nagra
National Cooperative for the
Disposal of Radioactive Waste

TECHNICAL REPORT 00-04

The Interaction of Radiolysis Products and Canister Corrosion Products and the Implications for Spent Fuel Dissolution and Radionuclide Transport in a Repository for Spent Fuel

February 2000

L.H. Johnson
P.A. Smith

Hardstrasse 73, CH-5430 Wettingen/Switzerland, Telephone +41-56-437 11 11

nagra
National Cooperative for the
Disposal of Radioactive Waste

TECHNICAL REPORT 00-04

The Interaction of Radiolysis Products and Canister Corrosion Products and the Implications for Spent Fuel Dissolution and Radionuclide Transport in a Repository for Spent Fuel

February 2000

L.H. Johnson [1)]
P.A. Smith [2)]

[1)] Nagra

[2)] Safety Assessment Management Limited

Hardstrasse 73, CH-5430 Wettingen/Switzerland, Telephone +41-56-437 11 11

This report was prepared on behalf of Nagra. The viewpoints presented and conclusions reached are those of the author(s) and do not necessarily represent those of Nagra.

ISSN 1015-2636

ABSTRACT

In this report, the release of radionuclides from the engineered barrier system of a deep geological repository for spent fuel is discussed and quantitative models are presented that will be used to support the concepts, models and parameter values to be used in future Nagra performance assessments. In the Nagra repository concept, the spent fuel will be contained in massive steel canisters, or copper canisters with steel inserts, that should ensure complete containment of radionuclides for at least 1000 years. When a canister is eventually breached, and water contacts the fuel, rapid release of an "instant release fraction" occurs, together with the much slower release of radionuclides incorporated in the fuel matrix, as the matrix dissolves. Processes that affect matrix dissolution include the failure of the Zircaloy cladding, the radiolysis of water contacting the fuel, with the generation of radiolytic oxidants that may react with the fuel, and the production of Fe^{2+} and H_2 from the corroding canister, that may scavenge radiolytic oxidants, and may also reduce the U(VI) released during fuel dissolution.

The failure of Zircaloy cladding is discussed. It is concluded that oxidants produced within the thin films of water surrounding the fuel pellets would have difficulty escaping by diffusion through the failed cladding. This provides the basis for a model of spent-fuel dissolution, in which it is assumed that all radiolytic oxidants that do not recombine with radiolytic reductants, react with the fuel surfaces. In order to apply this model, it is necessary to obtain a value for the effective yield of oxidants due to radiolysis, expressed as an effective *G*-value, that is suitably conservative for performance-assessment purposes. This report reviews evidence from laboratory experiments and natural analogues and concludes that a conservative value for performance-assessment calculations is 0.01 molecules of H_2O_2 per 100 eV.

If they are not scavenged by reductants inside the canister, such as H_2 and Fe^{2+}, radiolytic oxidants, and U(VI) from the dissolved fuel, may migrate from the breached canister into the surrounding bentonite buffer. The reducing minerals present in the bentonite, such as pyrite and siderite, will be depleted by these oxidants, forming an oxidising region, bounded by a redox front. Within this region, the solubilities of some safety-relevant radionuclides may be increased, and sorption diminished. For performance assessment, it is therefore important to assess the likely maximum penetration of the redox front.

In order to assess the scavenging by Fe^{2+}, the corrosion of carbon steel is reviewed and a model presented for the release of Fe^{2+} from a corroding steel canister. Release of Fe^{2+} occurs when iron corrodes to magnetite, but iron may be passivated by the formation of a low-porosity layer of maghemite on the magnetite. This model is incorporated in an assessment of the redox-front migration from a canister that is breached, either at a point or, more realistically for the assumed canister design, at a circumferential crack. The production of radiolytic oxidants decreases as a function of time, whereas the production of Fe^{2+} initially decreases but increases at longer times as a result of the formation of high surface area corrosion deposits. Eventually, all oxidants that are produced are likely to be scavenged. The time at which production of Fe^{2+} first exceeds that of radiolytic oxidants is also that time at which the oxidising region reaches its maximum extent.

The report presents calculations of redox-front penetrations for different fuel types (UO_2 and MOX fuels with a range of burn-ups) and for different assumptions regarding the nature of reductants in the bentonite and different canister lifetimes. It is concluded that

the scavenging of radiolytic oxidants by Fe^{2+} from canister corrosion is an important mechanism in limiting the extent of the oxidising region, but that it is also important to establish whether credit may be taken for the full potential of pyrite in the bentonite to provide a further scavenger of radiolytic oxidants.

ZUSAMMENFASSUNG

Im vorliegenden Bericht wird die Freisetzung von Radionukliden aus dem System der technischen Barrieren eines geologischen Tieflagers für abgebrannte Brennelemente diskutiert. Dabei werden quantitative Modelle vorgestellt, die zur Unterstützung der in künftigen Sicherheitsanalysen der Nagra verwendeten Konzepte, Modelle und Parameterwerte zum Einsatz kommen. Im Endlagerkonzept der Nagra werden die abgebrannten Brennelemente in massive Stahlbehälter oder Kupferbehälter mit Stahleinsatz eingelagert, die einen sicheren Einschluss der Radionuklide für mindestens 1000 Jahre gewährleisten sollen. Sollten irgendwann Risse in einem Behälter entstehen und Wasser in Kontakt mit dem Brennstoff gelangen, so wird eine "sofortige Freisetzungsmenge" an Radionukliden freigesetzt. Diese schnelle Freisetzung erfolgt zusammen mit der sehr viel langsameren Freisetzung von in der Brennstoffmatrix enthaltenen Radionukliden, wenn diese gelöst wird. Zu den die Matrixauflösung bewirkenden Prozessen zählen die Entstehung von Undichtigkeiten in den Zircaloy-Hüllrohren, die Radiolyse des Wassers in Kontakt mit dem Brennstoff, die Bildung von radiolytischen Oxidationsmitteln, die mit dem Brennstoff reagieren können und die Bildung von Fe^{2+} und H_2 aus den korrodierenden Behältern, die radiolytische Oxidationsmittel aufbrauchen und auch das während der Brennstofflösung freigesetzte U(VI) reduzieren können.

Die Konsequenzen von undichten Zircaloy-Hüllrohren werden im vorliegenden Bericht diskutiert. Daraus wird gefolgert, dass die innerhalb des dünnen, die Brennstoff-Pellets umgebenden Wasserfilms produzierten Oxidationsmittel Schwierigkeiten hätten, durch die undichten Hüllrohre hindurch zu diffundieren. Diese Erkenntnis bildet die Grundlage für ein Modell der Lösung von abgebrannten Brennstäben, wobei angenommen wird, dass alle radiolytischen Oxidationsmittel, die keine chemische Reaktion mit radiolytischen Reduktionsmitteln eingehen, mit den Brennstoffoberflächen reagieren werden. Für die Anwendung dieses Modells ist die Abschätzung eines Werts oder einer Reihe von Werten für die Netto-Ausbeute an radiolytischen Oxidationsmitteln erforderlich, ausgedrückt als effektiver G-Wert, der hinreichend konservativ für die Sicherheitsanalyse ist. Der vorliegende Bericht analysiert die Erkenntnisse aus Laborexperimenten und natürlichen Analoga und schliesst daraus, dass ein konservativer Wert für Sicherheitsberechnungen 0.01 Moleküle H_2O_2 pro 100 eV. beträgt.

Radiolytische Oxidationsmittel und U(IV) aus dem gelösten Brennstoff können durch im Behälter entstandene Risse in die umgebende Bentonitverfüllung migrieren, sofern sie nicht durch Reduktionsmittel innerhalb der Behälter verbraucht werden, wie z.B. durch Fe^{2+}. Die im Bentonit enthaltenen reduzierenden Mineralien, wie Pyrit und Siderit, werden durch diese Oxidationsmittel abgereichert. Es bildet sich eine Oxidationszone aus, die durch eine Redoxfront abgegrenzt wird. Innerhalb dieser Zone können die Löslichkeiten einiger sicherheitsrelevanter Radionuklide zunehmen und die Sorption verringert werden. Für die Sicherheitsanalyse ist es daher wichtig, die wahrscheinliche maximale Eindringtiefe der Redoxfront abzuschätzen.

Zur Abschätzung des Verbrauchs von Oxidationsmitteln durch Fe^{2+} wird das Korrosionsverhalten von Stahlguss überprüft und ein Modell der Fe^{2+}-Freisetzung aus einem korrodierenden Stahlbehälter vorgestellt. Fe^{2+} wird freigesetzt, wenn Eisen zu Magnetit oxidiert wird. Jedoch kann Eisen durch Bildung einer Maghemitschicht mit niedriger Porosität auf dem Magnetit passiviert werden. Dieses Modell wird in eine Abschätzung der Redoxfront-Migration aus einem Behälter mit entstandenen Rissen eingebunden, entweder an einem Punkt oder realistischer für die angenommene Behälterauslegung an einem umlaufenden Riss. Die Produktion radiolytischer Oxidationsmittel nimmt als

Funktion der Zeit ab, während die Produktion von Fe^{2+} zunächst abnimmt, dann aber nach längerer Zeit als Ergebnis der Bildung von Korrosionsablagerungen mit grosser Oberfläche zunimmt. Irgendwann sind wahrscheinlich alle produzierten Oxidationsmittel aufgebraucht. Die Zeit, in der die Fe^{2+}-Produktion erstmals diejenige der radiolytischen Oxidationsmittel übersteigt, entspricht ebenfalls der Zeit, zu der die Oxidationszone ihre maximale Ausdehnung erreicht.

Der vorliegende Bericht stellt die Berechnungen der Redoxfront-Eindringtiefe für unterschiedliche Brennstofftypen (UO_2- und MOX-Brennstoffe mit verschiedenen Abbränden) und für verschiedene Annahmen betreffend der Beschaffenheit der Reduktionsmittel im Bentonit und unterschiedlicher Behälterlebensdauer dar. Daraus wird gefolgert, dass der Aufbrauch der radiolytischen Oxidationsmittel durch Fe^{2+} aus der Behälterkorrosion ein wichtiger Prozess in der Begrenzung des Ausmasses der Oxidationszone ist. Es ist aber ebenfalls wichtig, zu ermitteln, ob auch das gesamte Pyritinventar im Bentonit als weiterer Verbraucher von radiolytischen Oxidationsmitteln berücksichtigt werden kann.

RÉSUMÉ

Ce rapport traite de la libération de radioéléments à partir du système de barrières techniques d'un dépôt pour combustible usagé en milieu géologique profond. Les modèles quantitatifs présentés servent à étayer les concepts, modèles et valeurs de paramètres à utiliser dans les futures évaluations de performance de la Cédra. Dans le concept d'entreposage de la Cédra, le combustible usagé sera placé dans des fûts massifs en acier, ou en cuivre avec un revêtement interne d'acier. Ces fûts sont conçus pour confiner complètement les radioéléments pendant au moins 1000 ans. Si un fût venait à s'endommager et que de l'eau entrait en contact avec le combustible, il s'ensuivrait une libération rapide de la « fraction de libération instantanée », ainsi qu'une libération beaucoup plus lente des radioéléments incorporés dans la matrice du combustible, au cours de la dissolution de cette dernière. Les processus qui affectent la dissolution de la matrice comprennent l'endommagement du revêtement de « Zircaloy », la radiolyse de l'eau au contact du combustible, avec la production d'oxydants radiolytiques pouvant réagir avec le combustible, ainsi que la production de Fe^{2+} et H_2 par corrosion du fût, pouvant mobiliser des oxydants radiolytiques mais aussi diminuer la libération de U(IV) lors de la dissolution du combustible.

Les conséquences de l'endommagement du revêtement de « Zircaloy » sont discutées dans le rapport. On en conclut que les oxydants produits dans les minces pellicules d'eau entourant les boulettes de combustible auraient de la peine à s'échapper par diffusion à travers le revêtement endommagé. Ce fait sert de base à un modèle de dissolution du combustible usagé, dans lequel on admet que tous les oxydants radiolytiques qui ne se combinent pas avec des réducteurs radiolytiques réagissent avec la surface du combustible. Pour appliquer ce modèle, il est nécessaire de disposer d'une valeur ou d'une fourchette de valeurs pour la production effective des oxydants issus de la radiolyse, exprimées comme valeurs-G effectives, suffisamment prudentes pour les besoins d'évaluation de la performance. Le rapport passe en revue les résultats d'expériences en laboratoire et les constats d'analogues naturels. Il en conclut qu'une valeur raisonnablement pessimiste pour les calculs d'évaluation de la performance peut être fixée à 0.01 molécules H_2O_2 pour 100 eV.

S'ils ne sont pas mobilisés par les réducteurs à l'intérieur du fût, les éléments tels que le Fe^{2+}, les oxydants radiolytiques et l'U(IV) issus de la dissolution du combustible peuvent migrer du fût endommagé vers le tampon de bentonite environnant. Les minéraux réducteurs présents dans la bentonite, tels que la pyrite et la sidérite, seront attaqués par ces oxydants, formant une région oxydante entourée d'un front redox. A l'intérieur de cette région, la solubilité de quelques radioéléments représentatifs pour les analyses de sécurité peut s'accroître, et l'adsorption peut diminuer. Il est donc important, pour l'évaluation de la performance, d'estimer la pénétration maximale probable du front redox.

Pour l'évaluation de la mobilisation par le Fe^{2+}, la corrosion de l'acier dur (riche en carbone) est passée en revue, et un modèle est présenté pour la libération du Fe^{2+} à partir d'un fût d'acier se corrodant. Du Fe^{2+} est libéré lorsque le fer se transforme en magnétite par corrosion, mais le fer peut être rendu passif par la formation d'une couche de maghémite sur la magnétite. Ce modèle est incorporé à une évaluation de la migration du front redox à partir d'un fût endommagé soit en un point, soit sur le pourtour par une fissure. Ce dernier cas de figure est plus réaliste, compte tenu du type de fût envisagé. La production d'oxydants radiolytiques décroît avec le temps, tandis que la production du Fe^{2+} commence par décroître pour croître ensuite à cause de la formation de dépôts

de corrosion à grande surface. En fin de compte, tous les oxydants produits seront probablement mobilisés. Le moment où la production de Fe^{2+} dépasse pour la première fois celle des oxydants radiolitiques correspond au moment du maximum d'extension de la région oxydante.

Le rapport présente les calculs de pénétration du front redox pour différents types de combustible (combustibles UO_2 et MOX avec un éventail de sous-produits de combustion) et différentes hypothèses sur la nature des réducteurs contenus dans la bentonite, ainsi que différentes durées de vie des fûts. On en conclut que la mobilisation des oxydants radiolytiques par le Fe^{2+} issu de la corrosion des fûts est un mécanisme important pour la limitation de l'extension de la région oxydante, mais qu'il est également important de savoir si l'on peut en compte toute la capacité de la pyrite contenue dans la bentonite à servir de mobilisateur supplémentaire des oxydants radiolytiques.

TABLE OF CONTENTS

LIST OF FIGURES

LIST OF TABLES

1 INTRODUCTION

The broad processes involved in the release of radionuclides from the near-field of a repository for spent fuel are summarised in Figure 1. Release from the fuel itself consists of two parts:

- the rapid release of an "instant-release fraction" (IRF) (JOHNSON & TAIT 1997) and
- congruent release, determined by slow, redox-dependent matrix dissolution.

The concentration of radionuclides in solution in the repository near field, and the rate of release from the near field to the geosphere, is a function of the release rate from the fuel, and of the solubility limits and sorption properties of the corresponding elements in the near-field environment.

A key uncertainty in evaluating these processes is the effect of redox conditions in the near field on the rate of UO_2 matrix dissolution and on solubility limits and sorption properties, which, in the case of some elements, are redox sensitive. For a repository sited in an anoxic host rock, it is generally acknowledged that the only significant source of oxidants that could attack the fuel matrix is that arising from radiolysis of groundwater[1]. Assuming that spent fuel is emplaced in canisters that have a lifetime of greater than about 500 years (the timescale associated with high beta/gamma activity arising from fission-product decay) the principal source of oxidant would be alpha-radiolysis of water that comes into contact with the fuel surface after failure of the canister and the Zircaloy cladding.

Oxidising species, including both radiolytic oxidants and the U(VI) that is released as the fuel is oxidised, may perturb redox conditions in the near field. A concern is that the transport of oxidising species through the near-field materials surrounding the fuel may produce a region within the near field, bounded by a redox front, where oxidising conditions prevail, and where the concentrations of some radionuclides in solution are affected by higher solubilities and lower sorption. In order to scope the possible consequences of such an oxidising region, four hypothetical cases were considered in SCHNEIDER *et al.* (1997), as illustrated conceptually in Figure 2(i) for crystalline basement rock. CASE 1, in which reducing conditions are assumed throughout the near field (including the fuel surface) is the most optimistic from the point of view of safety, but was considered to be difficult to support on the basis of current information and was not therefore evaluated quantitatively. The cases for which calculations of radionuclide release and transport were performed are:

CASE 2: The redox front penetrates a small distance into the bentonite (compared to its total thickness): sorption parameters and solubility limits are based on reducing conditions.

CASE 3: The redox front penetrates a considerable distance into the bentonite, but not beyond: sorption parameters for the bentonite are based on oxidising conditions and solubility limits are based on reducing conditions.

---

[1] Any oxygen trapped at the time of repository closure would be consumed by, for example, canister corrosion, and would not be expected to affect fuel dissolution.

CASE 4: The redox front penetrates into the host rock: sorption parameters and solubility limits are based on oxidising conditions.

For these latter three cases, the fractional dissolution rate of the fuel was taken from the time-dependent radiolytic dissolution model of VIENO *et al.* (1992), i.e., 5×10^{-6} a^{-1} for the time period 10^4 a to 10^5 a, 4×10^{-7} a^{-1} for the time period 10^4 a to 10^5 a and 2×10^{-7} a^{-1} beyond 10^6 a. The results of the calculations for the four cases showed that only for Case 4 does the resultant radiation dose come within one order of magnitude of the regulatory guideline of 0.1 mSv a^{-1} (Figure 2(ii)). In all other cases, doses were more than two orders of magnitude below the regulatory guideline. In the study, no attempt was made to quantify the rate of movement of a redox front through the buffer or to evaluate the importance of oxidant consumption by canister corrosion products such as magnetite.

The results of the preliminary calculations of SCHNEIDER *et al.* (1997) illustrate the importance of maintaining reducing conditions in the near field. In the present study, an attempt is made to evaluate several processes that will affect the near-field redox conditions. These include:

- the radiolytic oxidant production rate, including the effect of the recombination of radiolytic oxidants and reductants,
- the consumption of oxidants (either radiolytic oxidants such as H_2O_2, or U(VI) produced as a result of oxidation of the fuel) by the corrosion products of an iron-based canister and
- the consumption of oxidants by their reaction with reductants, such as pyrite and siderite, that are naturally present in the bentonite buffer that surrounds the canister in the Swiss repository concept[2].

A critical review of spent-fuel dissolution and radiolysis studies is presented in order to derive an effective *G* value for radiolytic oxidant production. This is used to calculate a time-dependent rate of fuel-matrix dissolution, based on the conservative assumption that all oxidants produced react with the fuel matrix. In addition, a model for the production of Fe(II) corrosion products during the anoxic corrosion of an iron-based canister is presented. The penetration of the redox front into the buffer is then calculated, incorporating both the effects of corrosion products and mineral reductants in the buffer on redox front movement.

---

[2] The redox buffering capacity due to reductants present in the groundwater is not considered in the present report.

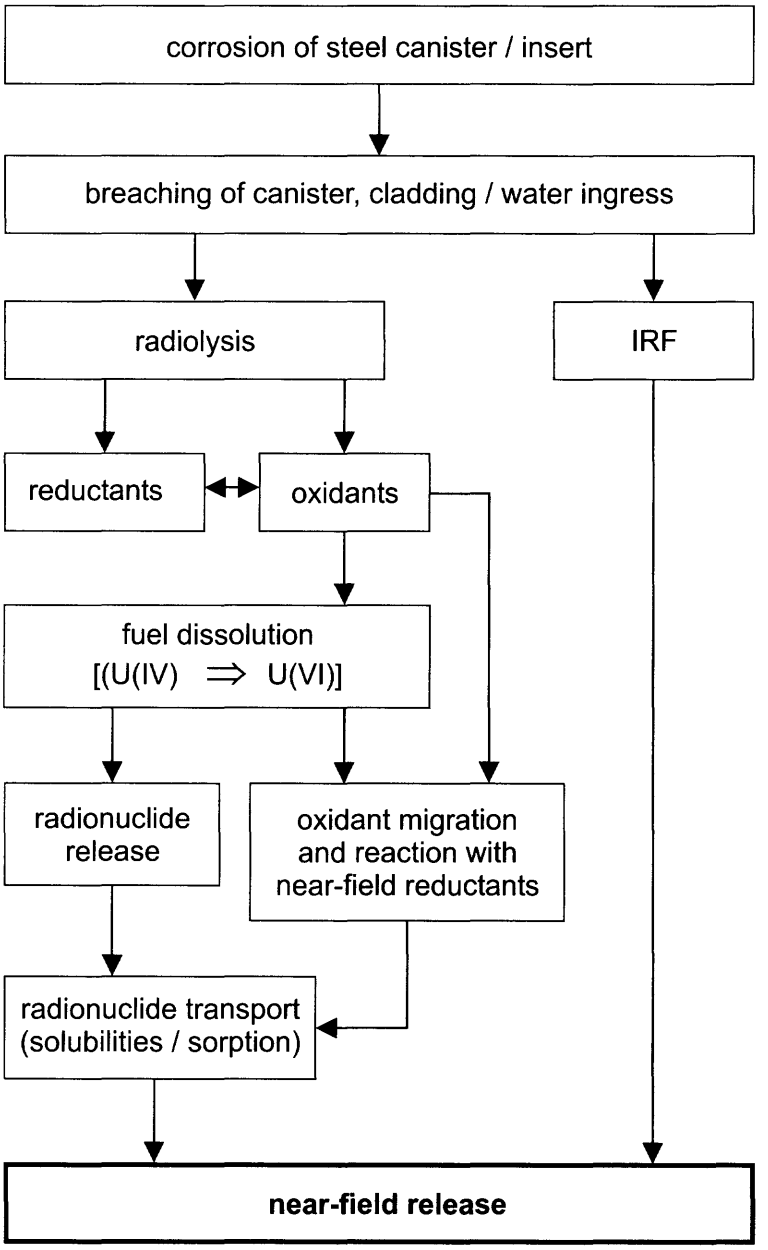

Fig. 1: Summary of broad processes involved in the release of radionuclides from the near field of a repository for spent fuel

	CASE 1	CASE 2	CASE 3	CASE 4 a/b	
fuel matrix dissolution rate	values for reducing conditions	values for oxidising conditions			
sorption	values for reducing conditions		values for oxidising conditions		
solubility limits	values for reducing conditions			values for oxidising conditions	
geosphere colloids	colloids generated at the redox front are filtered by the bentonite			filtration in geosphere	no filtration in geosphere
redox front migration	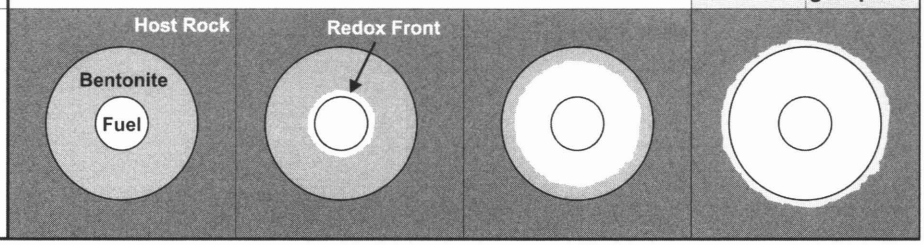				

Fig. 2(i): Calculational cases to evaluate sensitivity to position of a redox front (from SCHNEIDER *et al.* 1997).

Note: If the redox front is located in the geosphere (CASE 4), colloids may be transported through fractures in the host rock and, if they are prevented (due, for example, to their size) from diffusing into the stagnant pore water of the adjacent wall rock, then the radionuclides associated with these colloids would not be subject to the retarding effects of matrix diffusion and sorption on matrix pore surfaces. The distances over which such colloids would be transported through the host rock are highly uncertain and two extreme situations, within CASE 4, are evaluated in order to investigate the effects of this uncertainty:

CASE 4a: Colloids either do not form, or are transported only a short distance through host-rock fractures. Only solute transport is modelled in the geosphere.

CASE 4b: Colloids are transported, without either filtration or retardation, through host-rock fractures. Radionucide release from the near field is, in the model, assumed to be transferred instantaneously to the biosphere.

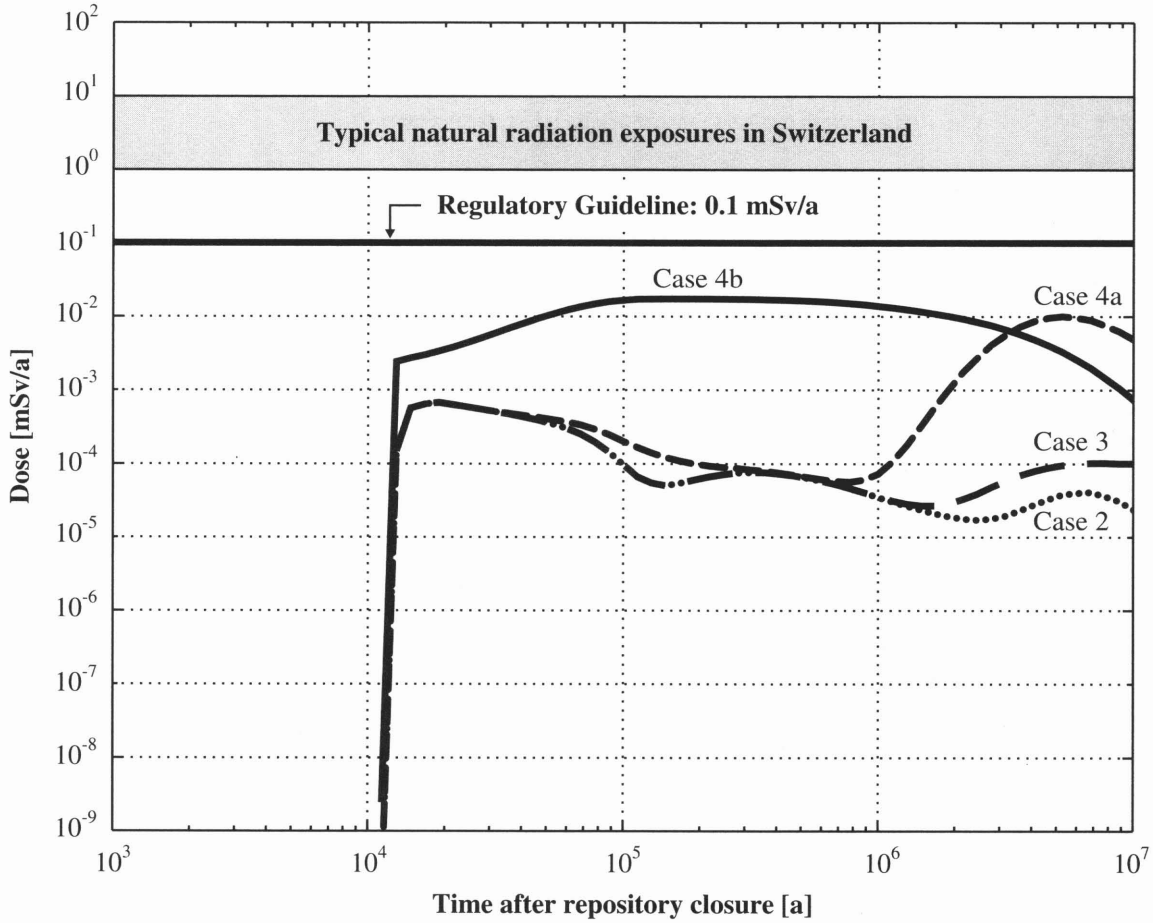

Fig. 2(ii): Annual individual dose from a repository in crystalline rock for UO_2 spent fuel as a function of time in CASE 2, CASE 3 and CASE 4 (SCHNEIDER *et al.* 1997).

2 PROCESSES OCCURRING IN A SPENT FUEL DISPOSAL CANISTER AFTER BREACHING

2.1 Canister design and overview of processes

In the present study, the use of a thick cast-steel or iron disposal canister, or a copper canister with a steel insert, is assumed. The canister has channels that would hold 4 PWR or 9 BWR assemblies of fuel elements[3], as shown in Figure 3. The fuel elements can be either UO_2 or MOX.

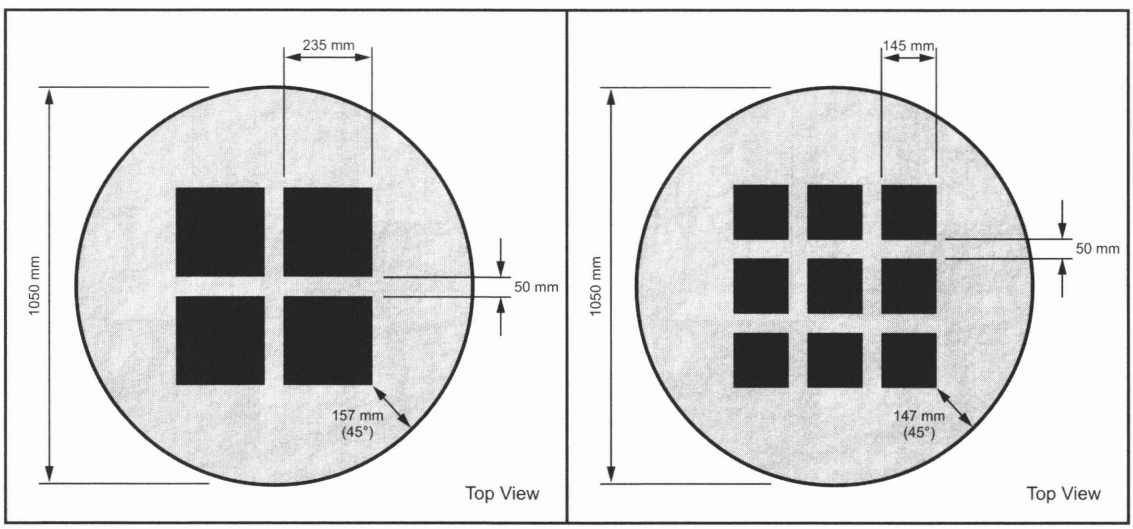

Fig. 3: Cross-section of the cast steel canister for PWR fuel (left) and for BWR fuel (right).

Following resaturation of the repository near field, the external surface of the canister would begin to corrode and would eventually be weakened sufficiently for breaching of the canister to occur. The canister is designed to remain unbreached for at least 1000 years (JOHNSON & McGINNES 1999). The physical and chemical processes occurring subsequent to breaching include:

- the failure of the Zircaloy cladding surrounding the fuel rods by a variety of potential mechanisms, including localised corrosion and hydrogen-induced cracking, with associated implications for mass transport,
- the radiolysis of water that contacts the fuel surface, producing radiolytic species that may interact with the fuel matrix, and lead to radionuclide release, and
- the corrosion of steel surfaces inside the canister to produce iron oxide phases, dissolved Fe(II) and H_2 (dissolved and gaseous)

The buffer material surrounding the canister ensures that all transport is diffusion controlled.

---

3 PWR = Pressurised water reactor. BWR = Boiling water reactor.

2.2 Failure of Zircaloy

The failure of cladding is discussed here principally because of the need to establish its role in influencing mass transport of oxidants produced at the fuel surface by α-radiolysis. Should cladding failure occur by localised corrosion or hydrogen-induced cracking, which is likely considering the very low general corrosion rate of Zircaloy, oxidants produced within the thin films of water within and surrounding the fuel pellets would escape slowly by diffusion through the point of cladding failure. As a result, oxidants are likely to react with the fuel. Alternatively, if there were numerous penetrations of the cladding, this might permit some fraction of the oxidants to escape and react with the Fe^{2+} that is produced by canister corrosion.

Hydriding, and general embrittlement of Zircaloy, would eventually lead to numerous penetrations in the cladding, such that it would likely have a limited role in reducing mass transport rates. Appendix A discusses the failure processes in more detail. However, because there are significant uncertainties in assessing the behaviour of the cladding, the calculations in this report conservatively emphasise the possibility of rapid cladding failure (as a result of hydrogen-induced cracking and possibly pitting corrosion), with trapping of oxidising radiolysis products at the fuel surface. The effect of more rapid transport of dissolved species through the failed cladding and the potential impact on fuel dissolution rates is discussed in Appendix B.

2.3 Radiolysis of water

2.3.1 Importance of alpha radiolysis in the generation of oxidants

In order to model the effects of radiolysis of water on spent fuel dissolution, it is necessary to describe the time-dependent concentration of oxidants present in the repository near field. It is generally assumed that the oxygen initially present in a sealed repository will be rapidly consumed and that, assuming a minimum canister lifetime of ~1000 years, the only possible source of oxidants to attack spent fuel would be that arising from alpha radiolysis.

In this report, the production rate of oxidants from alpha radiolysis is estimated by examining a number of theoretical and experimental studies. It is important to note that focusing solely on alpha as compared to low LET (linear energy transfer) beta/gamma radiation is appropriate if the modelling deals solely with time periods greater than several hundred years. If, however, early canister failures occur, low LET radiation is expected to have a greater impact than alpha radiation in contributing to radiolytic oxidation (CHRISTENSEN 1998, JOHNSON *et al.* 1996). A corollary of this point is that, in interpreting observed spent-fuel dissolution rates to obtain information about the radiolytic dissolution of spent fuel, one must acknowledge the potentially significant role that low LET radiation has in accelerating dissolution of spent fuel. This is an important point that will be dealt with later in the discussion about dissolution of spent fuel under anoxic conditions.

Alpha radiolysis, and the production of radiolytic oxidants, occurs where alpha particles interact with water molecules. Alpha particles generated within fuel pellets at distances greater than 11 μm from solid-liquid interfaces are absorbed by the fuel and do not contribute to oxidant production. Oxidants are produced due to alpha particles generated within the fuel, either near to the external surfaces of the fuel pellets or near to

internal, water-saturated fractures within the fuel[4]. In addition, following the initiation of fuel dissolution, alpha particles with the potential to generate radiolytic oxidants can originate:

- from within the porous precipitate (i.e. UO_3 hydrates incorporating alpha emitters such as ^{239}Pu), that may form within fuel fractures and in the fuel/sheath gap. The high porosity of precipitates may increase the volume of irradiated water, with only limited absorption of particles occurring in the solid hydrates,
- from dissolved alpha emitters in the water within the breached canister, which, in spite of their low concentration, may provide an efficient production route for oxidants since there is no absorption in solids and
- from alpha emitters that are sorbed on the buffer material, which again has a relatively high porosity (~ 40%), giving only limited absorption of alpha particles.

As discussed in Appendix C, these sources of radiolytic oxidants are of less importance than the alpha particles generated within the fuel, which is the focus of the present report.

2.3.2 Theoretical yields for alpha radiolysis

For alpha radiolysis, the dominant species produced are molecular, i.e., H_2 and H_2O_2, with radical species being produced in much lower quantities. The yield of H_2O_2 for a homogeneous acid solution has been measured and is ~1 molecule per 100 eV ($G = 1$) (BURNS & SIMS 1981; CHRISTENSEN 1998). Using this yield, attepts have been made to model the dissolution rate of UO_2 with limited success. The results show that in oxygen-free systems, modelled dissolution rates are orders of magnitude higher than measured dissolution rates (CHRISTENSEN & SUNDER 1998). For the complex heterogeneous system of interest here, the surface of spent fuel as influenced by Fe(II)/Fe(III) and H_2, both arising from canister corrosion, the yield cannot be directly measured but can be calculated if certain assumptions are made. The Fe(II)/Fe(III) couple is expected to undergo redox reactions leading to the decomposition of H_2O_2,

$$Fe^{3+} + e^-(aq) \rightarrow Fe^{2+} \quad (1)$$

$$Fe^{2+} + H_2O_2 \rightarrow FeOH^{2+} + OH^\bullet \quad (2)$$

resulting in an increase in H_2 concentration through the recombination of $H^\bullet$ radicals (CHRISTENSEN & BJERGBAKKE 1982). Some experimental evidence exists to support these arguments (SUNDER *et al.* 1997, LOIDA *et al.* 1996). CHRISTENSEN & BJERGBAKKE (1982) estimate an effective G value as low as 0.001 for the Fe(II)/(III) system. Calculations by TAIT & JOHNSON (1986) also show that quite moderate concentrations of H_2 ($\leq 10^{-5}$ mol l^{-1}) are sufficient to markedly suppress H_2O_2 production.Radiolytically produced hydroxyl radicals react with H_2 to produce $H^\bullet$ radicals

$$OH^\bullet + H_2 \rightarrow H^\bullet + H_2O \quad (3)$$

---

[4] Production at grain boundaries within the fuel is insignificant, due to the small volume of water that is present in these features.

which subsequently lead to the decomposition of peroxide,

$$H^{\bullet} + H_2O_2 \rightarrow OH^{\bullet} + H_2O \quad (4)$$

$$OH^{\bullet} + H_2O_2 \rightarrow HO_2^{\bullet} + H_2O \quad (5)$$

A *G* value as low as 0.001 might also be expected with H_2, particularly at the high H_2 partial pressures that would be experienced in the vicinity of a corroding iron canister.

Because such low yields have only been calculated, but have not been demonstrated for the system of interest, a more empirical approach is used in the present report to derive an effective *G* value (G_{eff}) for performance-assessment calculations of spent-fuel disposal.

2.3.3 Effective radiolytic yields used in performance-assessment models

In the model for spent-fuel dissolution used in the SKB-91 (SKB 1992) and TVO-92 (VIENO et al. 1992) performance assessments, which has also been used in preliminary performance-assessment calculations for Nagra (SCHNEIDER et al. 1997), the fractional dissolution rate of the fuel, *D* [a^{-1}], is assumed to be directly proportional to the α-activity R_α [GBq tHM^{-1}]:

$$D = 2.88 \times 10^{-10} R_\alpha \quad (6)$$

The constant of proportionality is derived from the results of the spent-fuel dissolution studies of WERME et al. (1990), performed under aerated conditions, in which ^{90}Sr release rates are considered indicative of the matrix dissolution rate. Converting the fractional dissolution rate to D_1 [mol a^{-1} tHM^{-1}], we have:

$$D_1 = D \times \frac{10^6 \text{ g tHM}^{-1}}{238 \text{ g mol}^{-1}} = 1.21 \times 10^{-6} R_\alpha \quad (7)$$

A G_{eff} value for this system is implicit in the constant in Eq. 7. In order to derive this implicit value, however, assumptions must be made regarding the proportion of α-activity that is absorbed by the fuel. Two alternative approaches are compared, below.

Approach 1

Water at the wetted surfaces of the fuel experience an α-flux, mainly from the top 11 μm of the fuel, as a result of the limited mean free path of the α-particles in solid UO_2 (NITZKI & MATZKE 1973). The fraction of the fuel that can give rise to α-particles penetrating the wetted surfaces and causing radiolysis is:

$$F_f = \frac{3\left(11 \times 10^{-6}\right) \times 0.15}{16\pi\left(5 \times 10^{-3}\right)^2} = 0.004 \quad (8)$$

where it is assumed that the wetted surface area of the fuel is 0.15 m^2 per metre of fuel rod, and the fuel-rod radius is 0.5 cm. The factor of 3/16 is included to take account of the random direction of α-particles generated near the fuel surfaces (LIU & NERET-NIEKS 1995). Thus, only 0.4% of the α-activity of the fuel gives rise to radiolysis, with the remainder of the energy being directly absorbed by the fuel.

The production rate, P_C [mol a^{-1} tHM^{-1}], of radiolytic H_2O_2 is given by:

$$P_C = QG_{eff}F_f \times \frac{\left[3.156\times10^{7}\ \mathrm{s\,a^{-1}}\right]}{\left[1.6\times10^{-17}\ \mathrm{J.(100\,eV)^{-1}}\right]\times\left[6.02\times10^{23}\ \mathrm{molecules\,mol^{-1}}\right]} = 0.013QG_{eff} \qquad (9)$$

where Q [W tHM^{-1}] is the heat output of the fuel. In this expression, If it is assumed that the dissolution rate of the fuel is equal to the production rate of radiolytic H_2O_2 in Eq. 9:

$$D_1 = P_C = 0.013QG_{eff} \qquad (10)$$

The heat output of the fuel is related to R_α by the expression:

$$R_\alpha = \frac{Q}{E}\cdot\frac{10^{-9}\ \mathrm{GBq\,Bq^{-1}}}{1.6\times10^{-19}\ \mathrm{J\,eV^{-1}}} = 6.25\times10^{9}\,\frac{Q}{E} \qquad (11)$$

where E [eV] is the average energy of an alpha particle, typically 5 × 10^6 eV. Thus, from Eq. 7 and Eq. 11:

$$D_1 = \frac{\left(1.21\times10^{-6}\right)\times\left(6.25\times10^{9}Q\right)}{5\times10^{6}} \qquad (12)$$

Equating D_1 in Eq. 10 and Eq. 12, and rearranging, the effective G value implicit in Eq. 7 is:

$$G_{eff} = \frac{\left(1.21\times10^{-6}\right)\times\left(6.25\times10^{9}\right)}{\left(5\times10^{6}\right)\times0.013} = 0.11 \qquad (13)$$

Approach 2

Another approach is to look at the dose rate at the surface of the samples in the spent-fuel experiments used to derive the rate values used in the dissolution models, starting with the calculations of CHRISTENSEN & BJERGBAKKE (1985). The alpha dose rate at the fuel surface, d [rad s^{-1}], together with the effective G value, gives the rate of production of radiolytic H_2O_2 per gram of irradiated water, P [mol a^{-1} g^{-1}], via the expression:

$$P = \frac{d \times 6.25 \times 10^{13}\ \text{eV rad}^{-1} \times 3.15 \times 10^{7}\ \text{s a}^{-1} \times 0.01 \times G_{eff}}{6.02 \times 10^{23}\ \text{molecules mol}^{-1}} = 3.27 \times 10^{-5} d G_{eff} \qquad (14)$$

The dissolution rate of the samples, can (as in Approach 1) be equated to the production rate, P_C, of radiolytic H_2O_2 per tonne of uranium:

$$D_1 = P_C = P \frac{M}{M_{HM}} \qquad (15)$$

where M [g] is the mass of irradiated water and M_{HM} [t_{HM}] is the mass of uranium in a sample. The fractional dissolution rate is:

$$D = 238\ \text{g mol}^{-1} \times 10^{-9}\ t_{HM}\ \text{g}^{-1} P_C = 2.38 \times 10^{-7} P \frac{M}{M_{HM}} \qquad (16)$$

The experiments of FORSYTH & WERME (1992) involved 16 g samples, which, assuming a typical surface area for spent fuel of 2×10^{-4} m^2 g^{-1} (JOHNSON 1982), would have an surface area of 3.2×10^{-3} m^2. Further assuming a 30 μm α-particle range in water, the mass of irradiated water would be:

$$M = 3.2 \times 10^{-3}\ \text{m}^2 \times 30 \times 10^{-6}\ \text{m} \times 10^{6}\ \text{g m}^{-3} = 0.096\ \text{g} \qquad (17)$$

16 g of fuel corresponds to a mass of uranium, M_{HM}, of:

$$M_{HM} = \frac{16\ \text{g} \times 238\ \text{g mol}^{-1} \times 10^{-9}\ t_{HM}\ \text{g}^{-1}}{270\ \text{g mol}^{-1}} = 1.41 \times 10^{-8}\ t_{HM} \qquad (18)$$

Substituting Eq. 14, Eq. 17 and Eq. 18 in Eq. 16, and rearranging:

$$G_{eff} = 1.89 \times 10^{4} \frac{D}{d} \qquad (19)$$

The measured fractional dissolution rate, D, was 1.1×10^{-4} a^{-1} for the aerated fuel dissolution experiment. The dose rate, d, for the fuel used in this experiment, at 15 years following unloading from a reactor (the age of the fuel in the original dissolution experiments of FORSYTH & WERME 1992)[5], is ~ 40 rad s^{-1}. Thus, according to this approach, the effective G value implicit in Eq. 7 is:

[5] The reported rate of 32 rad s^{-1} at 40 years following unloading is converted to ~ 40 rad s^{-1} at 15 years, based on an inspection of the total alpha decay curve for LWR fuel.

$$G_{eff} = \frac{(1.89\times10^{4})\times(1.1\times10^{-4})}{40} = 0.05 \qquad (20)$$

a value that agrees reasonably well with that derived by Approach 1.

It may be concluded that the G_{eff} values implicit in the results of these spent-fuel dissolution experiments are about 0.05-0.1. It follows that the assumption of a G value of 1 would significantly over-predict the yield of radiolysis products and that the predicted dissolution rate would be at least 10 times higher than the measured values indicate. Thus, an examination of a variety of experimental and natural analogue studies to provide a basis for G_{eff} values for performance-assessment calculations is worthwhile.

2.3.4 Effective yields from anoxic spent-fuel dissolution and natural-analogue studies

The following discussion is largely limited to the examination of matrix dissolution rate data for spent LWR and CANDU fuel[6] at low temperatures, and in the relatively low-salinity groundwaters that are of interest in the Nagra safety studies. In particular, the focus is on the SKB data (FORSYTH & WERME 1992) used to derive the constant for the rate model proposed in TVO-92 (VIENO et al. 1992), the flow-through dissolution experiments of TAIT & LUHT (1997) and the alpha radiolysis experiments of SUNDER *et al.* (1995, 1997). The importance of such factors as beta/gamma radiolysis vs. alpha radiolysis in experiments and extrapolation to temperatures of interest for repository safety analysis (~ 50 ^{0}C is assumed for a long-term repository average in Nagra studies) are also addressed.

Effect of oxic vs. anoxic experimental conditions

WERME *et al.* (1990) reported long-term average rates of dissolution of moderate burnup LWR fuel at 25 ^{0}C of 1.1 $\times$ 10^{-4} a^{-1} (based on Sr-90). This is the source of the rate of 1 $\times$ 10^{-4} a^{-1} quoted by VIENO et al. (1992) and of the effective G-value of 0.05 - 0.1 inferred in Section 2.3.3. The experiments were performed under aerated conditions. It has been shown (TAIT & LUHT 1997) that, in aerated water, the dissolution rate is very similar for both UO_2 and spent fuel. Thus, under aerated conditions, it can be inferred that:

- dissolution of spent fuel is driven principally by dissolved oxygen, not by alpha radiolysis;
- the effective G-value for spent-fuel dissolution in the anoxic conditions of interest in repository performance assessment is potentially even smaller than the 0.05 - 0.1 range inferred from the experiments.

The question of how much lower the dissolution rate of spent fuel is under anoxic conditions has been the subject of considerable debate, and there are few relevant carefully controlled measurements on which to rely. It is important to note that dissolution rate measurements for spent fuel, obtained in a variety of studies, show reasonable agreement (typically within a factor of five). For the purposes of this review, however, it

---

[6] It should be noted that the alpha activity of CANDU fuel is several times less than that of LWR fuel. Thus, if alpha radiolysis is an important factor in spent-fuel dissolution experiments, use in Nagra safety assessments of the CANDU fuel data for anoxic conditions might underestimate the rate of dissolution.

is the overall rate reduction in going from oxidising to anoxic conditions that is of most interest, rather than the absolute value of the rate. This is because the same test method and fuel are used in such comparative determinations.

WERME et al. (1990) reported that, under anoxic conditions, the dissolution rate was 1.1×10^{-5} a^{-1} (Sr-90), although a slightly higher value of 5.9×10^{-5} a^{-1} is reported in FORSYTH & WERME (1992). Thus, an average reduction in rate of between 2 and 10 is observed in going from oxic to anoxic conditions.

JOHNSON (1982) reported a dissolution rate for CANDU fuel of ~ 3.6×10^{-5} a^{-1} for aerated conditions, and observed a reduction in rate for anoxic conditions by a factor of five.

In a recent study, TAIT & LUHT (1997), using a flow-through technique with powdered spent CANDU fuel, observed a rate reduction of a factor of 30 to 40 on going from aerated to anoxic conditions. There are good reasons to believe that their study achieved more effective control of the oxygen concentration than the previously mentioned studies, including the use of a flow-through technique and an in-line oxygen analyser. The application of this data to performance assessment in a direct fashion may be unwise, because the flow-through technique may lead to sweeping away of radiolysis products that in a repository (or a static dissolution experiment with spent fuel) would be allowed to accumulate. It is also noted that the alpha activity of CANDU fuel is somewhat lower than that of LWR fuel.

Another study of spent-fuel dissolution that provides information on the effective G-value under anoxic conditions is that of ERIKSEN et al. (1995). They reported that a direct measurement of the H_2 yield for a sample of spent fuel in groundwater gave a yield of one tenth of the expected value, implying an effective *G*-value of 0.1.

Effect of beta-gamma dose rates

It has been noted by TAIT & LUHT (1997) that the decrease in dissolution rate for *unirradiated* UO_2 is a factor of > 100 in going from aerated to anoxic conditions compared to a factor of 30 – 40 for spent CANDU fuel. Furthermore, under aerated conditions, the dissolution rate of unirradiated UO_2 increased by a factor of 5 when the gamma radiation dose is increased to the range expected for spent CANDU fuel[7]. It seems reasonable to conclude that the relatively small rate reduction for spent fuel, as compared to unirradiated UO_2, in going from oxic to anoxic conditions arises because, under anoxic conditions, beta/gamma radiolysis contributes significantly to the dissolution rate of spent fuel. Under oxic conditions, dissolution is likely to be dominated by oxygen.

This is supported further by the data reported by SHOESMITH & SUNDER (1992) and by the alpha radiolysis studies of SUNDER *et al.* (1995), which suggest that very high alpha fields, well in excess of that at a spent-fuel surface, are required to cause significant oxidation of a UO_2 surface. This is not to say that alpha radiolysis has no effect and it must be noted that the geometry of the experiments in which such observations are made may underestimate radiolytic impacts because diffusive losses from the UO_2 electrode surface may also be contributing to the small observed radiolytic effect (as discussed in Appendix D, an effective G-value in the range 0.001 – 0.01 is apparent

[7] i.e. a range of 10^3 to 10^4 R hr^{-1} for the small amounts of powder used in the experiments of TAIT & LUHT (1997); dose rates may be above 10^4 R hr^{-1} for large clad segments of the type used in the experiments of FORSYTH & WERME (1992) and JOHNSON (1982).

when the diffusive losses are taken into account). It should, however, be noted that the total beta/gamma dose rate from spent fuel is approximately 100 times larger than the alpha dose rate (see TAIT & LUHT 1997, Fig. 15), whereas the H_2O_2 yield is similar (e.g. 0.98 for alpha radiolysis and 0.74 for beta radiolysis). Thus, the oxidative dissolution of spent fuel in experiments under anoxic conditions is likely to be driven principally by beta- and gamma-, rather than alpha-radiolysis. This is supported by a recent analysis of radiolysis effects in spent-fuel dissolution experiments by CHRISTENSEN (1998).

Given the above observations, it is reasonable to conclude that the rate of dissolution of spent fuel under anoxic conditions is at least five times lower than the rate under aerated conditions. It may well be even lower, but it is difficult to unequivocally demonstrate that this is the case, because of gamma/beta radiolysis effects.

Effect of temperature

Regarding the effect of temperature, the only reported measurement of spent fuel dissolution under anoxic conditions is that of TAIT & LUHT (1997), who report an activation energy of 18kJ mol^{-1}. Assuming a long-term (10^3 to 10^4 year) average repository temperature of ~ 50 °C, the rate of dissolution would be two to three times higher than at 25 °C. Returning to the question of effective G values, it appears that one could argue for a reduction in the G_{eff} value from 0.05 – 0.1 to ~ 0.02 – 0.05, based on the observation that the rate of dissolution decreases by a factor of five or more under anoxic conditions, but increases by a factor of two to three for a repository temperature of ~50 °C.

Effect of hydrogen

A study of spent fuel dissolution by SPAHIU & WERME (in press) illustrates clearly that a H_2 partial pressure of 5 MPa dramatically reduces the dissolution rate relative to that measured for anoxic conditions. In this study, essentially constant concentrations of fission products were observed (i.e., a dissolution rate cannot be derived from the change in concentration in solution of a matrix dissolution indicator such as ^{90}Sr). Furthermore, uranium concentrations well below 10^{-8} M were observed, indicating that U(IV) was the dominant oxidation state in solution. The authors noted that the mechanism may involve scavenging of radiolytic oxidants by hydrogen, or a catalytic effect of the UO_2 surface on dissolved hydrogen. KING et al. (1999) provide other evidence for the intensely reducing environment produced by the combination of radiation and high H_2 partial pressures. They measured potentials of –500 to –800 mV on UO_2 electrode surfaces with high gamma fields and a 5 MPa H_2 partial pressure. These values are far below the threshold for oxidative dissolution, a value of ~-100 mV where the surface composition is $UO_{2.33}$ (SHOESMITH et al. 1994). KING et al. (1999) interpreted their experiments as indicating that both homogeneous and surface reactions involving H_2 scavenge oxidizing species, essentially preventing any significant oxidation. SUNDER et al. (1990) also noted the effect of H_2 on suppressing oxidation of UO_2, in this case for alpha-radiolysis at low H_2 partial pressures at 100 °C. These studies have important implications, but it is not yet possible to infer G values from the results, although the G values must be assumed to be much lower than 0.01.

Evidence from natural analogues

Another perspective on the question of radiolytic yield is provided by the behaviour of uraninite in the Cigar Lake deposit (CRAMER & SMELLIE 1994). SMELLIE & KARLSSON (1996) have made a detailed review of the discrepancies between the predicted and observed radiolysis impacts on the deposit. They were unable to resolve the approximately one hundred-fold discrepancy and noted that the most obvious reason was uncertainty in the important boundary condition for water distribution and grain-size distribution in the deposit. The effective *G*-value of 0.01 proposed by LIU & NERETNIEKS (1995) is an attempt to account for the discrepancy. The use of this *G*-value in performance assessment calculations for spent fuel, however, implicitly assumes that the conditions of exposure to radiolysis for spent fuel in a repository are the same as for Cigar Lake ore.

2.3.5 Summary of G_{eff}-values

The following table summarises the G_{eff}-values discussed above, along with their sources and some key observations:

G_{eff} –value	Origin	Comments
1	Primary yield in homogeneous solution.	Predicts dissolution rates approximately 10 times higher than actually measured for spent fuel in aerated water; also not consistent with Cigar Lake observations.
~ 0.1	Effective *G* in TVO-92; derived from spent fuel rate in aerated water.	Overestimate because O_2 and beta/gamma radiation can explain the rate under these conditions.
0.1	Based on Eriksen *et al.* (1995).	Actual measurement of H_2 yield for spent fuel in deaerated water; beta/gamma effects may be dominant.
~ 0.02 – 0.05	Derived from spent fuel dissolution rates under anoxic conditions, adjusted for temperature.	Beta/gamma effects may be dominant.
0.01	Derived from Cigar Lake natural-analogue study.	Significant uncertainties remain.
< 0.01	Effective *G* from spent CANDU fuel dissolution in deaerated water.	May underestimate the rate, due to diffusive losses from the experimental system.
0.001 – 0.01	Derived from the alpha-radiolysis experiments of SUNDER *et al.* (1997).	Uncertainties in the treatment of diffusive losses from apparatus and the effect of H_2O_2 decomposition (Appendix D).
0.001	Consistent with calculations of CHRISTENSEN (1985), for Fe^{2+}acting as a recombiner.	
<0.001	Implied by experiments of SPAHIU & WERME (in press)	G_{eff} cannot be directly calculated

The above discussion suggest that a G_{eff} value of 0.01, derived directly from spent fuel dissolution measurements, can be considered to have a sufficient degree of conservatism for use in performance-assessment calculations. It is noted that this value predicts a significant dissolution rate for spent fuel for reducing repository conditions, whereas experiments indicate negligible dissolution at high hydrogen partial pressures. The oxidant production rates and dissolution rates for spent UO_2 and MOX fuels, based on a G_{eff} value of 0.01, are discussed in Section 4.

2.4 The corrosion of carbon steel canisters

2.4.1 Importance of the process

Upon breaching of the canister, water would gradually fill the void space and corrosion of the inside of the canister would begin. In addition, the Zircaloy cladding would be expected to fail, exposing the fuel to groundwater. The products of steel corrosion (various Fe oxides and H_2), could interact with radiolysis products, leading to a mitigation of radiolysis effects. In particular, this might cause:

- a suppression of the rate of fuel matrix dissolution, if the rates of reaction of Fe^{2+} or H_2 with radiolytic H_2O_2 are similar to, or greater than, that of H_2O_2 with UO_2, and
- chemical reduction of U(VI) and redox-sensitive fission products and actinides, released by fuel matrix dissolution, due to the large reducing capacity provided by the corrosion products of the steel canister.

Accounting for the latter effect in performance-assessment calculations has been questioned because of the possibility of passivation of the corroding steel, which might greatly reduce the potential for Fe^{2+} to participate in redox reactions. The corrosion reactions in question are examined here to determine if the redox-buffering capacity associated with the steel can be convincingly argued to slow or prevent migration of a redox front.

2.4.2 Iron-oxide phase relationships

Corrosion of carbon steel under repository conditions will produce magnetite (Fe_3O_4):

$$3Fe + 4H_2O = Fe_3O_4 + 4H_2 \qquad (21)$$

as well as Fe(III) oxide phases:

$$4Fe_3O_4\,(s) + O_2\,(g) + xH_2O\,(l) = 6Fe_2O_3{\cdot}xH_2O\,(s) \qquad (22)$$

The quantities of the latter are likely to be small, due to the limited quantity of oxidants in the repository environment. Before discussing the quantities and properties of the various oxides that might form, and their effect on the release of Fe^{2+} to solution, it is worthwhile briefly reviewing iron-oxide phase relationships.

There have been numerous reviews published of the complex relationships among the various iron oxides and oxyhydroxides (see, e.g., SCHWERTMANN & CORNELL (1991), LANGMUIR (1969), BLESA & MATIJEVIC (1989), TAYLOR (1987), WAY-CHUNAS (1991), GREENLAND & MOTT (1978) and JOBE *et al.* (1997)). It is clear from these studies that one of the major uncertainties in characterising the products of corrosion of a steel canister is the identification of the particular Fe(III) oxide phase(s) that could form. The further oxidation of magnetite can potentially produce a variety of phases, including:

- $Fe(OH)_3$(am), probably a transient phase in the repository environment,
- γ-FeOOH (lepidocrocite), slightly less stable than goethite,

- γ-Fe_2O_3, (maghemite), with a stability similar to lepidocrocite,
- α-FeOOH (goethite), the commonest crystalline oxyhydroxide, and
- α-Fe_2O_3, (hematite), the most stable oxide.

Several other less abundant and synthetic oxyhydroxides exist. The K_{sp} values of the various phases vary from ~10^{-37} for freshly precipitated $Fe(OH)_3$ to 10^{-42} for well-crystallised hematite. It is worth noting that crystallinity and particle size effects can influence the relative stability of the various oxides (LANGMUIR 1971).

A potential-pH diagram for iron at 25°C is shown in Figure 4, reproduced from JOBE *et al.* (1997). The diagram is drawn assuming K_{sp} (25°C) for the "$Fe(OH)_3$" phase is 10^{-40}, corresponding to well-crystallised maghemite or lepidocrocite, or poorly crystallised goethite or hematite. The dotted line adjacent to the Fe_3O_4/"$Fe(OH)_3$" boundary is the U_4O_9/U_3O_7 boundary, considered to be the redox potential above which oxidative dissolution becomes relatively rapid. As indicated, siderite ($FeCO_3$) could also form, although only at very reducing potentials. Because of the uncertainties regarding crystallinity and particle size and the similar stabilities of various phases, there appears to be little prospect of predicting the Fe(III) oxide phase(s) that might form under repository conditions. There is, nonetheless, some evidence that, in addition to magnetite as the major phase forming from carbon-steel corrosion under mildly oxidising conditions, lepidocrocite and hematite can also form, as these phases have been observed in steel-corrosion studies at 60-180°C (SAWICKI & BRETT 1993). Whether conditions in the repository will be sufficiently oxidising to form significant quantities of these phases is open to question.

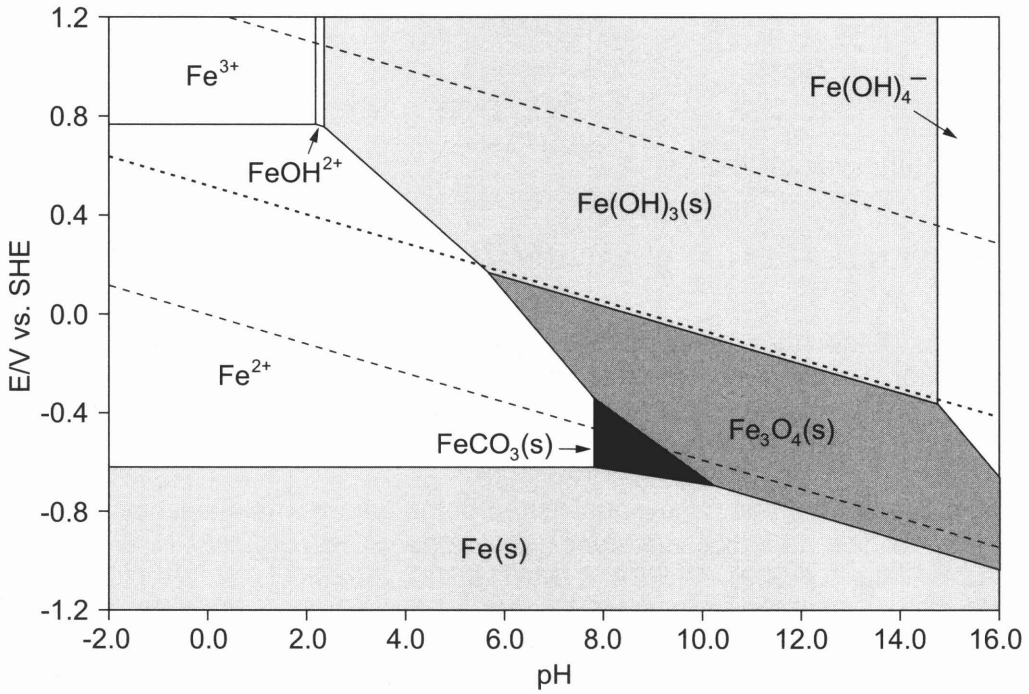

Fig. 4: Calculated Potential-pH Diagram for Iron (10^{-5} mol/kg) at 25°C, with $\{C_T\} = 10^{-3}$ mol/kg, $\{Cl^-\} = 10^{-2}$ mol/kg, and K_{sp} (25°C) for "$Fe(OH)_3$" = 10^{-40} (from Jobe et al. 1997)

Although it is generally considered that H_2 is relatively unreactive at temperatures below 100°C, it should be noted that the hydrogen partial pressure may be very high, probably greater than 10 MPa (NASH *et al.* 1998), at the canister surface as a consequence of the iron-water reaction and the relative impermeability of the buffer to hydrogen transport. If thermodynamic equilibrium is achieved, Figure 4 illustrates that any Fe(III) oxides formed could well be reduced to magnetite. In fact, it has been shown that Fe(II) can react with lepidocrocite to form magnetite under anaerobic conditions at room temperature (TAMAURA *et al.* 1983, ISHIKAWA *et al.* 1998). Were this to occur, the only iron phases present would be Fe_3O_4 and the residual steel of the canister, and the oxidant produced would be readily consumed, thus there would be no redox-front migration. While this may occur, the possibility that the Fe_3O_4 surface may be passivated by a film of Fe(III) oxide, thus diminishing Fe^{2+} release, cannot be discounted.

2.4.3 Passive-film formation

Possible conceptual models for film-formation processes on carbon steel are illustrated in Figures 5 to 7.

Figure 5 represents the equilibrium situation in which the high H_2 partial pressure sustains reduction of any Fe(III) oxide films that might form. Under such a condition, the solubility of Fe^{2+} is ~10^{-5} to 10^{-6} M. Alternatively, an Fe(III) oxide film could form as a result of oxidation of magnetite by radiolysis products, decreasing the rate of Fe^{2+} release from the underlying magnetite. This is represented in Figure 6. Some of the Fe(III) oxide phases form by oxidation of Fe^{2+}, followed by hydrolysis of Fe^{3+}, thus the resultant oxide is anticipated to be porous and probably incapable of fully passivating the surface of the Fe_3O_4. An exception to this case involves the selective dissolution of Fe^{2+} under anoxic (but not reducing) conditions, where magnetite can convert to maghemite.

$$(Fe^{2+}Fe_2^{3+})O_4 + 2H^+ = [Fe_2^{3+}]O_3 + Fe^{2+} + H_2O \qquad (23)$$

a phase that forms topotactically, thus preserving the structure and morphology of the underlying magnetite (WHITE *et al.* 1994). The result is a continuous film, albeit with some porosity, potentially capable of greatly diminishing the flux of Fe^{2+} into the solution.

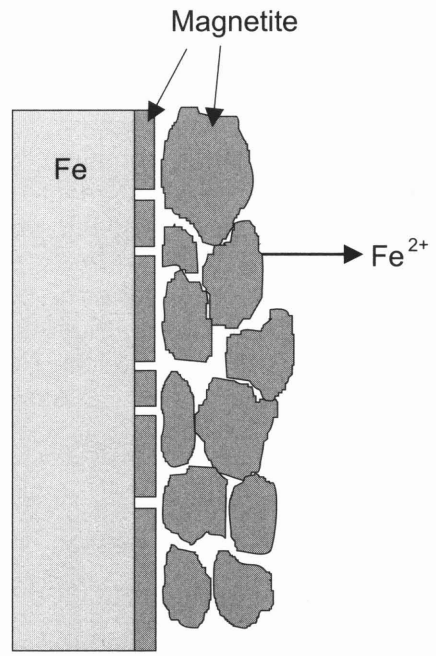

Fig. 5: Corrosion of carbon steel under reducing conditions with formation of magnetite

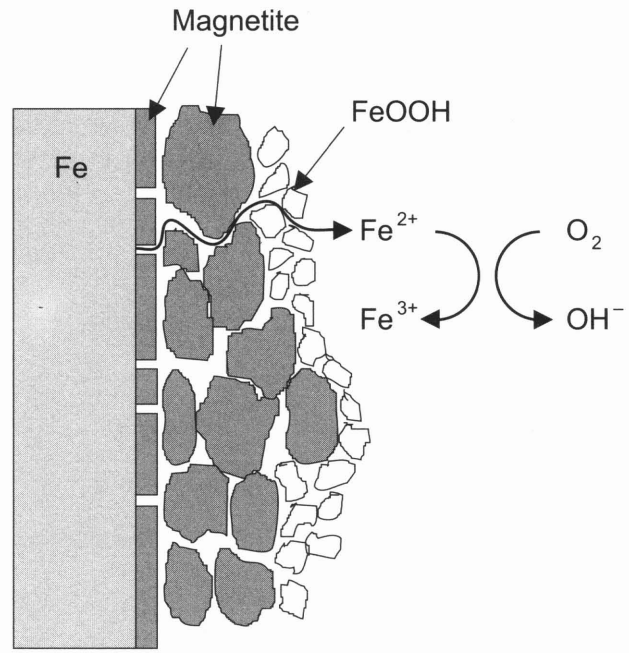

Fig. 6: Corrosion of carbon steel under oxidizing conditions with formation of magnetite and Fe(III) oxyhydroxides

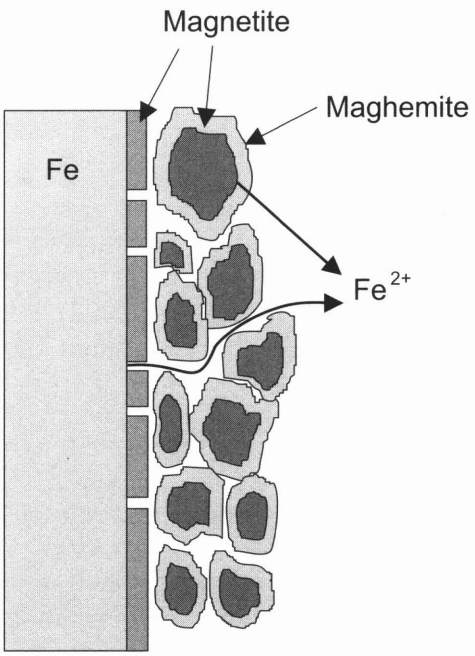

Fig. 7: Corrosion of carbon steel with formation of magnetite and maghemite

It is worth noting at this point that magnetite films on steel, while protective, are porous, the porosity permitting continuing access of groundwater to the underlying steel to sustain the corrosion reaction (POTTER & MANN 1961, CASTLE & MASTERSON 1966). The reduction in corrosion rate of carbon steel from ~10 μm a^{-1} to ~0.1 μm a^{-1} in going from aerated to anoxic conditions (MARSH & TAYLOR 1987, FUJISAWA *et al.* 1997, SKB 1997) provides an indication of the extent of this protection. The structure of the magnetite film is of great importance in attempting to develop a conservative conceptual model for Fe^{2+} release to solution. There is considerable evidence that magnetite films consist of a thin adherent layer with a loosely-adherent outer layer of discrete crystals (POTTER & MANN 1961, CASTLE & MASTERSON 1966, FIELD *et al.* 1966, CASTLE 1964). The surface areas of such films have been determined by CASTLE & MASTERSON (1966). They report values of 0.15 - 2.5 m^2g^{-1} for magnetite recovered from boiler tubes corroded at 300 ^{0}C. There appears to be no information available on the surface area of magnetite films formed on carbon steel at 25 to 100 ^{0}C. Returning to the selective dissolution of magnetite to form maghemite, this is then realistically represented in Figure 7, which takes account of the large surface area of the magnetite film. As the magnetite film is continuously formed, it releases Fe^{2+}, concurrently forming a gradually thickening layer of maghemite. It is probable that, because magnetite is a semiconductor, galvanic coupling with the underlying steel will occur, preventing passivation. Nonetheless, it is also conceivable that spalling or separation of the film may occur, as depicted in Figure 7, preventing reduction of the film.

It thus appears from examining Figure 5 to 7 that the most appropriate model for estimating the potential release of Fe^{2+} to solution is that of Figure 7, because it conservatively accounts for complete passivation of the magnetite by maghemite, but uses a realistic representation of the film structure.

3 A MODEL FOR RELEASE OF Fe^{2+} FROM A CORRODING STEEL CANISTER

3.1 Basis of the model

This section presents a film-growth model, which can be used to assess the rate of Fe^{2+} release arising from corrosion of carbon steel and to compare this rate with that of radiolytic-oxidant production. The time-dependent release of Fe^{2+} from magnetite is calculated based on the model of WHITE *et al.* (1994), which describes the growth of maghemite (γFe_2O_3) on magnetite and the associated Fe^{2+} release, according to Eq. 23.

The model is applied to the canister shown in Figure 3, which contains 4 PWR UO_2 or MOX fuel elements. In assessing the potential release of Fe^{2+} to solution, it is assumed that, at $t = 1000$ years, the water penetrates the external shell, fills the channels and the fuel cladding fails. The carbon steel is expected to corrode with the formation of magnetite, according to Eq. 21 and to rapidly achieve a constant corrosion rate of 0.1 to 1 μm a^{-1} (SKB 1997). The growth of maghemite on magnetite, together with the migration of Fe^{2+} by diffusion through the maghemite film, is illustrated in Figure 7.

3.2 The governing equations

The time t [a] to produce a maghemite layer of thickness y [cm] is given by WHITE *et al.* (1994) as[8]:

$$t = \frac{1}{aC_A}\left(\frac{y}{k_S} + 1.5\frac{y^2}{V_0 D_A}\right) \qquad (24)$$

where D_A [$cm^2\ s^{-1}$] is the diffusion coefficient in the maghemite film, C_A [mol cm^{-3}] is the concentration of H^+, k_S [$cm^4\ mol^{-1}\ s^{-1}$] is the intrinsic reaction rate at the magnetite-maghemite interface, V_0 [$cm^3\ mol^{-1}$] is the specific molar volume of magnetite[9] and a [$s\ a^{-1}$] is the number of seconds in a year. When the rate constant, k_S, is sufficiently large, the diffusion term on the right-hand side of Eq. 24 will dominate and:

$$t \approx \frac{1.5y^2}{aC_A V_0 D_A} \qquad (25)$$

Eq. 25 can be rearranged, to give an expression for the thickness of the maghemite film:

---

8 Since the first drafting of the present report, it has been realised that the factor of 1.5 in Eq. 24 from WHITE *et al.* (1994) is an error. The flux of H^+ through the layer is given by $F_H = aD_AC_A/y$. Neglecting the reaction rate (i.e. the first term inside the brackets in Eq. 24), the rate of growth of the layer is $dy/dt = F_HV_0/2$, since 2 moles of H^+ are required to release one mole of Fe^{2+}. Combining these two equations, and integrating dy/dt, $y^2 = D_AC_AV_0t$, i.e. $t = y^2 / (aD_AC_AV_0)$, without the factor of 1.5 that appears in Eq. 24. The consequences of this error are, however, small compared to other uncertainties in the analysis, especially since the factor 1.5 is taken inside a square root term for the evaluation of redox-front penetration (Eq. 28).

9 In WHITE *et al.* (1994), Eq. 24 was written in terms of concentration, rather than specific molar volume. The one is simply the reciprocal of the other.

$$y=\left(\frac{V_0 D_A a t C_A}{1.5}\right)^{1/2} \tag{26}$$

The flux of Fe^{2+} from the magnetite, F [mol cm^{-2} a^{-1}], can be equated to the rate of maghemite film growth:

$$F=\frac{1}{V_0}\frac{dy}{dt}=\frac{1}{2V_0}\left(\frac{2aD_A V_0 C_A}{3t}\right)^{1/2}=\left(\frac{aD_A C_A}{6tV_0}\right)^{1/2} \tag{27}$$

and, if the layer has a time-dependent area $A(t)$ [cm^2], the total release rate from the layer, R [mol a^{-1}] is:

$$R=A(t)\left(\frac{aD_A C_A}{6tV_0}\right)^{1/2} \tag{28}$$

3.3 Calibration of the model

WHITE *et al.* (1994) made measurements of Fe^{2+} release at pH values from 1 to 6, from which they derived D_A values[10]. These ranged from ~$10^{-15.5}$ cm^2 s^{-1} at pH 1 to $10^{-12.3}$ cm^2 s^{-1} at pH 6. These values are extrapolated[11] to a pH of ~8, the expected pH in the pore water in the canister, giving a predicted D_A value at 25ºC of $10^{-11.2}$. For a long-term repository temperature of ~50 to 60 ^{0}C, the rate would be ~2.5 times higher (White *et al.* 1994), thus we adopt a D_A value of $10^{-10.8}$ cm^2 s^{-1}. The specific molar volume of magnetite, V_0, is 44.5 cm^3 mol^{-1}. The Fe flux (mol cm^{-2} a^{-1}) at time t [a] after canister failure is thus given by

$$F=\left[\frac{\left(10^{-10.8}\,\mathrm{cm^2\,s^{-1}}\right)\times\left(10^{-11}\,\mathrm{mol\,cm^{-3}}\right)\times\left(3.15\times10^{7}\,\mathrm{s\,a^{-1}}\right)}{6t\times\left(44.5\,\mathrm{cm^3\,mol^{-1}}\right)}\right]^{1/2}=\left(\frac{1.9\times10^{-17}}{t}\right)^{1/2} \tag{29}$$

The internal surface area of the channels in a canister is A_0 = 1.77 x 10^5 cm^2. The total release of Fe^{2+} per canister as a function of time can be calculated by assuming that

---

[10] White *et al.* (1994) postulated that H^+ diffusion (D_A) through the maghemite layer is the rate-determining step, which appears to be unlikely based on other studies of passive film behaviour that suggest that Fe^{2+} transport through defects in the film is rate limiting (MCDONALD & URQUIDI- MCDONALD (1994) and BRUZZONI & RIECKE (1994)). In spite of this concern about the validity of the mechanism postulated by WHITE *et al.* (1994), their analysis appears to produce the correct result, because, in evaluating their Fe^{2+} release dissolution data, they determined the product of D_A and C_A, which represents the flux through the passive film. Using their data at a pH of 6, (D_A C_A) = $10^{-21.3}$ mol $cm^{-1}s^{-1}$, which agrees reasonably well with the value of $10^{-22.3}$ mol $cm^{-1}s^{-1}$ for neutral pH reported by MCDONALD & URQUIDI- MCDONALD (1994). The latter is based on D_{Fe}= 5 x 10^{-20} cm^2 s^{-1} and a defect concentration of 10^{-3} mol cm^{-3} in the film. Thus although there are reservations about the model of WHITE et al. (1994), we retain their formulation because it produces the correct result and permits the direct use of their Fe^{2+} release data in our model.

[11] For the present report, extrapolation was performed by eye, by fitting a linear best fit through a plot of log D_A vs. pH

the release initially occurs from a surface area equal to that of the channels in the canisters, with the surface area for release, $A(t)$, increasing as the porous magnetite film thickens. The contribution to the surface area for release made by the magnetite film, $A_f(t)$ [cm^2], can be derived from the production rate of magnetite, which is related to the corrosion rate of steel, R_s [mol a^{-1}], and the specific area of magnetite, Ψ [cm^2 g^{-1}].

$$A(t) = A_0 + A_f(t) = 1.77 \times 10^5 + \frac{R_s}{3} \Psi t \qquad (30)$$

where the factor of three arises from the fact that the corrosion of 3 moles of steel is required for the production of one mole of magnetite.

The molar corrosion rate of the steel, R_s, is given by:

$$\begin{aligned} R_s &= 0.1\ \mu m\ a^{-1} \times 7.84\ g\ cm^{-3} \times 17.7 \times 10^4\ cm^2 \times 1\ mol\ Fe/55\ g \times 10^{-6}\ m\ \mu m^{-1} \\ &= 0.252\ mol\ a^{-1} \end{aligned} \qquad (31)$$

The value of 0.1 µm a^{-1} assumed for the anaerobic corrosion rate may be somewhat low, but, for the purposes of this report, the intention of which is to estimate the quantity and surface area of magnetite, it is a conservative value.

The specific area of magnetite, Ψ, is taken to be 0.15 m^2 g^{-1}, the low end of the range measured by CASTLE & MASTERSON (1966). Thus, from Eqs. 28-31, the total release of Fe^{2+} from the canister and the growing magnetite film is given by:

$$R = \left(1.77 \times 10^5 + 2.9 \times 10^4 t\right)\left(\frac{1.9 \times 10^{-17}}{t}\right)^{1/2} \qquad (32)$$

and plotted in Figure 8.

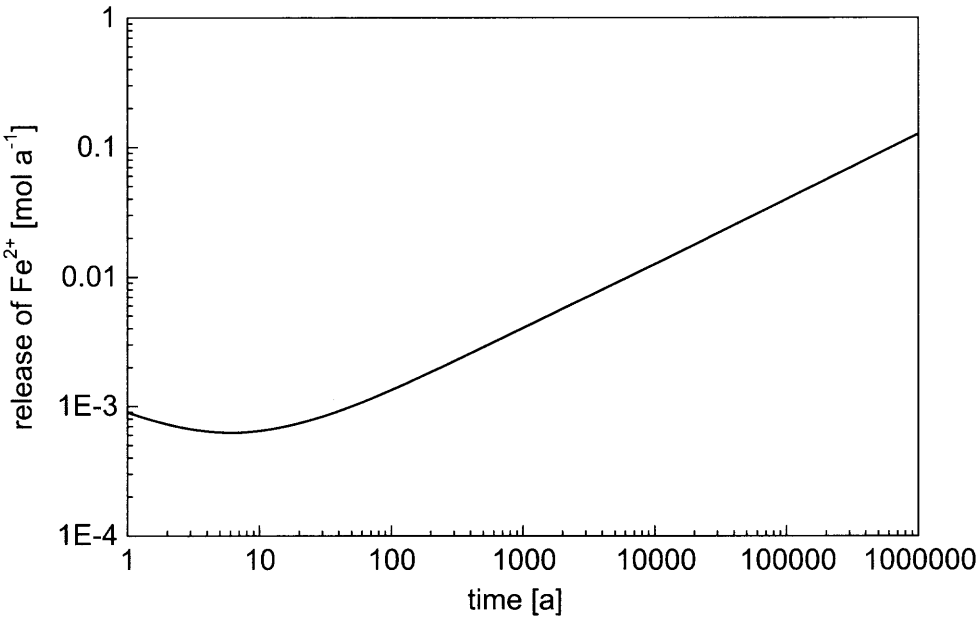

Fig. 8: The release rate of Fe^{2+} from a corroding steel canister, according to the film-growth model.

4 MODELLING SPENT-FUEL DISSOLUTION

4.1 Basis of the model

Having derived a conservative effective G-value in Section 2, the impact of this value on the rates of spent-fuel dissolution for different fuel types, for use in performance-assessment calculations, can be evaluated. An approach is adopted in this section in which all the molecular radiolytic oxidants that are produced following canister failure react with the fuel. The supply of water to the fuel surfaces is assumed to be unlimited and the supply of reductants from repository materials (e.g. Fe^{2+} release from canister-corrosion processes; Section 3) and from groundwater is neglected. The effect of Fe^{2+} is, however, taken into account in evaluating the migration of a redox front in Section 5. Moreover, a less conservative approach to the evaluation of fuel-dissolution rates, in which radiolytic oxidants may either react with the fuel or with Fe^{2+} from canister corrosion, is presented in Appendix B, indicating that, in reality, oxidative dissolution of spent fuel may be significantly less, with fuel dissolution ceasing after a few thousands of years. There are, however, considerable uncertainties involved in this calculation, and the simpler approach is used here, in order to derive conservative fuel dissolution rates for Nagra performance assessments.

4.2 Application of the model

Since one mole of radiolytically-generated H_2O_2 oxidises one mole of U(IV) to U(VI), the fractional dissolution rate of the fuel, *D*, is:

$$D = P_C \times \left[238 \text{ g mol}^{-1}\right] \times \left[10^{-6} \text{ tonnes g}^{-1}\right] \qquad (33)$$

where P_C, the production rate of radiolytic H_2O_2, is given by Eq. 9. Q ("Total Alpha") is presented in Table 1, for both UO_2 and MOX spent fuels, and for a range of burn-ups. Table 2 and Figure 9 present the fractional dissolution rates of the fuels.

Table 1: Energy output of the fuel due to alpha radiation (Watts per tonne of original heavy metal), as a function of time and burn-up for UO2 and MOX spent fuels.

	Time [a]										
	1.00E+01	3.00E+01	1.00E+02	3.00E+02	1.00E+03	3.00E+03	1.00E+04	3.00E+04	1.00E+05	3.00E+05	1.00E+06
Burn-up [MWd/tIHM]	Energy output for UO_2 spent fuel due to alpha radiation [W/tIHM]										
33 000	2.10E+02	2.35E+02	2.09E+02	1.40E+02	6.06E+01	2.45E+01	1.49E+01	6.02E+00	1.15E+00	5.75E-01	3.93E-01
48 000	4.42E+02	4.13E+02	3.13E+02	1.90E+02	7.68E+01	2.91E+01	1.73E+01	6.82E+00	1.43E+00	8.21E-01	5.19E-01
55 000	6.15E+02	5.27E+02	3.62E+02	2.10E+02	8.39E+01	3.20E+01	1.87E+01	7.14E+00	1.55E+00	9.26E-01	5.64E-01
	Energy output for MOX spent fuel due to alpha radiation [W/tIHM]										
33 000	1.98E+03	1.73E+03	1.25E+03	7.86E+02	3.22E+02	1.17E+02	6.45E+01	2.15E+01	3.91E+00	2.11E+00	1.41E+00
48 000	2.92E+03	2.16E+03	1.25E+03	7.44E+02	2.97E+02	1.05E+02	5.72E+01	1.84E+01	3.64E+00	2.20E+00	1.38E+00
55 000	3.42E+03	2.35E+03	1.21E+03	6.99E+02	2.80E+02	1.01E+02	5.49E+01	1.74E+01	3.53E+00	2.17E+00	1.32E+00

Table 2: Fractional dissolution rate of UO_2/MOX fuel with different burn-ups as a function of time for a G-value of 0.01 molecules of H_2O_2 per 100 eV.

Time	Fractional dissolution rates [a^{-1}]					
[a]	UO_2 33000	UO_2 48000	UO_2 55000	MOX 33000	MOX 48000	MOX 55000
1000	1.86E-06	2.36E-06	2.58E-06	9.89E-06	9.12E-06	8.60E-06
1225	1.56E-06	1.96E-06	2.14E-06	8.17E-06	7.47E-06	7.05E-06
1501	1.31E-06	1.62E-06	1.77E-06	6.73E-06	6.11E-06	5.78E-06
1840	1.10E-06	1.34E-06	1.47E-06	5.54E-06	5.00E-06	4.75E-06
2254	9.30E-07	1.12E-06	1.23E-06	4.59E-06	4.13E-06	3.94E-06
2762	7.97E-07	9.51E-07	1.05E-06	3.84E-06	3.45E-06	3.31E-06
3384	6.97E-07	8.23E-07	9.05E-07	3.28E-06	2.95E-06	2.84E-06
4146	6.25E-07	7.32E-07	8.04E-07	2.88E-06	2.58E-06	2.50E-06
5080	5.73E-07	6.68E-07	7.32E-07	2.60E-06	2.32E-06	2.25E-06
6225	5.35E-07	6.22E-07	6.79E-07	2.39E-06	2.13E-06	2.06E-06
7627	5.03E-07	5.84E-07	6.35E-07	2.22E-06	1.97E-06	1.90E-06
9345	4.70E-07	5.46E-07	5.91E-07	2.04E-06	1.82E-06	1.74E-06
11450	4.30E-07	4.98E-07	5.37E-07	1.84E-06	1.63E-06	1.56E-06
14030	3.81E-07	4.41E-07	4.73E-07	1.60E-06	1.41E-06	1.34E-06
17190	3.28E-07	3.78E-07	4.03E-07	1.33E-06	1.17E-06	1.11E-06
21060	2.73E-07	3.13E-07	3.31E-07	1.07E-06	9.28E-07	8.82E-07
25810	2.20E-07	2.51E-07	2.64E-07	8.21E-07	7.07E-07	6.70E-07
31620	1.74E-07	1.96E-07	2.05E-07	6.10E-07	5.21E-07	4.93E-07
38750	1.34E-07	1.51E-07	1.57E-07	4.47E-07	3.79E-07	3.58E-07
47480	1.02E-07	1.16E-07	1.20E-07	3.26E-07	2.75E-07	2.60E-07
58170	7.70E-08	8.78E-08	9.14E-08	2.39E-07	2.03E-07	1.92E-07
71280	5.74E-08	6.68E-08	7.02E-08	1.79E-07	1.56E-07	1.48E-07
87330	4.27E-08	5.15E-08	5.50E-08	1.39E-07	1.26E-07	1.21E-07
107000	3.23E-08	4.08E-08	4.45E-08	1.12E-07	1.06E-07	1.03E-07
131100	2.53E-08	3.37E-08	3.75E-08	9.36E-08	9.22E-08	9.05E-08
160700	2.12E-08	2.94E-08	3.32E-08	8.11E-08	8.25E-08	8.15E-08
196800	1.90E-08	2.70E-08	3.07E-08	7.33E-08	7.60E-08	7.52E-08
241200	1.81E-08	2.59E-08	2.94E-08	6.84E-08	7.15E-08	7.07E-08
295500	1.77E-08	2.53E-08	2.85E-08	6.51E-08	6.78E-08	6.69E-08
362100	1.72E-08	2.44E-08	2.73E-08	6.18E-08	6.41E-08	6.30E-08
443700	1.64E-08	2.31E-08	2.58E-08	5.83E-08	6.01E-08	5.89E-08
543600	1.55E-08	2.16E-08	2.39E-08	5.47E-08	5.59E-08	5.45E-08
666100	1.44E-08	1.98E-08	2.19E-08	5.10E-08	5.15E-08	4.99E-08
816100	1.33E-08	1.79E-08	1.96E-08	4.72E-08	4.70E-08	4.53E-08
1000000	1.21E-08	1.59E-08	1.73E-08	4.33E-08	4.24E-08	4.05E-08

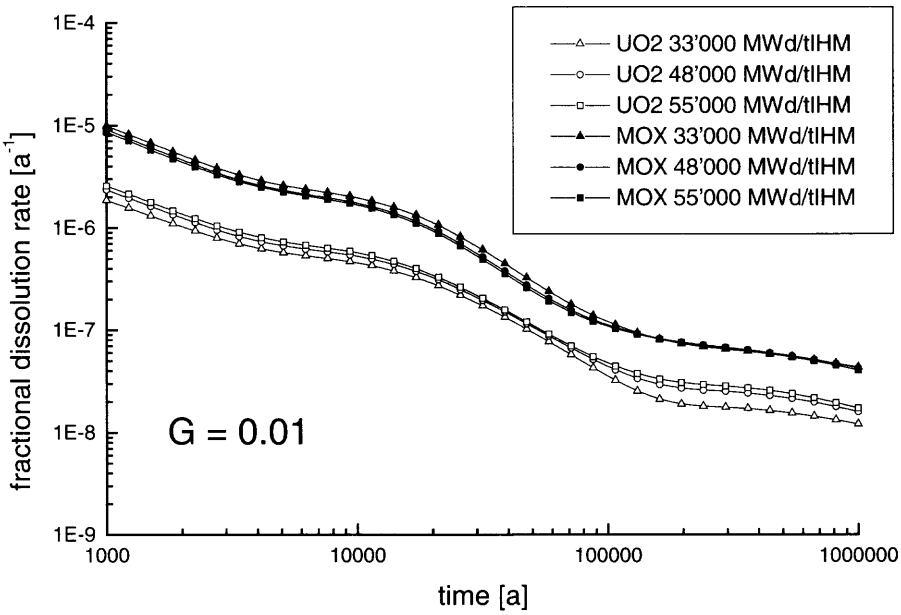

Fig. 9: Fractional dissolution rate as a function of time for a G-value of 0.01 molecules of H_2O_2 per 100 eV.

5 MODELLING THE MIGRATION OF THE REDOX FRONT

5.1 Basis of the model

As discussed in previous Sections 2 and 3, U(VI) complexes that diffuse away from the fuel surfaces may react with Fe^{2+}, originating from canister corrosion processes. LIGER et al. (1999) have shown that Fe^{2+} will reduce U(VI) adsorbed on Fe(III) oxide. In the present report, no attempt has been made to model the kinetics of this process, as the kinetic parameters are not yet clearly defined. Instead, a mass balance approach is used. The total release per year of Fe^{2+} from corrosion processes is given by R in Eq. 32. The release of U(VI), per mole of original U(IV) in the fuel, is given by D in Eq. 33. If the release of oxidising equivalents (e.g. in the form of U(VI))[12] exceeds that of Fe^{2+}, then oxidants may migrate through the breached canister and into the surrounding bentonite buffer. The oxidants will then react with reductants in solution and with mineral surfaces, which will gradually become depleted, forming an oxidised zone within the bentonite.

Figure 10 shows the time-integrated production of radiolytic oxidants, and the time-integrated production of Fe^{2+} from canister corrosion, assuming a canister-failure time of 1000 a. It can be see that the inventory of fuel is sufficient to react with all the radiolytic oxidants, giving rise to U(VI) in solution. Depending on the fuel type (MOX or UO_2) and, to a lesser extent, the burn-up, U(VI) dissolved following reaction of the fuel will exceed the Fe^{2+} produced by canister corrosion for a period of 10^4 to 10^5 years following canister failure. During this period, it is possible that U(VI) will diffuse from the canister into the bentonite.

The figure also shows the inventory of reducing equivalents (in the form of pyrite and siderite) present in the bentonite around a canister. Only a small part of this inventory is required in order to react with the U(VI) in solution, reducing it to U(IV). If, however, the canister is breached at a localised point of failure, then only a small part of the bentonite needs to be exposed to diffusing U(VI) in order for the oxidised zone to contact the outer boundary of the bentonite.

In order to construct a simple, conservative model to investigate this possibility, a single breach in the canister is assumed, in the form of either a single, small hole or a single circumferential crack. The assumption of a single hole (rather than, for example, multiple holes or one or more cracks) is the most conservative, in that, if all oxidants are released from a single location, then the likelihood of an oxidised zone forming that spans the entire thickness of the bentonite is greatest. It may, however, be unrealistic, in that the time required for water inflow through a small defect to initiate release is likely to be many thousands of years (Vieno *et al.* 1992). The case of a circumferential crack (e.g., a failure along the weld region) is likely to be more realistic. In this case, water ingress could occur more rapidly and initiate the production of radiolytic oxidants, although there is a larger volume of bentonite potentially available to provide reductants. In either case, if the reaction with reductants in the bentonite is rapid, and the diffusion of reductants in solution inwards towards the fuel is conservatively neglected (due to the current lack of the necessary data and model concepts), then a front will form at a distance r_f [m] from the hole. This front defines the outer boundary of the zone in which reductants have been consumed.

---

[12] The additional effects of dissolved, precipitated and absorbed alpha-emitters on radiolytic oxidant production in the near field are discussed in Appendix C, and shown not to be important.

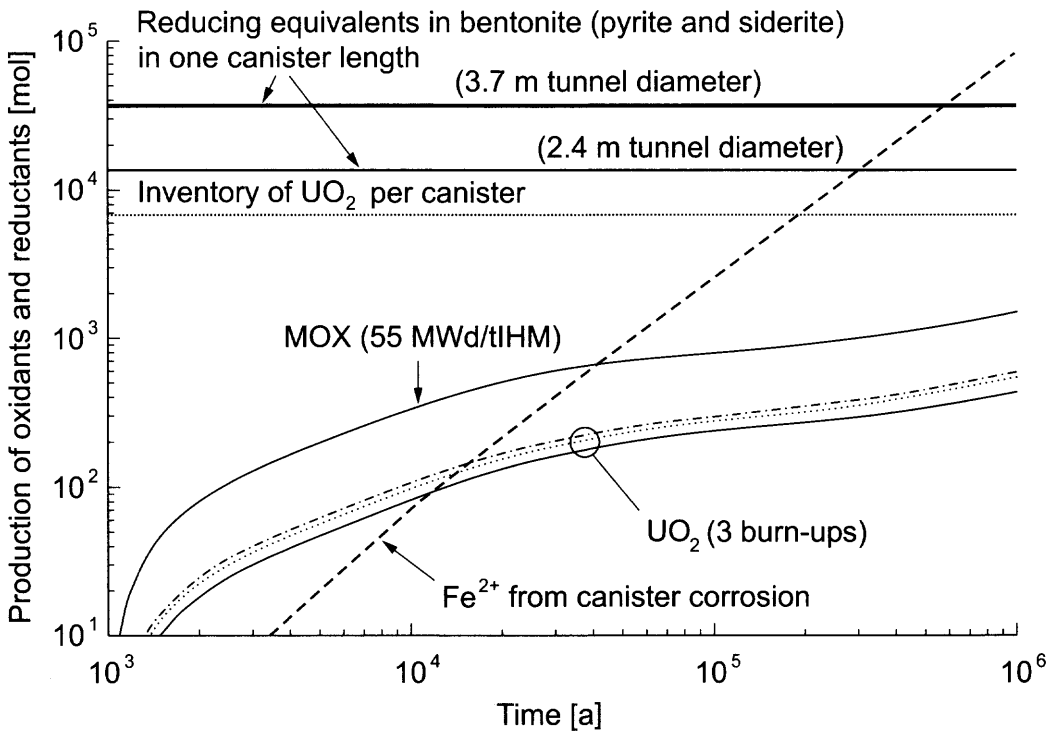

Fig. 10: Integrated production of radiolytic oxidants, compared to the inventory of UO_2 per canister, the generation of Fe^{2+} by canister corrosion and the inventories of reductants in the bentonite (reducing equivalents from pyrite and siderite)

The key assumptions of the model are summarised as follows:

- There is unlimited supply of water to fuel and canister surfaces.
- Failure occurs at a single hole or crack.
- Reduction reactions of U(VI) are fast with respect to transport processes.
- Transport processes are fast with respect to expansion of redox front (i.e. growth is based on material balance).
- Direct access of U(VI) to primary canister corrosion product (magnetite) is impeded by a maghemite layer.
- The rate of production of Fe^{2+} controlled by diffusion through maghemite layer.

5.2 The governing equations

r_f will increase with time as further reductants are consumed at the front. The volume V [m^3] of the oxidised zone is given by:

$$V = \begin{cases} \pi^2 r_f^2 \left(r_a + \frac{4}{3} r_f \right) & \text{for a circumferential crack} \\ \frac{2}{3} \pi r_f^3 & \text{for a hole} \end{cases} \quad (34)$$

where r_a [m] is the external radius of the canister (where, in the case of the hole, the curvature of the canister surface is neglected).

If the initial concentration of reductants in the bentonite is C [mol m^{-3}], the initial inventory of U(IV) in the fuel is I [mol], and the production rate of oxidising equivalents per canister (not consumed by reaction with Fe^{2+} from canister corrosion) is equal to $2DI - R$[13], the balance between production and the number of reducing equivalents originally contained within a volume V gives:

$$\int_{t_f}^{t} (2DI - R) dt = CV \quad (35)$$

where t_f [a] is the time at which the canister is breached and fuel dissolution and iron corrosion commence. From Eqs. (34) and (35):

$$\frac{1}{C} \int_{t_f}^{t} (2DI - R) dt = \begin{cases} \pi^2 r_f^2 \left(r_a + \frac{4}{3} r_f \right) & \textit{for a circumferential crack} \\ \frac{2}{3} \pi r_f^3 & \textit{for a hole} \end{cases} \quad ; \; 2DI > R \,. \quad (36)$$

5.3 Application of the model

Eq. 36 is solved numerically for r_f, using the energy-output data in Table 1, and the results are plotted in Figure 11 for the case of a circumferential crack. A time of canister breaching of 1000 a and an inventory of U(IV) per canister of I = 6723 moles are assumed, the latter corresponding to 1.6 t_{HM} per canister. The penetration into the bentonite of the redox front is compared to the thickness of the bentonite for a 3.7 m tunnel diameter (corresponding to the Nagra repository concept for a crystalline host rock) and for a 2.4 m tunnel diameter (for the Opalinus Clay host rock). In calculating the bentonite thickness from the canister outer surface to the tunnel wall, the canister diameter is taken to be 1.05 m. A concentration of near-field reductants of C = 742 mol

[13] The factor of 2 arises since each mole of U(VI) dissolved is considered to release 2 moles of oxidising equivalents to solution.

m^{-3} is also assumed, based on the combined inventories of siderite ($FeCO_3$) and pyrite (FeS_2) in MX-80 bentonite (Appendix F).

Eventually, the production of Fe^{2+} from canister corrosion exceeds that of radiolytic oxidants and no oxidants escape to the bentonite, as illustrated in Figure 12, where $2Dl/R$ is plotted as a function of time. For a 1000 year canister lifetime, this occurs at about 4000 – 5000 years after canister breaching (5000 – 6000 years after unloading of the fuel from the reactor) for UO_2 spent fuel and at about 20000 years after canister breaching in the case of MOX. Following these times, the redox front is assumed to remain stationary.

A number of parameter variations have been performed using this model. Figures 13-15 (for a crack) and 16-17 (for a hole) present the maximum distance into the bentonite reached by the redox front in 10^6 years. To illustrate the effects of canister corrosion products, these effects are omitted in the calculations for Figure 14. In addition, variations are considered in:

- fuel type (UO_2 and MOX spent fuels, each with 3 different burn-ups);
- nature of the reductants in the bentonite (pyrite and siderite, siderite only and pyrite only);
- canister lifetime (10^3 a, 10^4 a and 10^5 a).

The variation of redox front penetration with time for all of these cases is shown in the figures in Appendix E.

Comparison of the histograms in Figures 13 and 14, for a canister lifetime of 1000 a, clearly illustrates the effect of Fe^{2+} release from canister corrosion products on stabilising the position of the redox front. For example, for UO_2 fuel with a burn-up of 55000 MWd/t_{HM} , the redox front penetration is limited to ~ 0.1 m if pyrite is reactive and canister corrosion products release Fe^{2+} (Figure 13). Without the effect of canister corrosion products, the redox front penetrates ~ 0.3 m. (Figure 14). Inspection of the Figures in Appendix C (1000 a cases) illustrates that redox front penetration is halted after several thousand years as a result of Fe^{2+} release from the increasing quantity of canister corrosion products becoming significant.

For a bentonite thickness of either 0.7 m or 1.3 m, indicated by the dotted and dashed lines in Figure 16, complete penetration of the redox front does not occur for any of the fuel types if pyrite in the buffer is reactive, irrespective of the canister lifetime. The assumption that pyrite is reactive is considered reasonable based on various studies of pyrite dissolution (NICHOLSON et al. 1988, 1990).

The effect of canister lifetime is interesting to note. There is limited reduction in the redox front penetration when canister lifetime is increased from 1000 a to 10000 a (Figures 13 and 15); however, for a 100,000 year canister lifetime, the model indicates that no redox front is formed.

Figures 16-17 show that the case of a point defect gives higher redox-front penetrations than that of a circumferential crack, due to the smaller volume of bentonite that is potentially available for the consumption of oxidants. For a 1000 year canister lifetime, the redox front almost penetrates the bentonite in the case of the smaller tunnel diameter, if pyrite and siderite are reactive, and penetrates the wall of the larger diameter tunnel if only siderite in the buffer is reactive. A 100 000 a canister lifetime is required

to ensure containment of the redox front in the buffer for all parameter variations, in which case that model again indicates that no redox front is formed.

The case of a point defect, is, however, considered to be unduly pessimistic. The most likely failure mechanism for a steel canister is mechanical failure following a period of corrosion, as thinning of the canister would weaken it structurally and the imposed load (hydrostatic plus buffer swelling pressure) would cause buckling and fracture. At typical corrosion rates of 0.1 to 1 μm a^{-1} and a corrosion allowance of 80 mm (JOHNSON, in preparation), this is likely to take tens of thousands of years.

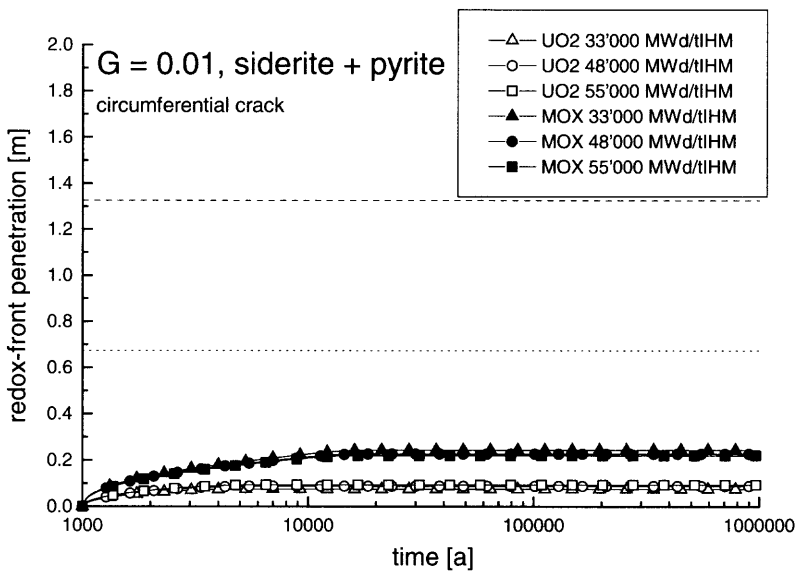

Fig. 11: Redox-front penetration into the bentonite, as a function of time, for a G-value of 0.01, a 1000 a canister lifetime, and assuming that Fe^{2+}, and both siderite and pyrite in the bentonite, are available as reductants.

Note: Dashed and dotted lines = bentonite thickness for 3.7 m and 2.4 m tunnel diameters, respectively.

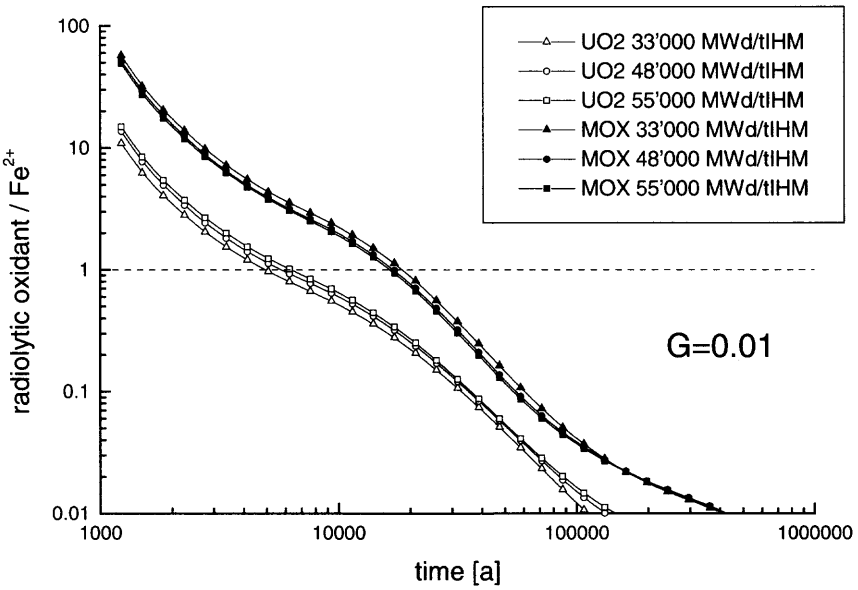

Fig. 12: The ratio of radiolytic oxidant production to the production of Fe^{2+} from canister ($2Dl/R$) as a function of time, for a G-value of 0.01 and a 1000 a canister lifetime.

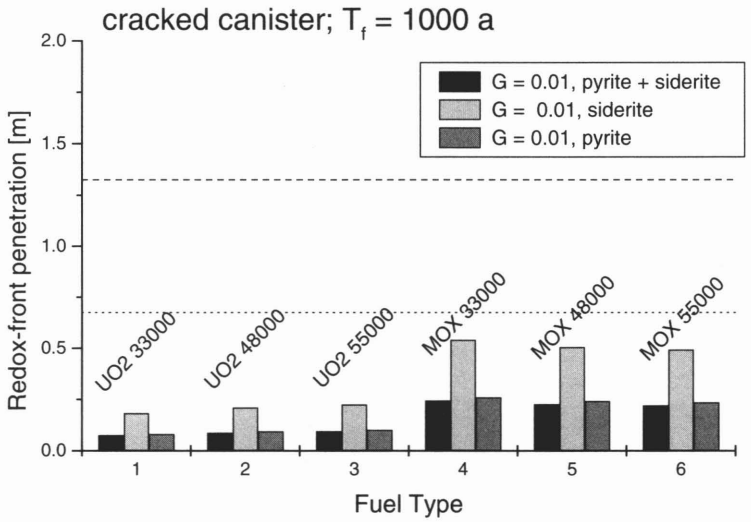

Fig. 13: The maximum distance into the bentonite reached by the redox front in the case of a 1000 a canister lifetime (before failure along a circumferential crack), as a function of fuel type, and of the minerals assumed to act as reductants in the bentonite.

Note: Dashed and dotted lines = bentonite thickness for 3.7 m and 2.4 m tunnel diameters, respectively.

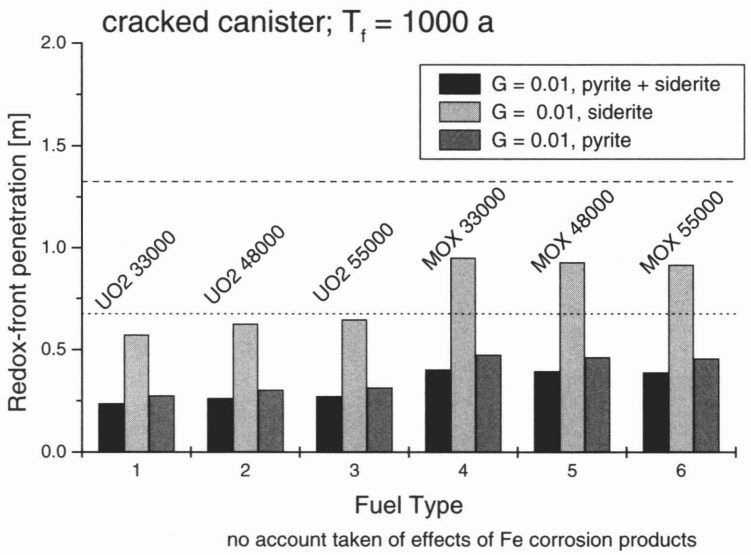

Fig. 14: The maximum distance into the bentonite reached by the redox front in the case of a 1000 a canister lifetime (before failure along a circumferential crack), as a function of fuel type if no credit is taken for reaction of oxidants with canister-corrosion products.

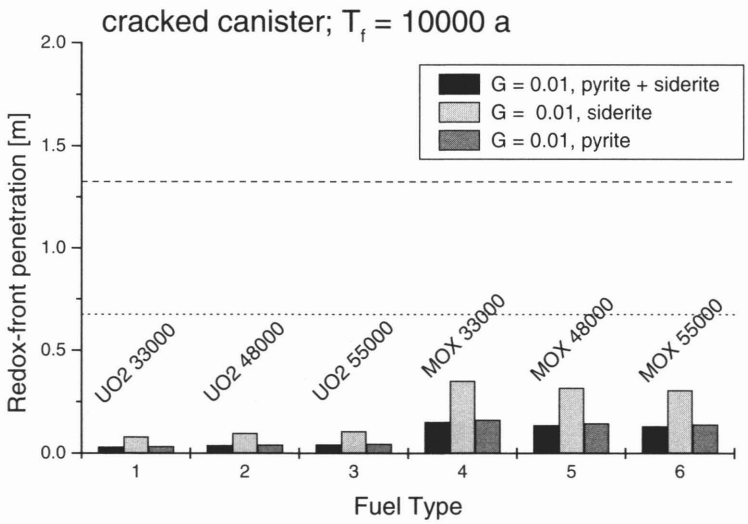

Fig. 15: The maximum distance into the bentonite reached by the redox front in the case of a 10000 a canister (before failure along a circumferential crack), as a function of fuel type, and of the minerals assumed to act as reductants in the bentonite.

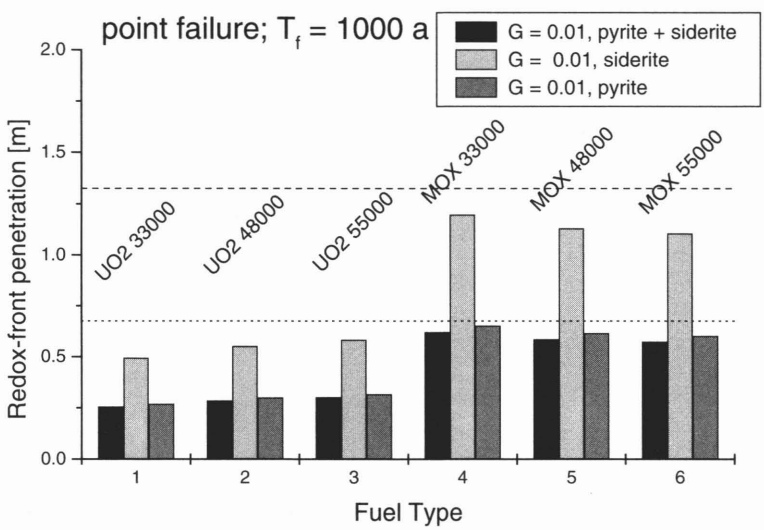

Fig. 16: The maximum distance into the bentonite reached by the redox front in the case of a 1000 a canister lifetime (before failure at a single point), as a function of fuel type, and of the minerals assumed to act as reductants in the bentonite.

Note: Dashed and dotted lines = bentonite thickness for 3.7 m and 2.4 m tunnel diameters, respectively.

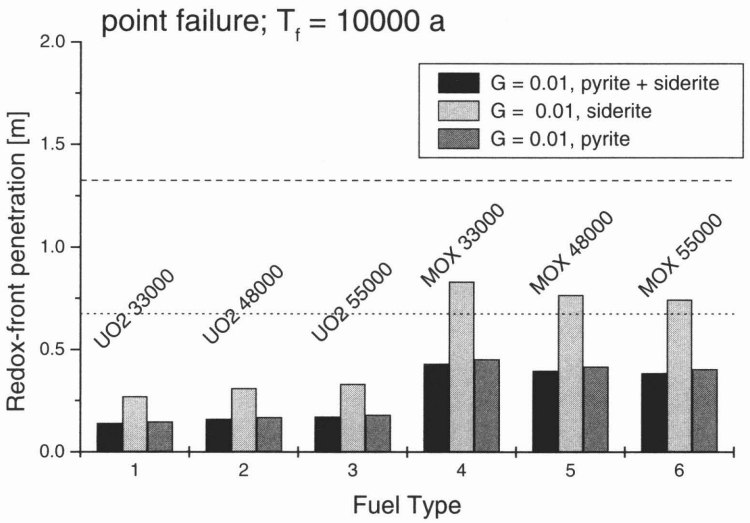

Fig. 17: The maximum distance into the bentonite reached by the redox front in the case of a 10000 a canister lifetime (before failure at a single point), as a function of fuel type, and of the minerals assumed to act as reductants in the bentonite.

5.4 Discussion of Model Limitations

The model presented here describes oxidant formation due to α-radiolysis, Fe^{2+} release from corroding steel and oxidant (H_2O_2, O_2, or U(VI)) migration through a hole or circumferential crack in the canister into the surrounding bentonite. Ferrous minerals in the bentonite are assumed to be oxidized at a rate governed by the rate at which oxidants are released from the canister defect. Selection of the modelling approach involves numerous compromises and the use of expert judgement in balancing realism with a degree of conservatism appropriate for a peformance assessment model used to bound possible performance over hundreds of thousands of years.

It is judged that the model is conservative in the following respects:

1) a G value of 0.01, derived from relevant experiments and inferred from natural analogues, is expected to overestimate oxidant production, because reducing agents such as H_2 and Fe^{2+} would be present within a failed canister and would scavenge primary radiolytic oxidizing species, further decreasing the effective oxidant yield. This is supported by the experiments of SPAHIU & WERME (in press) and KING et al. (1999).

2) Redox equilibrium is assumed not to be achieved. An important example of this is that complete passivation of the magnetite corrosion layer on the steel by maghemite is assumed to occur. If equilibrium were attained at the high hydrogen partial pressure expected, this would prevent passive film formation and magnetite would control the solubility of Fe^{2+}. Under such conditions the fuel oxidation rate would be negligible.

3) Under conditions of passive film formation, consumption of oxidants is assumed to occur only through oxidation of Fe^{2+} released from the film, whereas it is expected that oxidants would migrate through pores in the film and be reduced by the underlying magnetite and metal.

4) The geometry of the canister defect (hole or crack) maximizes redox front penetration. Furthermore, transport of oxidants from the fuel to the redox front via the defect is assumed to be instantaneous. If transport resistance of the defect and other retardation processes were included, the redox front would migrate more slowly.

Uncertainties in some of the data used in the model may be significant, thus it may be prudent to retain the conservatisms until a better understanding of the processes and improved data are available. For example, the use of specific surface area data from magnetite corrosion products produced at high temperatures may lead to an overestimate of the Fe^{2+} release from the film. Similarly, although pyrite in the bentonite can reasonably be considered to be an effective agent for reducing migrating U(VI), it is possible that processing and storage of the bentonite prior to its emplacement may lead to oxidation of a significant fraction of the material initially present. This can easily be overcome by the addition of a redox agent at a level of ~0.5 wt.% prior to bentonite emplacement.

Some elements of the model are rather simplistically represented. For example, the oxidizing species that migrates into the buffer is not specified, thus it may be considered to be either radiolytic hydrogen peroxide (or oxygen) or U(VI). Given that the migration path into the buffer would be a crack or corrosion penetration through the thick steel canister, it is inconceivable that hydrogen peroxide or oxygen could be the migrating species, as the rapid reaction rate with steel would prevent its escape. Uranium(VI) must then be assumed to be the migrating oxidized species. It is expected that U(VI) would be reduced by pyrite in the bentonite or by Fe(II) on the surface of iron oxides (LIGER et al. 1999).

Examination of some of these model limitations would aid in both increasing confidence in the models and in eliminating unnecessary conservatisms.

3) Under conditions of passive film formation, consumption of oxidants is assumed to occur only through oxidation of Fe^{2+} released from the film, whereas it is expected that oxidants would migrate through pores in the film and be reduced by the underlying magnetite and metal.

4) The geometry of the canister defect (hole or crack) maximizes redox front penetration. Furthermore, transport of oxidants from the fuel to the redox front via the defect is assumed to be instantaneous. If transport resistance of the defect and other retardation processes were included, the redox front would migrate more slowly.

Uncertainties in some of the data used in the model may be significant, thus it may be prudent to retain the conservatisms until a better understanding of the processes and improved data are available. For example, the use of specific surface area data from magnetite corrosion products produced at high temperatures may lead to an overestimate of the Fe^{2+} release from the film. Similarly, although pyrite in the bentonite can reasonably be considered to be an effective agent for reducing migrating U(VI), it is possible that processing and storage of the bentonite prior to its emplacement may lead to oxidation of a significant fraction of the material initially present. This can easily be overcome by the addition of a redox agent at a level of ~0.5 wt.% prior to bentonite emplacement.

Some elements of the model are rather simplistically represented. For example, the oxidizing species that migrates into the buffer is not specified, thus it may be considered to be either radiolytic hydrogen peroxide (or oxygen) or U(VI). Given that the migration path into the buffer would be a crack or corrosion penetration through the thick steel canister, it is inconceivable that hydrogen peroxide or oxygen could be the migrating species, as the rapid reaction rate with steel would prevent its escape. Uranium(VI) must then be assumed to be the migrating oxidized species. It is expected that U(VI) would be reduced by pyrite in the bentonite or by Fe(II) on the surface of iron oxides (LIGER et al. 1999).

Examination of some of these model limitations would aid in both increasing confidence in the models and in eliminating unnecessary conservatisms.

6 CONCLUSIONS

In this report, the release of radionuclides from the engineered barrier system of a deep geological repository for spent fuel has been discussed and quantitative models are presented that will be used to support the concepts, models and parameter values to be used in future Nagra performance assessments. The following conclusions are drawn:

Failure of Zircaloy:

- Should the Zircaloy cladding fail by localised corrosion or hydrogen-induced cracking, oxidants produced within the thin films of water surrounding the fuel pellets would have difficulty escaping by diffusion through the point of cladding failure, and would be likely to react with the fuel. This provides the basis for a model of spent-fuel dissolution, in which it is assumed that all radiolytic oxidants, that do not recombine with radiolytic reductants, react with the fuel surfaces.

Radiolysis of water:

- Production near to the external surfaces of fuel pellets and near to internal, water-saturated fractures within the fuel is the most important source of oxidants due to alpha radiolysis, being larger than the production from precipitated, dissolved or sorbed alpha emitters, that are released once fuel dissolution commences.
- Alpha radiolysis is likely to dominate over beta/gamma radiolysis for canister lifetimes of 1000 years or more. Theoretical effective yields for alpha radiolysis have been calculated and are very low (an effective *G*-value as low as 0.001), but have not been demonstrated for the system of interest, necessitating an empirical approach to derive an effective *G*-value for performance assessment.
- In assessing laboratory experiments that give information on the radiolysis of water, it is noted that the experimental conditions (oxic vs. anoxic, temperature and the effects of beta-gamma dose rates) must be taken into account, as these can significantly influence findings. Reviewing such evidence, and also evidence from natural analogues, a conservative *G*-value for performance-assessment calculations of 0.01 is derived.

Modelling of spent-fuel dissolution:

- Spent fuel dissolution has been modelled for both UO_2 and MOX spent fuels, and for a range of burn-ups, based on the assumption that radiolytic oxidants are produced according to the conservative *G*-value, and then react with the fuel surfaces. The resulting dissolution rates, as a function of time, should provide input to future Nagra safety-assessment calculations.

The corrosion of carbon steel:

- While it is possible that the only iron phases present inside a breached canister would be magnetite and the residual steel of the canister, and that any radiolytic oxidants would be entirely consumed by the resulting Fe^{2+} release, the possibility that the magnetite surface may be passivated by a film of Fe(III) oxide, thus reducing the Fe^{2+} release, cannot be discounted.
- If the Fe(III) oxide is composed of maghemite, formed topotactically (preserving the structure and morphology of the underlying magnetite), the film would be expected

to be continuous, with low porosity, and potentially capable of greatly diminishing the flux of Fe^{2+} into solution. This, in turn, may allow some radiolytic oxidants, and U(VI) from fuel dissolution, to escape from the breached canister, without being scavenged by Fe^{2+}, forming an oxidising region in the surrounding bentonite.

Modelling the migration of the redox front:

- The migration of the redox front that bounds the oxidising region in the bentonite has been modelled, including the effects of Fe^{2+} from canister corrosion. The production of Fe^{2+} initially decreases but increases at longer times as a result of the production of high surface area corrosion deposits. The rate of production of radiolytic oxidants decreases relatively rapidly and, eventually, all oxidants that are produced are likely to be scavenged. The time at which production of Fe^{2+} first exceeds that of radiolytic oxidants is also that time at which the oxidising region reaches its maximum extent. The scavenging of radiolytic oxidants by Fe^{2+} from canister corrosion is found to be an important mechanism in limiting the extent of the oxidising region.
- Calculations of redox-front penetrations for different fuel types (UO_2 and MOX fuels with a range of burn-ups), and for different assumptions regarding the nature of reductants in the bentonite and different canister lifetimes, indicate that it is important to establish whether credit may be taken for the full potential of pyrite in the bentonite in providing a further scavenger of radiolytic oxidants. For bentonite thicknesses appropriate to Nagra repository concepts, complete penetration of the bentonite does not occur for any of the fuel types provided pyrite is fully reactive, irrespective of canister lifetime.
- Uncertainty in the extent of the oxidising region, indicated by the modelling results, will be taken into account in establishing calculational cases for future Nagra performance assessments and in setting near-field solubility limits and sorption constants for these cases.

7 ACKNOWLEDGEMENTS

The authors would like to thank I. Neretnieks of the Royal Institute of Technology, Stockholm, for preliminary discussions related to some concepts discussed in this report, and D. Mancey of AECL for his input arising from his critical review of data on magnetite dissolution and passivation, which aided in the justification of data used in the Fe^{2+} release model. The manuscript also benefitted from reviews by D.W. Shoesmith of the University of Western Ontario and F.J. Pearson of PSI.

8 REFERENCES

BLESA, M.A. & MATIJEVIC, E. (1989): Phase transformations of iron oxides, oxohydroxides, and hydrous oxides in aqueous media. Advances in Colloid and Interface Science 29, 173-221.

BRUZZONI, P. & RIECKE, E. (1994): Hydrogen and iron transport through passive oxide films on electropolished iron. European Symposium on Modification of Passive Films, Paris, 1993. Edited by P. Marcus, B. Baroux and M. Keddam. Published for The European Federation of Corrosion by The Institute of Materials. European Federation of Corrosion Publication No. 12.

BURNS, W.G. & SIMS, H.E. (1981): J. Chem. Soc., Faraday Trans. 1, 77, 2803.

CASTLE, J.E. & MASTERSON, H.G. (1966): The role of diffusion in the oxidation of mild steel in high temperature aqueous solutions, Corrosion Science, 6, 93-104.

CHRISTENSEN, H. (1998): Calculations simulating spent-fuel experiments, Nucl. Tech. 124.

CHRISTENSEN, H. & BJERGBAKKE, E. (1982). Radiolysis of groundwater from spent fuel. SKBF/KBS TR82-18, Swedish Nuclear Fuel Supply Co./ Div. KBS, Stockholm.

CHRISTENSEN, H. & BJERGBAKKE, E. (1985): Alpha-radiolysis of aqueous solutions, in Mat. Res. Soc. Symp. Proc. Vol. 50, pp. 401-408, Materials Research Society.

CHRISTENSEN, H. & SUNDER,S. (1988): Current state of knowledge in radiolysis effects on spent fuel corrosion. Studsvik Report STUDSVIK/M-98/71.

CRAMER, J.J. & SMELLIE, J. (1994): Final report of the AECL/SKB Cigar Lake analog study. Atomic Energy of Canada Limited Report, AECL-10851, COG-93-147.

ERIKSEN, T.E., EKLUND, U-B. WERME, L.O. & BRUNO, J. (1995): Dissolution of irradiated fuel: A radiolytic mass balance study, J. Nucl. Mat. 227, pp. 76-82.

FORSYTH, R. & WERME, L.O. (1992): Spent fuel corrosion and dissolution, J. Nucl. Mat. 190, pp3-19

FUJISAWA, R., CHO, T., SUGAHARA, K., TAKIZAWA,Y., HORIKAWA, Y., SHIOMI, T. & HIRONAGA, M. (1997): The corrosion behavior of iron and aluminum under waste disposal conditions, Mat. Res. Soc. Symp. Proc. Vol. 465, Materials Research Society.

GREENLAND, D.J. & MOTT, C.J.B. (1978): Surfaces of soil particles. In: The Chemistry of Soil Constituents (D.J. Greenland and M.H.B. Hayes, editors), Wiley, Chichester, U.K., 321-353.

ISHIKAWA, T., KONDO, Y., YASUKAWA, A. & K. KANDORI, (1998): Formation of magnetite in the presence of ferric oxyhydroxides, Corrosion Science 40, pp. 1239-1251.

JOBE, D.J., LEMIRE, R.J. & TAYLOR, P. (1997): Iron oxide redox chemistry and nuclear fuel disposal, Atomic Energy of Canada Limited Report AECL-11667, COG-96-487-I.

JOHNSON, L.H. (1982): The dissolution of irradiated UO_2 Fuel in Groundwater, Atomic Energy of Canada Limited Report AECL-6837

JOHNSON, L.H., LENEVEU, D.M., KING, F., SHOESMITH, D.W., KOLAR, M., OSCARSON, D.W., SUNDER, S., ONOFREI, C. & CROSTHWAITE, J.L. (1996): The disposal of Canada's nuclear fuel waste: a study of postclosure safety of in-room emplacement of used CANDU fuel in copper canisters in permeable plutonic rock. Volume 2: Vault model. Atomic Energy of Canada Limited Report AECL-11494-2, COG-95-552-2.

JOHNSON, L.H. & McGINNES, D. (1999): Canister options for the direct disposal of spent fuel, unpublished Nagra report.

JOHNSON, L.H. & TAIT, J.C. (1997): Release of Segregated Radionuclides from Spent Fuel, SKB Technical Report 97-18

KING, F., QUINN, M.J. & MILLER, N.H. 1999: The effect of hydrogen and gamma radiation on the oxidation of UO_2 in 0.1 mol dm^{-3} NaCl solution. SKB Technical Report TR-99-27.

LANGMUIR, D. (1969): The Gibbs free energies of substances in the system $Fe–O_2–H_2O$-CO_2 at 25°C. U.S. Geological Survey Professional Paper 650-B, B180-B184.

LANGMUIR, D. (1971): Particle size effect on the reaction goethite = hematite + water. American Journal of Science 271, 147-156 (and correction (1972), ibid. 272, 972).

LIGER, E., CHARLET, L. & VAN CAPELLEN, P. 1999: Surface catalysis of uranium (VI) reduction by iron(II), Geochimica et Cosmochimica Acta 63, 2939-2955.

LIU, J. & NERETNIEKS, I. (1995): Some evidence of radiolysis in a uranium ore body - quantification and interpretation, In Proc. Mat. Res. Soc. Symp. Vol. 353, pp 1179-1186, Kyoto, ed. T. Murakami and R.C. Ewing, Materials Research Society.

LOIDA, A., GRAMBOW, B. & GECKEIS, H: (1996): Anoxic corrosion of high burnup spent fuel samples. J. Nucl. Materials 238, 11-22.

MARSH, G.P. &. TAYLOR, K.J. (1988): An assessment of carbon steel containers for radioactive waste disposal. Corrosion Science 28, 289-320.

MACDONALD, D. D. & URQUIDI-MACDONALD, M. (1994): Fundamental aspects in the design of passive alloys. European Symposium on Modification of Passive Films, Paris, 1993. Edited by P. Marcus, B. Baroux and M. Keddam. Published for The European Federation of Corrosion by The Institute of Materials. European Federation of Corrosion Publication No. 12.

NASH, P.J., SWIFT, B.T., GOODFIELD, M. &. RODWELL, W.R. (1998): Modelling gas migration in bentonite, Posiva Report 98-08, Posiva, Helsinki, Finland.

NICHOLSON, R.V., GILLHAM., R.W. & REARDON, E.J. (1988): Pyrite oxidation in carbonate-buffered solution: 1. Experimental kinetics. Geochim. Cosmochim. Acta 52, 1077-1085.

NICHOLSON, R.V., GILLHAM., R.W. & REARDON, E.J. (1990): Pyrite oxidation in carbonate-buffered solution: 2. Rate control by oxide coatings. Geochim. Cosmochim. Acta 54, 395-402.

POTTER, E.C. & MANN, G.M.W. (1961): Oxidation of mild steel in high temperature aqueous systems, First International Congress on Metallic Corrosion.

SAWICKI, J.A. & BRETT, M.E. (1993): Mossbauer study of corrosion products from a CANDU secondary system, Nucl. Instr. Methods Phys. Res. B76, 254-257.

SCHNEIDER, J., ZUIDEMA, P., SMITH, P. GRIBI, P. & NIEMEYER, P. (1997): Preliminary calculations of radionuclide release and transport from a repository for spent nuclear fuel in Switzerland, In Proc. Waste Management '97, Tucson, Arizona.

SCHWERTMANN, U. &. CORNELL, R.M. (1991): Iron oxides in the laboratory: Preparation and characterization. VCH, Weinheim, Germany, 137 pp.

SHOESMITH, D. W. & JOHNSON, L.H. (1997): Models for Used Nuclear Fuel Corrosion Under Waste Disposal Conditions, Ontario Hydro Report No. 06819-REP-01200-0012 R00

SHOESMITH, D.W. & SUNDER, S. (1992): The prediction of nuclear fuel (UO_2) dissolution rates under waste disposal conditions. J. Nucl. Mater. 190, 20-35.

SHOESMITH, D.W., SUNDER, S. & W.H. HOCKING. 1994. Electrochemistry of UO_2 nuclear fuel In: The Electrochemistry of Novel Materials, (Editors J Lipkowski and P.N. Ross), VCH, New York, p297-337.

SKB. (1997): SKB Annual Report (1996). SKB Technical Report 96-25.

SMELLIE, J. & KARLSSON, F. (1996): A reappraisal of some Cigar Lake issues of importance to performance assessment. SKB Technical Report 96-08.

SMITH, P. & McKINLEY, I.G. (1995): Production of Radiolytic Oxidants and Penetration of a Redox Front into the Bentonite in the Cases of UO_2 and MOX Spent Fuel, unpublished Nagra report.

SPAHIU, K. & WERME, L. In press: The influence of near field hydrogen on actinide solubilities and spent fuel leaching, to be published in Radiochimica Acta.

SUNDER, S., BOYER, G.D. & MILLER, N.H. 1990. XPS studies of UO_2 oxidation by alpha radiolysis of water at 100 °C. J. Nucl. Mater. 175, 163-169.

SUNDER, S., SHOESMITH, D.W. & MILLER, N.H. (1995): Prediction of the oxidative dissolution rates of used nuclear fuel in a geological disposal vault due to the al-

pha-radiolysis of water. In Mat. Res. Soc. Symp. Proc. 353, ed. T. Murakami & R.C. Ewing, pp. 617-624.

SUNDER, S., SHOESMITH, D.W. & MILLER, N.H. (1997): Oxidation and dissolution of nuclear fuel (UO_2) by the products of the alpha radiolysis of water. J. Nucl. Mater. 24, 66-74.

TAIT, J.C. & JOHNSON, L.H. (1986): Computer modelling of alpha radiolysis of aqueous solutions in contact with used UO_2 fuel. In Proceedings of the 2nd International Conference on Radioactive Waste Management, Winnipeg, MB, Sept. 7-11 (1986), Canadian Nuclear Society, Toronto, 611-615

TAIT, J.C. & LUHT, J.L. (1997): Dissolution Rates of Uranium from Unirradiated UO_2 and Uranium and Radionuclides from Used CANDU Fuel Using the Single-pass Flow-through Apparatus. Ontario Hydro Used Fuel Disposal Program Report 06819-REP-01200-0006 R00.

TAMAURA, Y., ITO, K. & KATSURA, T. (1983): Transformation of γ-FeO(OH) to Fe_3O_4 by adsorption of iron(II) ion on γ-FeO(OH). Journal of the Chemical Society, Dalton Transactions, 189-194.

TAYLOR, R.M. (1987): Non-silicate oxides and hydroxides. In Chemistry of Clays and Clay Minerals (A.C.D. Newman, editor). Mineralogical Monograph No. 6. John Wiley and Sons, New York, NY, 129-201.

VIENO, T., HAUTOJARVI, A., KOSKINEN, L., & NORDMAN, H. (1992): TVO-92 Safety Analysis of Spent Fuel Disposal. Nuclear Waste Commission of Finnish Power Companies Report, YJT-92-33E.

WAYCHUNAS, G.A. (1991): Crystal chemistry of oxides and oxyhydroxides. In Oxide Minerals: Petrologic and Magnetic Significance. Reviews in Mineralogy 25 (D.H. Lindsley, editor), Chapter 2.

WERME, L.O., SELLIN, P. & FORSYTH, R. (1990): Radiolytically induced oxidative dissolution of spent nuclear fuel, SKB Technical Report 90-08.

WHITE, A.F., PETERSON, M.L., & HOCHELLA, M.F., Jr. (1994): Electrochemistry and Dissolution Kinetics of Magnetite and Ilmenite, Geochim. et Cosmochim. Acta 58, 1859-1875.

APPENDIX A: FAILURE OF SPENT-FUEL CLADDING

Although the general corrosion rate of Zircaloy cladding is very low (< 0.01 μm a^{-1}), little is known about its susceptibility to localised corrosion in neutral pH groundwaters. Furthermore, the environment within a canister after breaching may lead to hydrogen-induced cracking and embrittlement of cladding as a result of hydrogen absorption. This might occur because of the high hydrogen pressure within a breached canister arising from the combined effects of the anaerobic corrosion of steel and the relative impermeability of buffer to hydrogen transport. Recent studies illustrate that break-through pressures for hydrogen escape from the buffer are likely to exceed 10 MPa (NASH *et al.*1998). Unfortunately, little is known about H_2 permeation into Zircaloy at high H_2 partial pressures. Despite many studies, there is still no satisfactory value for the diffusion coefficient of H_2 in ZrO_2 (COX & WONG 1999), which protects the Zircaloy from uptake of H_2, thus it is difficult to even crudely estimate long-term hydriding effects at low temperatures. Under in-reactor conditions within failed fuel elements, it is known that at a high ratio of hydrogen to steam pressure (>100), the impermeable nature of ZrO_2 can be lost and rapid H_2 uptake can occur (CLAYTON 1989). Unfortunately, the studies have all been performed under high temperature in-reactor conditions that are probably not relevant to repository conditions.

Given the large uncertainties associated with projecting the lifetime of cladding, it appears reasonable to consider that its lifetime is short under anoxic repository conditions. Because the failure mode is likely to be local due to the high resistance of Zircaloy to general corrosion, but the number of penetrations cannot be predicted, it also seems logical to retain conceptual models for fuel dissolution that consider both the trapping of all radiolytic oxidants at the fuel surface and their possible escape to react with Fe^{2+}. Appendix B examines the implications for fuel dissolution for the case of numerous penetrations in the cladding arising from, e.g., hydrogen-induced failure.

References

CLAYTON, J. C. (1989). Internal Hydriding in Irradiated Defected Zircaloy Fuel Rods. *Zirconium in the Nuclear Industry: Eighth International Symposium.* ASTM STP 1023, pp. 266-288. Philadelphia, Pennsylvania: American Society for Testing and Materials.

COX, B. & WONG, Y.-M. (1999). A hydrogen uptake micro-mechanism for Zr alloys. J. Nucl. Mat. 270, 134-146.

NASH, P.J., SWIFT, B.T., GOODFIELD, M. &. RODWELL, W.R. (1998): Modelling gas migration in bentonite. Posiva Report 98-08.

APPENDIX B: A REACTION-DIFFUSION MODEL FOR THE INTERACTION OF RADIOLYTIC OXIDANTS WITH SPENT FUEL AND FE^{2+}

M. Kolar (AECL) and L. H. Johnson

Although it may be sufficient to show that a redox front would not migrate beyond the buffer, it is interesting to examine, in addition, the potential effect of Fe^{2+} on the spent-fuel dissolution process itself. As well as reacting with UO_2, radiolytic oxidants may also react with Fe^{2+}, thus slowing the fuel-dissolution reaction. This process can be examined if some simplifying assumptions are made.

In the following model, it is assumed that there are numerous penetrations in the cladding. The release of Fe^{2+} from corrosion products is calculated using Eq. 32 (Section 3). When the solution concentration of Fe^{2+} in the water within the canister reaches a value of 10^{-6} mol dm^{-3} (the solubility of magnetite), the concentration is assumed to remain constant.

The radiolytically generated H_2O_2 is assumed to react with UO_2 at the rate proposed by BRUNO *et al.* (1997). For the reaction of Fe^{2+} with H_2O_2, the latter is assumed to decompose rapidly to O_2, according to

$$H_2O_2 = ½\ O_2 + H_2O \qquad (B1)$$

Oxygen may then undergo diffusion and reaction with Fe^{2+} only in the 5 cm wide water-filled space between the external surface of the fuel element and the surrounding iron parts of the canister. It is expected that the reaction of O_2 with Fe^{2+} at neutral pH is slower than that of H_2O_2, so this should be a conservative assumption. The system simulated is shown in Figure B1.

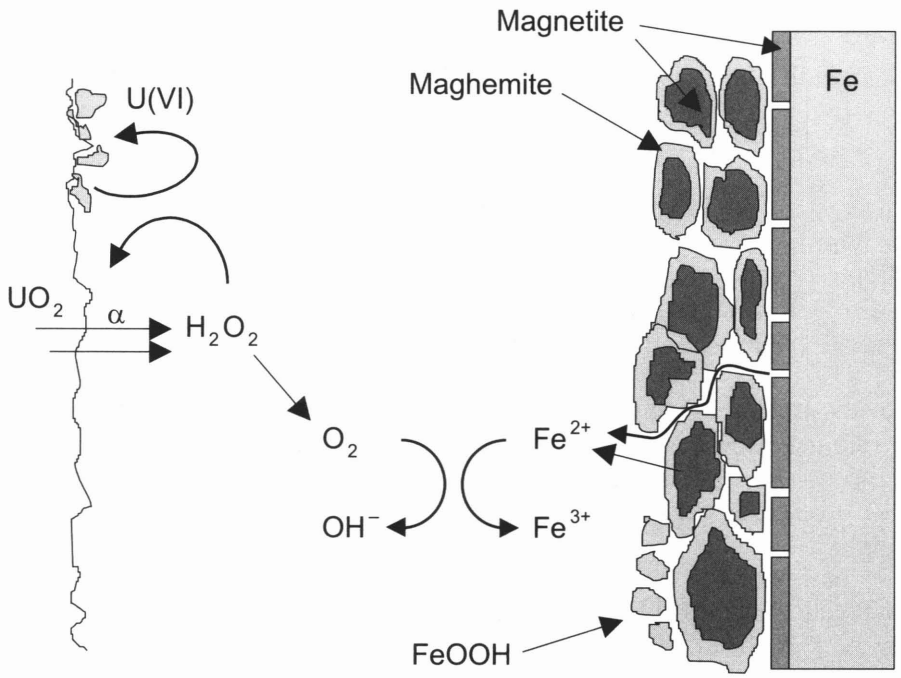

Fig. B1: Dissolution processes and solution reactions represented in the reaction diffusion model

The external surface of the fuel assembly is assumed to be the source of the release of radiolytic H_2O_2. The surface area of the assembly, which is 0.215 x 0.215 x 4.3 m, A_a, is given by

$$A_a = (4\times4.3\times0.215 + 2\times0.215^2)\ \mathrm{m}^2 = 3.79\ \mathrm{m}^2 = 379\ \mathrm{dm}^2 \qquad \text{(B2)}$$

The production rate of oxidants per tonne of original heavy metal is given by P_C in Eq. 9. If a canister is assumed to contain a mass of original heavy metal of 1.6 tonnes, within 4 fuel assemblies, the production rate per unit surface area of an assembly [mol dm^{-2} a^{-1}] is then:

$$\frac{1.6P_C}{4A_a} = 1.32\times10^{-5} QG_{eff} \qquad \text{(B3)}$$

where Q is the time-dependent energy production of the fuel due to alpha decay.

The dissolution rate of fuel per unit surface area of an assembly [mol dm^{-2} a^{-1}] is given by:

$$\frac{(3\times10^{-10}\ dm\,s^{-1})\times(32400\ dm^{2})\times(3.15\times10^{7}\ s\,a^{-1})c_0}{4A_a} = 0.202c_0 \qquad \text{(B4)}$$

where 32 400 dm^2 is the total surface area of the fuel in a canister, c_0 is the surface concentration of H_2O_2, and 3 x 10^{-10} dm s^{-1} is the rate constant for the reaction of H_2O_2 with UO_2, taken from BRUNO *et al.* (1997).

The total release of Fe^{2+} per unit surface area of an assembly [mol dm^{-2} a^{-1}], for the case of canister breaching occurring at 1000 years is, from Eq. 32:

$$\frac{R}{4A} = \frac{r_1}{\sqrt{t-1000}} + r_2\sqrt{t-1000} \qquad \text{(B5)}$$

where r_1 = 5.09×10^{-7} mol dm^{-2} $a^{-0.5}$, and r_2 = 8.34×10^{-8} mol dm^{-2} $a^{-1.5}$. The rate of consumption of Fe^{2+} due to its reaction with O_2 [mol dm^{-2} a^{-1}] is:

$$\frac{dc_1}{dt} = -\frac{2\times10^{13}}{60}c_1\,pO_2[OH^-]^2 \qquad \text{(B6)}$$

(DAVISON & SEED 1983). Here, c_1 is the concentration of iron, [OH^-] = 10^{-7} mol·dm^{-3}, and pO_2 is the partial pressure of O_2 in water, which can be obtained from Henry's law:

$$pO_2 = 4.3\times10^{4}\ \text{atm mol}^{-1}c_0V_{H_2O} \qquad \text{(B7)}$$

where 4.3×10^4 atm mol^{-1} is the Henry's Law constant, V_{H_2O} = 0.0181 dm^3 is the molar volume of water and c_0 is the concentration of oxygen. If all these values are substituted into Eq. B6, one obtains:

$$\frac{dc_1}{dt} = -k\,c_1\,c_0 \qquad \text{(B8)}$$

where k = 8.19×10^7 dm^3 mol^{-1} a^{-1}

When we add diffusion and the precipitation of iron, representing the fact that the concentration of iron cannot exceed the saturation value of c_1^{sat} (the solubility of magnetite), we obtain the following simple 1D model:

$$\frac{\partial c_0}{\partial t} = D_0 \frac{\partial^2 c_0}{\partial x^2} - \frac{1}{2} k c_0 c_1$$
$$\frac{\partial c_1}{\partial t} = D_1 \frac{\partial^2 c_1}{\partial x^2} - k c_0 c_1 - k_p \max(0, c_1 - c_1^{sat}) \qquad \text{(B9)}$$

Here, D_0 = 5.36 dm^2 a^{-1} is the diffusion rate of oxygen, and D_1 = 1.58 dm^2·a^{-1} is that of iron. k_p is a rather arbitrary rate of precipitation of iron, which operates only when the iron concentration exceeds the saturation value. We have used the value $k_p = 3.16 \times 10^7$ a^{-1}, although calculations show that the results are relatively insensitive to the value used. The model extends from $x = 0$ on the surface of a fuel element, to $x = L = 0.5$ dm, representing the inner surface of the canister from which iron is released. We have to add the following boundary conditions using the values defined above:

At $x = 0$ (from Eq. B3 and Eq. B4):

$$-D_0 \frac{\partial c_0}{\partial x}\Big|_{x=0} = 1.32 \times 10^{-5} Q G_{eff} - 0.202 c_0, \qquad \frac{\partial c_1}{\partial x}\Big|_{x=0} = 0 \qquad \text{(B10)}$$

At $x = L$:

$$\frac{\partial c_0}{\partial x}\Big|_{x=L} = 0, \qquad D_1 \frac{\partial c_1}{\partial x}\Big|_{x=L} = \frac{r_1}{\sqrt{t - 1000}} + r_2 \sqrt{t - 1000} \qquad \text{(B11)}$$

Initial values are $c_0 = c_1 = 0$ throughout the model.

This set of partial differential equations is solved numerically. As in Sections 4 and 5, an effective G value of 0.01 is assumed for the radiolytic yield. The heat output of the fuel, $Q(t)$, is taken from Table 1, assuming UO_2 spent fuel with a burn-up of 48000 MWd/tHM). The U(VI) produced by oxidation of the fuel is assumed to have no effect on the reaction of Fe^{2+} with O_2.

The integrated production of H_2O_2 and UO_3 hydrate as a function of time is shown in Figure B2. The difference between the two curves represents the consumption of the radiolytic oxidant by Fe^{2+}. As a result, fuel dissolution ceases after ~7000 a. The drop in H_2O_2 concentration at the fuel surface as a result of the scavenging of oxidant by Fe^{2+} is shown in Figure B3. In Figure B4, it can be seen that only 0.4 % of the fuel matrix dissolves in 10^5 a.

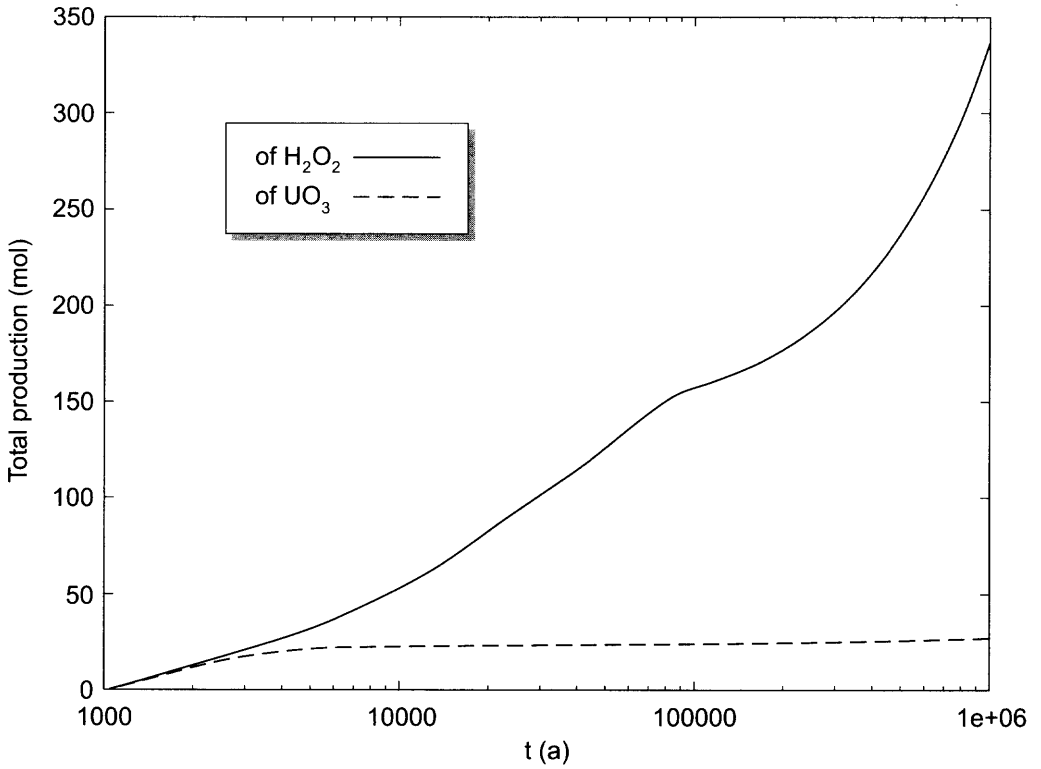

Fig. B2: The integrated production of H_2O_2 and UO_3 hydrate as a function of time.

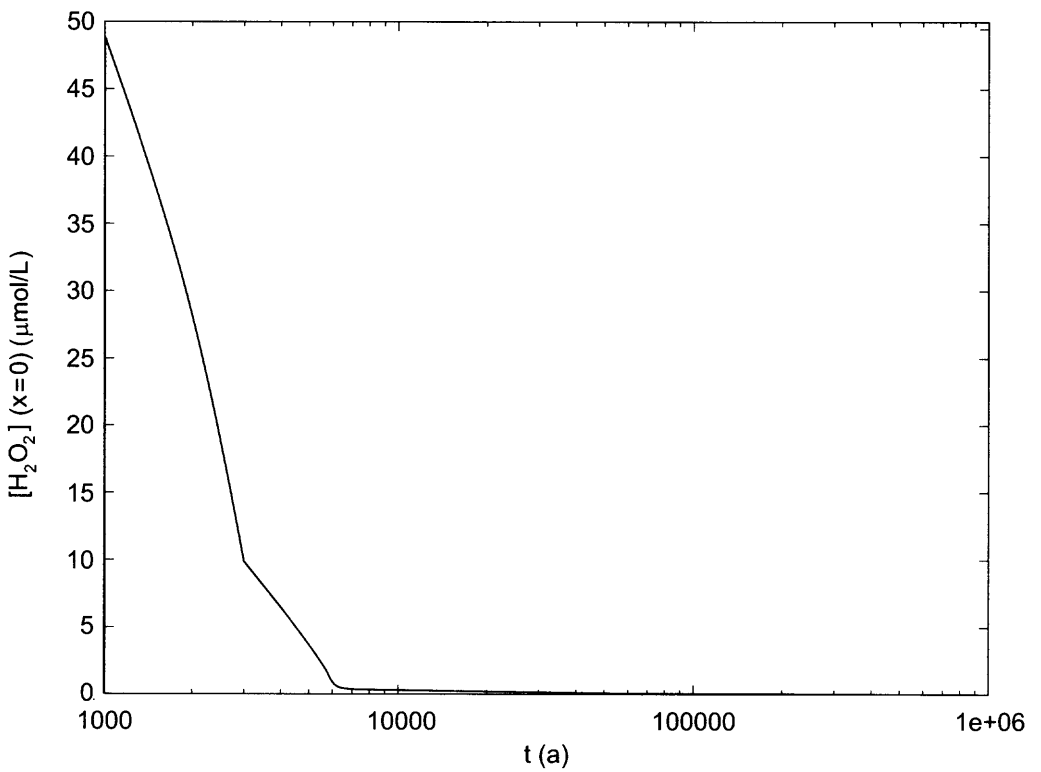

Fig. B3: The change in H_2O_2 concentration at the fuel surface as a result of the scavenging of oxidant by Fe^{2+}.

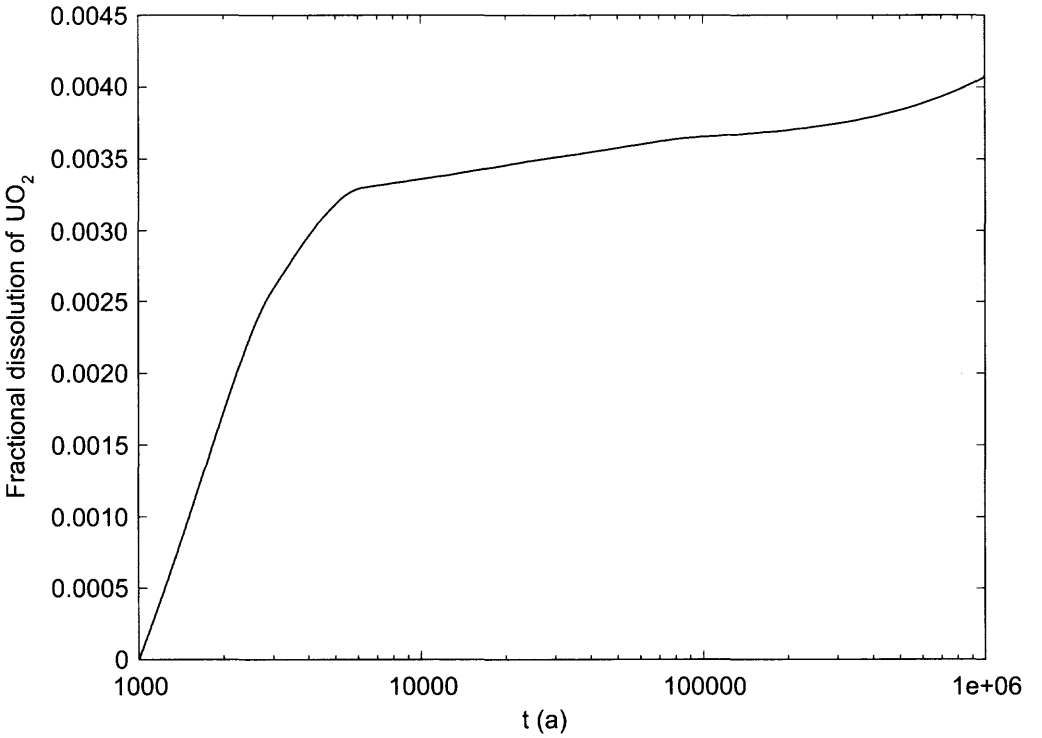

Fig. B4: Fractional dissolution of UO_2 spent fuel as a function of time.

References

BRUNO, J., CERA, E., DURO, L., ERIKSEN, T.E., SELLIN, P., SPAHIU, K. & WERME, L.O. (1997): A kinetic model for the stability of spent fuel matrix under oxic conditions: Model development against experimental evidence. In Mat. Res. Soc. Symp. Proc. Vol 465, pp. 491-502.

DAVISON, W. & SEED, G. (1983): The kinetics of oxidation of ferrous iron in synthetic and natural waters, Geochimica et Cosmochimica Acta 47, pp. 67-79.

APPENDIX C: THE EFFECT OF PRECIPITATED, DISSOLVED AND SORBED ALPHA EMITTERS ON OXIDANT PRODUCTION IN THE NEAR FIELD

Radiolytic oxidants are produced by the interaction between water and alpha particles generated within the fuel, either near to the external surfaces of the fuel pellets or near to internal, water-saturated fractures within the fuel. In addition, following the initiation of fuel dissolution, alpha particles with the potential to generate radiolytic oxidants can originate:

- from within the porous precipitate (i.e. UO_3 hydrates incorporating alpha emitters), that may form in the fuel fractures and in the fuel/sheath gap and, due to its porosity, which is higher than that of the fuel itself, may increase the volume of irradiated water, with only limited absorption of particles in the solid hydrates,
- from dissolved alpha emitters in the water within the breached canister, which, in spite of their low concentration, may provide an efficient production route for oxidants since there is no absorption on solids and
- from alpha emitters that are sorbed on the buffer material, which again has a relatively high porosity (~ 40%), giving only limited absorption of alpha particles.

In the following scoping calculations, each of these mechanisms is examined to determine if their contribution to oxidant production is significant compared to that arising from radiolysis of water at the fuel surface. The calculations of the effects of precipitated alpha emitters are generic, in that they apply to any alpha emitter, on the conservative assumption that the concentrations in the precipitate are the same as those in the fuel. To simplify the calculations of the effects of dissolved and sorbed alpha emitters, only the most important alpha emitter, ^{239}Pu, is considered.

The effect of precipitated alpha emitters

As fuel dissolution proceeds, U(VI) complexes (as well as some primary radiolytic oxidants) either diffuse away from the fuel surfaces, or are precipitated in the void spaces within the fuel pellets and in the gap between the fuel pellets and the cladding, eventually filling these spaces. Such precipitation has been observed in both static dissolution experiments (STROES-GASCOYNE *et al.* 1997) and unsaturated drip tests (WRONKIEWICZ *et al.* 1997) with spent fuel. The precipitates themselves, with the radionuclides that they incorporate, provide a source of alpha particles, but may also absorb alpha particles originating from within the fuel.

These two competing effects are scoped by considering a hypothetical case where all voids are filled with precipitates. The fraction, η_1, of alpha radiation generated in a medium of porosity, ε, that interacts with water molecules is given by (LIU & NERETNIEKS 1994)[14]:

$$\eta_1 = \frac{3\varepsilon\delta_{\alpha,f}}{8(1-\varepsilon)\delta_{\alpha,w}} \qquad \text{(C1)}$$

[14] The equation was applied by LIU & NERETNIEKS to the Cigar Lake uranium ore body, but should be equally applicable to a fuel pellet with filled cracks.

where $\delta_{\alpha,f}$ and $\delta_{\alpha,w}$ are, respectively, the ranges of alpha particles in fuel and water (~ 11 μm and 40 μm). For simplicity, no distinction is made between the range in fuel and the range in precipitate, which are, in any case, expected to be similar. For a fuel rod comprising pellets of radius r = 5 mm and surface area A_S = 0.15 m^2 m^{-1}, with 45 μm voids[15] filled with a hydrate precipitate of porosity 0.45 (KING & BETTERIDGE 1998), the overall porosity is:

$$\varepsilon = \frac{0.15\ \mathrm{m\ m^{-2}}.4.5\times10^{-5}\ \mathrm{m}\times0.45}{\pi\left(5\times10^{-3}\ \mathrm{m}\right)^2} = 0.0387 \qquad \text{(C2)}$$

giving $\eta_1 = 0.004$

This can be compared to the case where no precipitate is present (which is the basis of Eq. 9), where the fraction, η_2, of alpha radiation generated in the medium that crosses wetted surfaces and interacts with water molecules is given by:

$$\eta_2 = \frac{3A_S\delta_{\alpha,f}}{16\pi r^2} = 0.004 \qquad \text{(C3)}$$

Since $\eta_1 \sim \eta_2$, the competing effects that arise when voids are filled with precipitates, namely additional alpha-particle generation, and a reduction in the volume of water available for radiolysis, roughly cancel each other. The effects of precipitates are therefore neglected in this report.

The effect of dissolved alpha emitters

For the case of dissolved ^{239}Pu, the production of radiolytic oxidants is limited by the relatively low solubility of Pu. Irrespective of the quantity of fuel dissolved, the oxidant production rate from dissolved Pu will remain constant with time. The void volume of a spent fuel canister is 706 litres (SMITH 1998; value for PWR fuel). Assuming a Pu solubility of 10^{-8} M (BRUNO et al. 1997) and a specific activity for ^{239}Pu of 2.3×10^9 Bq g^{-1}, the total activity of dissolved ^{239}Pu is 3.88×10^6 Bq $canister^{-1}$. Assuming a G value of 1 (an appropriate value for homogeneous solution radiolysis), the H_2O_2 production rate is given by:

3.88×10^6 Bq $canister^{-1}$ × 5×10^6 eV Bq^{-1} × 0.01 molecule eV^{-1} × 1 mole/(6.02×10^{23})

= 3.22×10^{-13} moles s^{-1}.

The cumulative production to 10^5 years[16] is thus 1.37 mol, which represents a very small fraction of the ~150 mol produced by radiolysis of water at the fuel surface over the same duration.

The effect of sorbed alpha emitters

---

[15] In the fuel pellets, 50-60 micron cracks are common, with typical fuel-sheath gaps of 20-40 microns.

[16] The half life of ^{239}Pu is 2.41×10^4 years, and so this isotope would, in any case, not be expected to contribute significantly to radiolysis after about 10^5 years (4 half lives), since its inventory will have decayed substantially by this time.

For the case of irradiation of pore water in the bentonite, we consider the following scenario. The canister is assumed to be breached along a crack of aperture W [m]. Neglecting the curvature of the canister/bentonite interface, but taking into account diffusion from the crack and radioactive decay, the steady-state concentration, c, of ^{239}Pu in solution in the buffer is governed the equation:

$$\frac{1}{r'}\frac{d}{dr'}\left(r'\frac{dc}{dr'}\right)-c=0 \qquad \text{(C4)}$$

where

$$r'=\frac{r}{\mu} \qquad \text{(C5)}$$

$$\mu=\sqrt{\frac{D_b}{R_b\lambda}} \qquad \text{(C6)}$$

and

$$R_b=1+\rho_b K_d\left(\frac{1-\varepsilon_b}{\varepsilon_b}\right) \qquad \text{(C7)}$$

r [m] is a radial coordinate, extending from the crack into the surrounding bentonite, with its origin at the centre of the crack, D_b = 0.0166 m^2 a^{-1} is the pore diffusion coefficient of bentonite, ε_b = 0.38 is the bentonite porosity, ρ_b = 2760 kg m^{-3} is its solid density, K_d = 5 m^3 kg^{-1} is the "realistic-conservative" sorption constant for plutonium on bentonite (all data from NAGRA 1994) and λ [a^{-1}] = ln $2/t_{1/2}$, where $t_{1/2}$ is the half life of ^{239}Pu (2.41×10^4 years).

If the concentration of ^{239}Pu is maintained at its solubility limit of 10^{-8} M, i.e. at $c_0 = 10^{-5}$ mol m^{-3}, at the crack/bentonite interface[17], and the effects of the outer boundary of the bentonite are neglected, the solution of Eq. C4, in terms of modified Bessel functions, is:

$$\frac{c}{c_0}=\frac{K_0(r')}{K_0(r'_D)} \qquad \text{(C8)}$$

where

$$r_D=\frac{W}{\pi} \qquad \text{(C9)}$$

[17] For mathematical simplicity, the interface is assumed to describe a semi-circle in a plane normal to the canister axis, with the same length as the crack aperture (W).

The total amount of ^{239}Pu in solution, N [mol], is given by:

$$N = 2\pi r_a \int_{r_D}^{\infty} \pi r c dr \qquad \text{(C10)}$$

for a canister of external radius r_a = 0.4 m. Substituting Eq. C8 in Eq. C10,

$$N = \frac{2\pi^2 r_a c_0 \mu^2}{K_0(r'_D)} \int_{r_D}^{\infty} r' K_0(r') dr' = \frac{2\pi^2 r_a c_0 \mu^2 r'_D K_1(r'_D)}{K_0(r'_D)} \qquad \text{(C11)}$$

The amount sorbed on mineral surfaces in the bentonite is very much larger, because of the high sorption capacity of the buffer for plutonium, and is given by $N(R_b\text{-}1)$:

$$N(R_b - 1) = \frac{2\pi^2 r_a c_0 \mu^2 (R_b - 1)}{K_0(r'_D)} \int_{r_D}^{\infty} r' K_0(r') dr' = \frac{2\pi^2 r_a c_0 \mu^2 (R_b - 1) r'_D K_1(r'_D)}{K_0(r'_D)} \qquad \text{(C12)}$$

Taking the specific activity of ^{239}Pu as 2.3 × 10^9 Bq g^{-1}, the H_2O_2 production in 10^5 years is given by:

$N(R_b\text{-}1)G \times \eta \times 239$ g $mol^{-1} \times 2.3 \times 10^9$ Bq $g^{-1} \times 5 \times 10^6$ eV $Bq^{-1} \times 0.01$ molecule $eV^{-1} \times 3.16 \times 10^7$ s $a^{-1} \times 10^5$ a × 1 mole/(6.02×10^{23}).

where η is the fraction of alpha radiation from the decay of ^{239}Pu that interacts with water molecules (LIU & NERETNIEKS 1994):

$$\eta = \frac{3\varepsilon_b \delta_{\alpha,b}}{8(1-\varepsilon_b)\delta_{\alpha,w}} \qquad \text{(C13)}$$

and $\delta_{\alpha,b}$ and $\delta_{\alpha,w}$ are, respectively, the ranges of alpha particles in the bentonite minerals and water, which, in this case, are conservatively assumed to be equal.

This production is given in Table C1 as a function of G and the crack aperture, W.

Table C1: H_2O_2 production in 10^5 years as a function of G and of crack aperture, W.

Crack aperture [m]	H_2O_2 production in 10^5 a [moles]		
	G = 1	G = 0.1	G = 0.01
10^{-3}	239	23.9	2.39
10^{-4}	174	17.4	1.74

For a G value of about 0.1 or less, the production is again considerably smaller than the ~150 mol produced by radiolysis of water at the fuel surface over the same duration, and is insensitive to the crack aperture. ERIKSEN & NDALAMBA (1988) studied

α-radiolysis of water-saturated bentonite and determined that $G(H_2O_2) = 0.69$, although the measurements were not at the high H_2 partial pressures that would be expected to arise from corrosion of steel, which would be expected to reduce the yield considerably. Estimates of radiolytic oxidant production in the Cigar Lake deposit by LIU & NERETNIEKS (1995) suggest that the effective G value is ~0.01 for a fine-grained ore with a porosity of 10%. The low efficiency of oxidant production was assumed to arise from recombination of oxidants and reductants. Although it is unclear if recombination would occur to the same extent for Pu absorbed within a bentonite buffer, a *G* value of greater than 0.1 seems unlikely, as discussed in Section 2.3, because dissolved iron species and H_2 that enhance recombination would be present in significant concentrations in the buffer.

In conclusion, the calculations illustrate that radiolysis of water at the spent fuel surface is likely to be largest contributor to oxidant production and that other mechanisms for oxidant production are much less important.

It is further noted that the production of oxidants within the bentonite would not be expected to contribute significantly to the movement of a redox front into the bentonite. This is because the O_2 or H_2O_2 produced would be consumed by corrosion of the outer surface of the steel canister. This can be seen by substituting a typical oxic corrosion rate for carbon steel (i.e., ~10 μm a^{-1}) into Equation 31, which gives a molar corrosion rate of ~25 mol a^{-1} per canister. This is far in excess of the quantities of oxidant produced by radiolysis (see Table C1), thus most of the oxidants produced would be expected to diffuse back towards the canister and react with the steel.

References

BRUNO, J., E. CERA, J. DE PABLO, L.DURO, S. JORDANA & D. SAVAGE. (1997): Determination of radionuclide solubility limits to be used in SR-97 Uncertainties associated to calculated solubilities. SKB Technical Report 97-33.

ERIKSEN,T. & NDALAMBA, P. (1988). On the formation of a moving redox-front by α-radiolysis of compacted water saturated bentonite. SKB Technical Report 88-27.

KING, F. & BETTERIDGE, J. S. (1998): Ex situ measurements of the porosity of precipitated corrosion products on oxidised UO2, Ontario Hydro Report UFDP (*in preparation*).

LIU, J. & NERETNIEKS, I. (1995): Some evidence of radiolysis in a uranium ore body - quantification and interpretation, In Proc. Mat. Res. Soc. Symp. Vol. 353, pp 1179-1186, Kyoto, ed. T. Murakami and R.C. Ewing, Materials Research Society.

NAGRA (1994): Kristallin-I safety assessment report, Nagra Technical Report Series, NTB 93-22, Nagra, Wettingen, Switzerland.

SMITH, P. A. (1998): The significance of the instant-release fraction for a repository for spent nuclear fuel, Nagra unpublished report.

STROES-GASCOYNE, S., JOHNSON, L.H., TAIT, J.C., MCCONNELL, J.C. & PORTH, R.J. (1997): Leaching of used CANDU fuel: Results from a 19-year leach test under oxidizing conditions, In Mat. Res. Soc. Symp. Proc. Vol. 465, pp. 511-518, Materials Research Society.

WRONKIEWICZ, D. J., BUCK, E.C. & J. K. BATES. (1997): Grain boundary corrosion and alteration phase formation during the oxidative dissolution of UO_2 fuel pellets, In Mat. Res. Soc. Symp. Proc. Vol. 465, pp. 519-526, Materials Research Society.

APPENDIX D: ESTIMATION OF AN EFFECTIVE *G*-VALUE RANGE FROM AECL ALPHA-RADIOLYSIS EXPERIMENTS

The AECL experimental apparatus, which consists of a thin-layer electrochemical cell, is shown schematically in Figure D1.

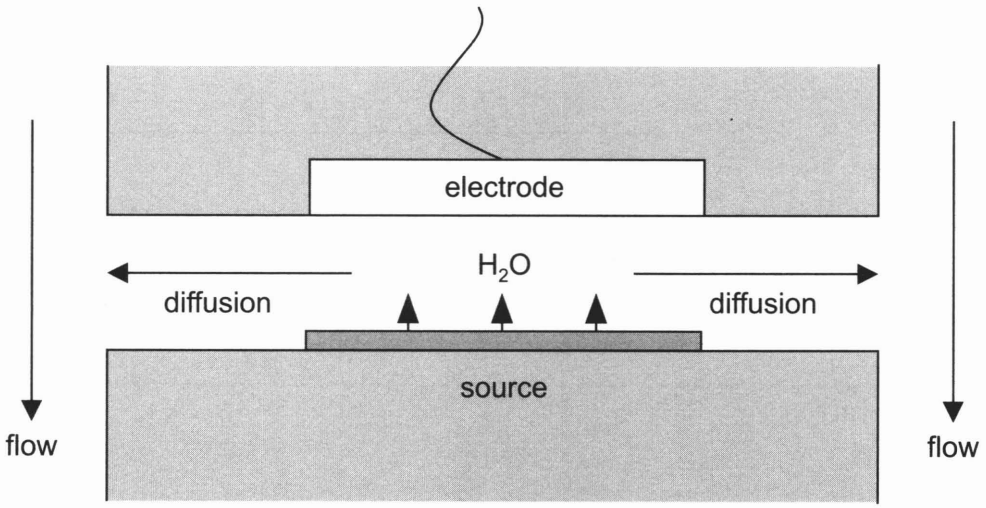

Fig. D1: The AECL electrochemical cell from which data on the corrosion rate of a UO_2 electrode, for a given α source strength, are derived (from SHOESMITH & SUNDER 1992).

Mass balance

Radiolysis occurs in the water-filled gap above an alpha source of strength S [Ci]. H_2O_2, generated by radiolysis at a rate P [mol a^{-1}], may react with an unirradiated UO_2 electrode of area A [m^2], the dissolution rate of which, D [mol m^{-2} a^{-1}], is derived from its steady-state corrosion potential via an electrochemical model. H_2O_2 may also be transported by diffusion, at a rate F [mol a^{-1}] to the outside of the cell, where it is removed by advection.

Mass balance gives:

$$P - DA = F \qquad (D1)$$

Diffusive transport

The rate of diffusive transport can be estimated assuming that the fluid in the gap between the α-source and the electrode has a uniform hydrogen peroxide concentration $[H_2O_2]_0$ and that the outer boundary of the gap has a zero concentration, on account of the advective flow around the cell (Fig D2).

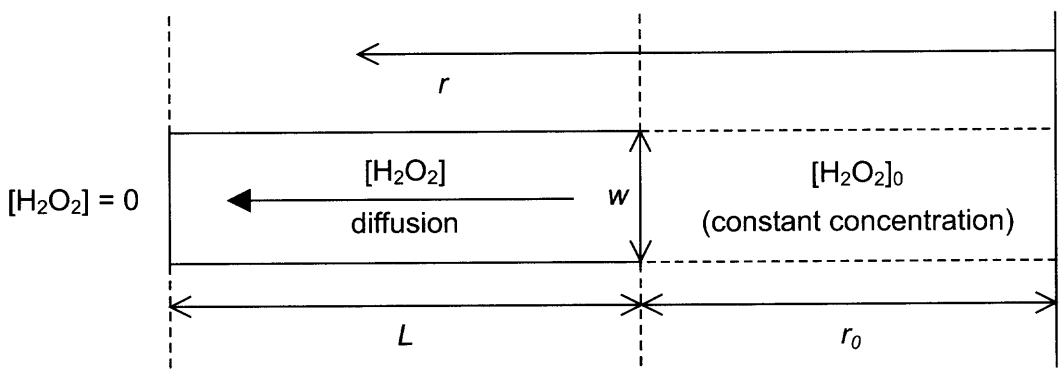

Fig. D2: Estimating the diffusive flux through the gap in the AECL electrochemical cell.

Assuming that source and electrode are circular, with radii $r_0 \approx 10^{-2}$ m (SHOESMITH & SUNDER 1992), that the distance from the perimeter of the source to the outer boundary of the gap is $L \approx 10^{-2}$ m (based on Fig. 19 in SHOESMITH & SUNDER 1992) and that the width of the gap $w = 25 \times 10^{-6}$ m (SHOESMITH & SUNDER 1992), and taking the diffusion coefficient of H_2O_2 in water to be $D_0 \approx 10^{-9}$ m^2 s^{-1} = 0.032 m^2 a^{-1}, the steady-state concentration of H_2O_2, $[H_2O_2]$, is given by:

$$\frac{[H_2O_2]}{[H_2O_2]_0} = \frac{\log_e\left(\frac{r}{r_0 + L}\right)}{\log_e\left(\frac{r_0}{r_0 + L}\right)} \qquad \text{(D2)}$$

The flux of H_2O_2 through the gap, F, is then given by:

$$F = -2\pi r w D_0 \frac{d}{dr}[H_2O_2] = -2\pi w D_0 \frac{[H_2O_2]_0 \times 1000\,\mathrm{l\,m^{-3}}}{\log_e\left(\frac{r_0}{r_0 + L}\right)} = 7.3\times10^{-3}[H_2O_2]_0 \qquad \text{(D3)}$$

Hydrogen peroxide production

Assuming an average α-particle energy of 5 MeV, the production rate of H_2O_2 is:

$$P = 0.5 \times \frac{SG_{eff} \times 10^{-2} \times [3.7 \times 10^{10}\ \mathrm{Bq\,Ci^{-1}}] \times [5 \times 10^{6}\ \mathrm{eV}] \times [3.16 \times 10^{7}\ \mathrm{sa^{-1}}]}{6.02 \times 10^{23}\ \mathrm{molecules\,mol^{-1}}} = 4.86 \times 10^{-2}\, SG_{eff}$$

(D4)

where the factor of 0.5 accounts for the fact that not all α-particles are released into the water-filled gap (50 % are assumed to be ejected away from this region), and the factor of 10^{-2} converts the units of G_{eff} from molecules of H_2O_2 per 100 eV to molecules per eV.

Spent fuel dissolution rate

The results of the AECL experiments take the form of measured dissolution rates for different source strengths and are plotted in Figure D3, together with a "best fit" function, that takes the form:

$$D = 3.16 \times 10^{6} S^{4.3} \qquad (D5)$$

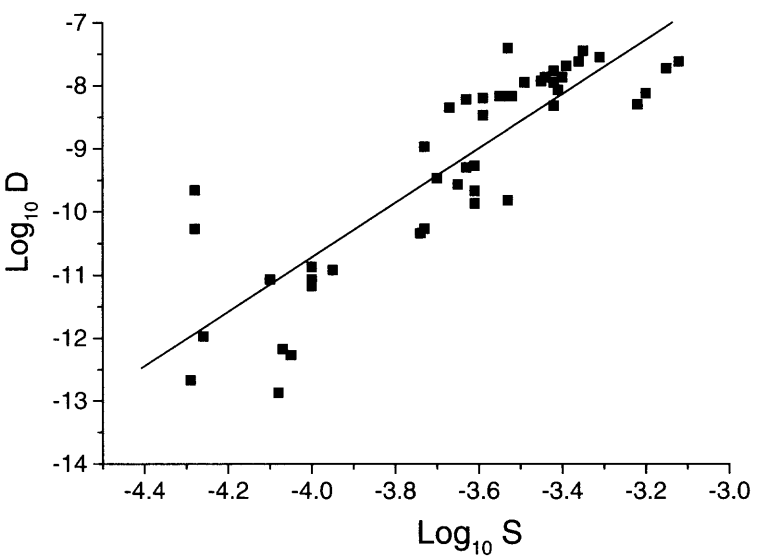

Fig. D3: Dissolution rate of UO_2, D [mol cm^{-2} a^{-1}] as a function of alpha source strength, S [Ci]. Individual points are experimental results from Sunder et al. 1997, and the best fit to these points (Eq. D5) is shown by the solid line.

Estimating G_{eff}

Substituting the rates of production (Eq. D4) and diffusion (Eq. D3) in the mass balance (Eq. D1), and rearranging:

$$S = \frac{7.3\times10^{-3}[H_2O_2]_0 + AD}{4.86\times10^{-2}G_{eff}} \qquad (D6)$$

Substituting Eq. D6 in Eq. D5:

$$D = 3.16\times10^{6}\left(\frac{7.3\times10^{-3}[H_2O_2]_0 + AD}{4.86\times10^{-2}G_{eff}}\right)^{4.3} = \left(\frac{36.5[H_2O_2]_0 + D}{7.48G_{eff}}\right)^{4.3} \qquad (D7)$$

for a UO_2 electrode of wetted surface area A = 2×10^{-4} m^2.

Eq. D7 can be solved numerically to obtain D as a function of $[H_2O_2]_0$, for any assumed G_{eff} value. These solutions can be compared to the results of some further experiments on the electrochemical cell, reported in SHOESMITH & SUNDER (1992), in which corrosion potentials on a UO_2 electrode were measured in H_2O_2 solution of known concentration. The comparison is made in Figure D4 across the range of D for which Eq. D7 is valid (i.e. the range for which Eq. D5 approximates to the AECL experiments).

The results of the experiments using H_2O_2 solution of known concentration follow the trend predicted by Eq. D7 and are consistent with a G_{eff} value in the range of about 0.001 to 0.01. One must view the inference of such a low G_{eff} value from the radiolysis experiments with some caution. Even though diffusive losses of H_2O_2 have been accounted for in the above analysis, the uncertainties regarding the rate of decomposition of H_2O_2 and the slow rate of reaction of the resultant O_2 with the UO_2 electrode have not been accounted for (i.e. some of the O_2 may diffuse out of the gap before reacting), and these factors may cause underestimation of G_{eff}. Nonetheless, the results suggest that G_{eff} is significantly less than 1 for α-radiolysis at a UO_2 surface.

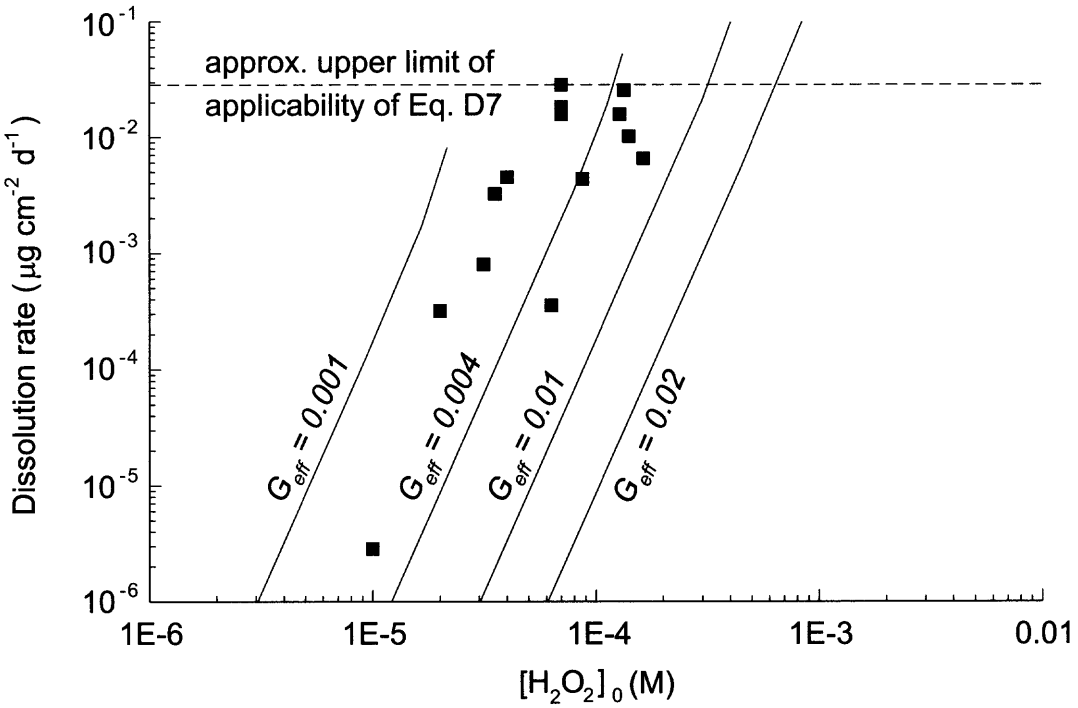

Fig. D4: Dissolution rate of the UO_2 electrode as a function of H_2O_2 concentration in the cell, $[H_2O_2]_0$. The results of experiments that use a known H_2O_2 concentration are compared to those using an α source to generate H_2O_2, where the H_2O_2 concentration is derived using Eq. D7 assuming different G_{eff} values.

References

SHOESMITH, D. W. & SUNDER, S. (1992): An electrochemistry-based model for the dissolution of UO_2, AECL-10488, Atomic Energy of Canada Limited, Whiteshell Laboratories, Pinawa, Canada.

SUNDER, S., SHOESMITH, D. W. & MILLER, N. H. (1997): Oxidation and dissolution of nuclear fuel (UO_2) by the products of alpha radiolysis of water, J. Nucl. Mater., 244, 66-74, AECL-11537.

APPENDIX E: RESULTS OF PARAMETER VARIATIONS IN THE MODELLING OF THE MIGRATION OF THE REDOX FRONT

(i) Canister failure along a circumferential crack

1000 a canister lifetime, variations in bentonite minerals acting as reductants.

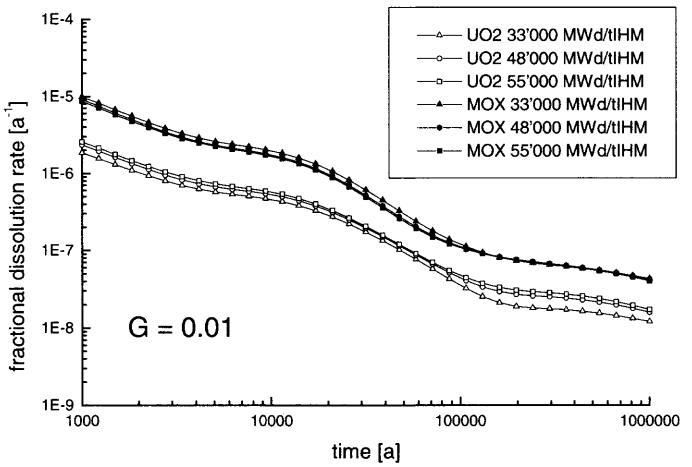

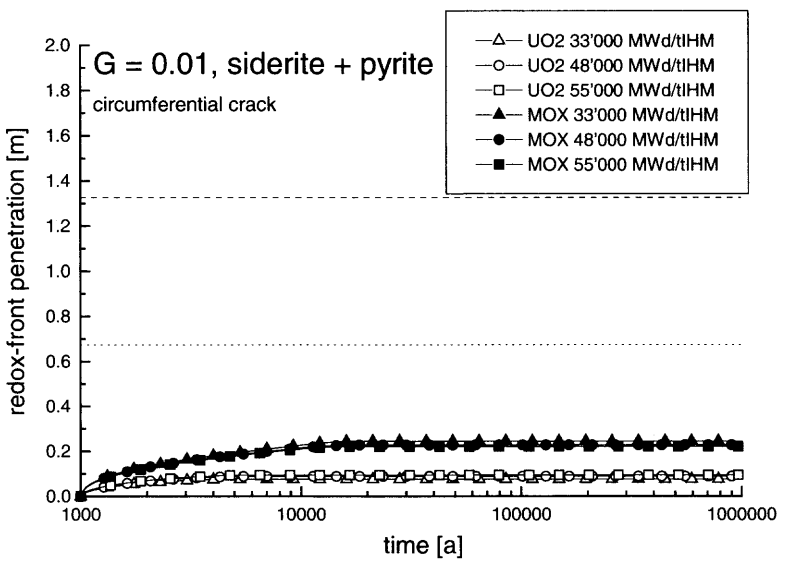

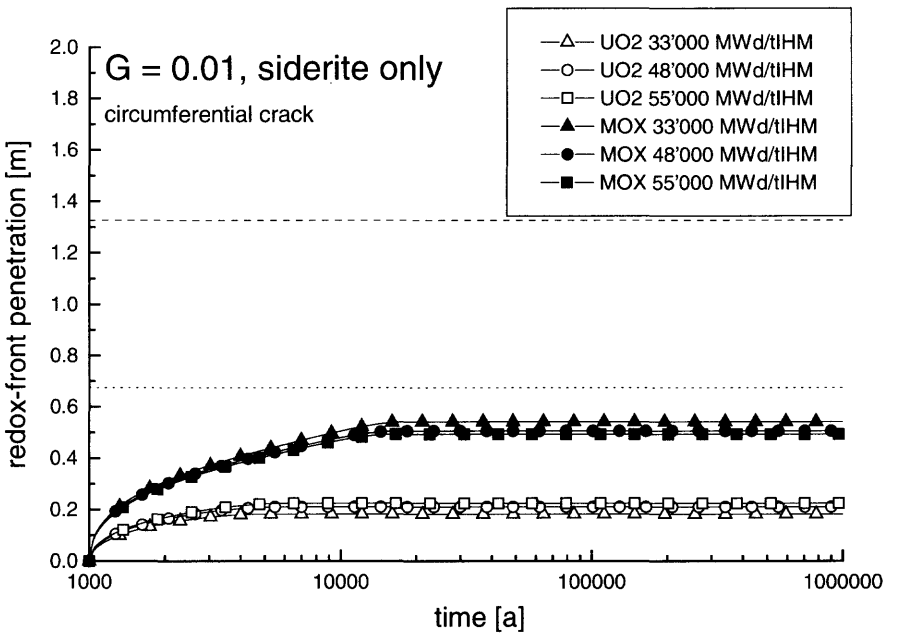
G = 0.01, siderite only
circumferential crack
UO2 33'000 MWd/tIHM
UO2 48'000 MWd/tIHM
UO2 55'000 MWd/tIHM
MOX 33'000 MWd/tIHM
MOX 48'000 MWd/tIHM
MOX 55'000 MWd/tIHM
redox-front penetration [m]
time [a]
2.0
1.8
1.6
1.4
1.2
1.0
0.8
0.6
0.4
0.2
0.0
1000
10000
100000
1000000

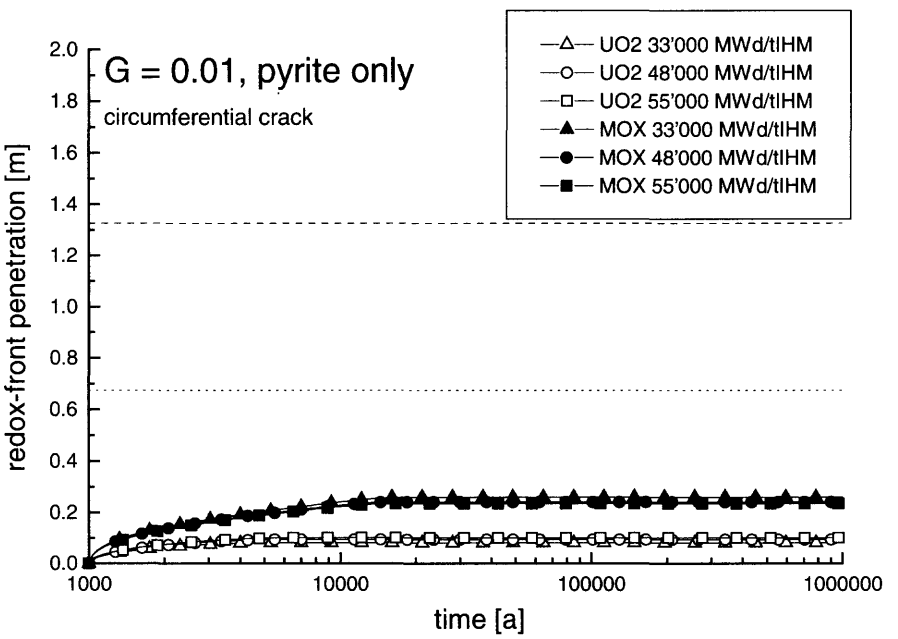
G = 0.01, pyrite only
circumferential crack
UO2 33'000 MWd/tIHM
UO2 48'000 MWd/tIHM
UO2 55'000 MWd/tIHM
MOX 33'000 MWd/tIHM
MOX 48'000 MWd/tIHM
MOX 55'000 MWd/tIHM
redox-front penetration [m]
time [a]
2.0
1.8
1.6
1.4
1.2
1.0
0.8
0.6
0.4
0.2
0.0
1000
10000
100000
1000000

10000 a canister lifetime, variations in bentonite minerals acting as reductants.

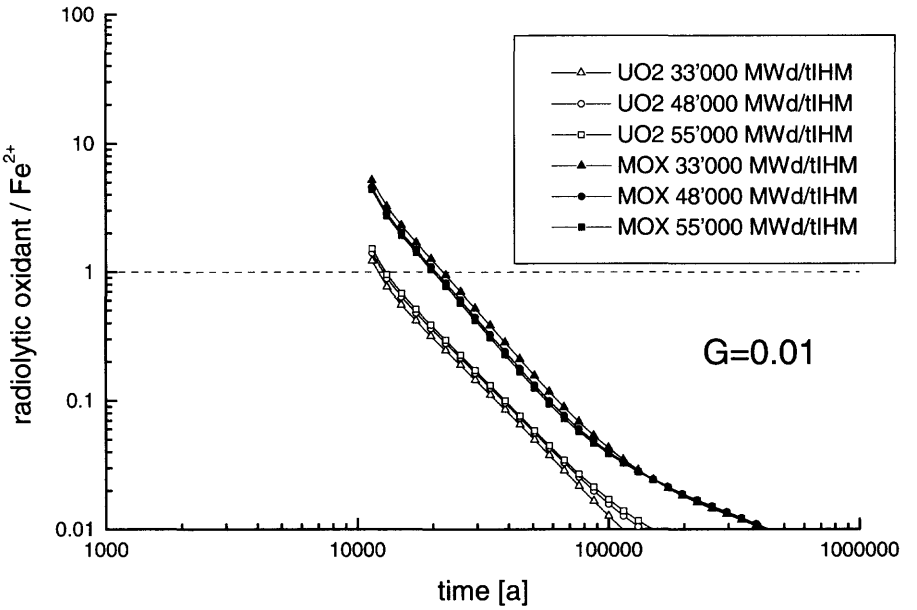

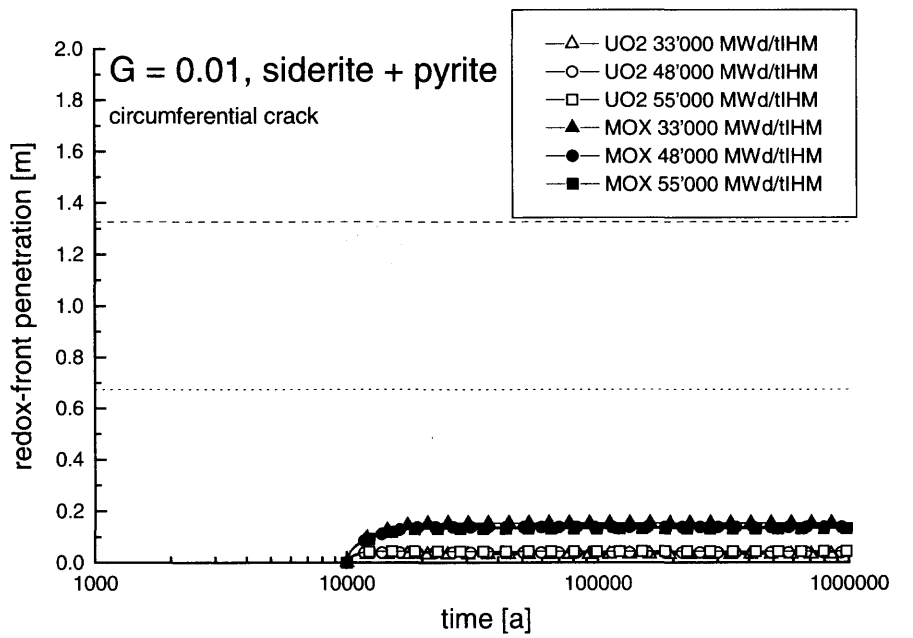

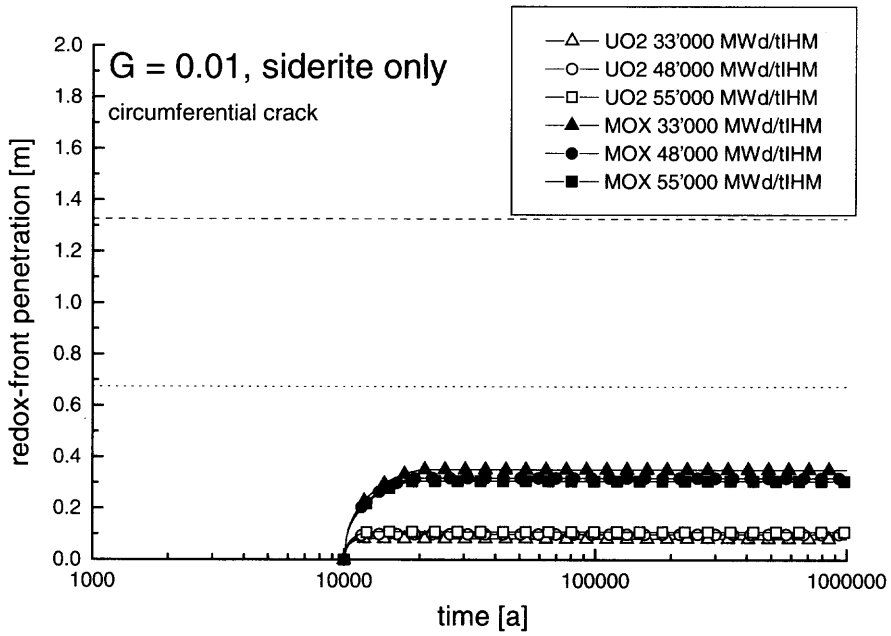
G = 0.01, siderite only
circumferential crack
UO2 33'000 MWd/tIHM
UO2 48'000 MWd/tIHM
UO2 55'000 MWd/tIHM
MOX 33'000 MWd/tIHM
MOX 48'000 MWd/tIHM
MOX 55'000 MWd/tIHM
redox-front penetration [m]
time [a]
2.0
1.8
1.6
1.4
1.2
1.0
0.8
0.6
0.4
0.2
0.0
1000
10000
100000
1000000

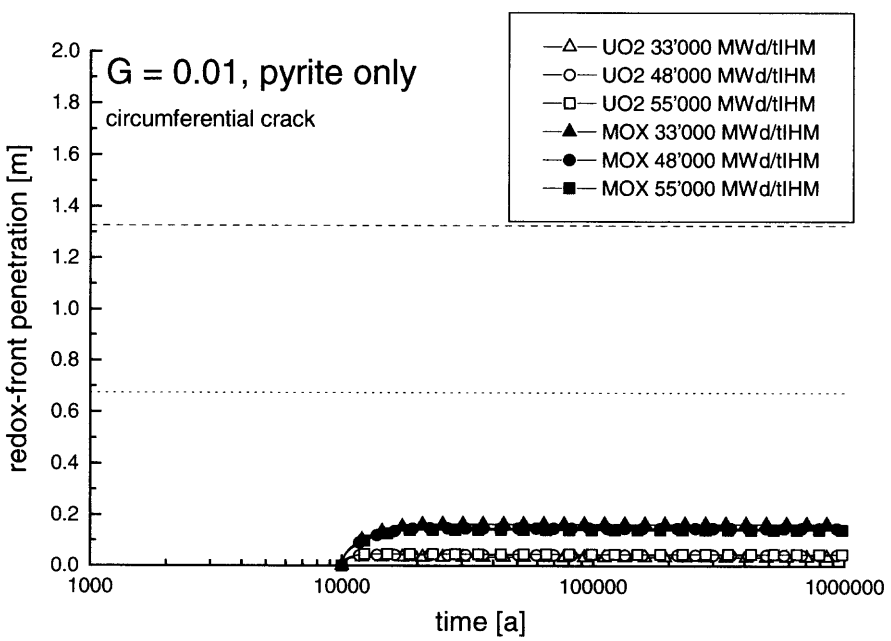
G = 0.01, pyrite only
circumferential crack
UO2 33'000 MWd/tIHM
UO2 48'000 MWd/tIHM
UO2 55'000 MWd/tIHM
MOX 33'000 MWd/tIHM
MOX 48'000 MWd/tIHM
MOX 55'000 MWd/tIHM
redox-front penetration [m]
time [a]
2.0
1.8
1.6
1.4
1.2
1.0
0.8
0.6
0.4
0.2
0.0
1000
10000
100000
1000000

100000 a canister lifetime.

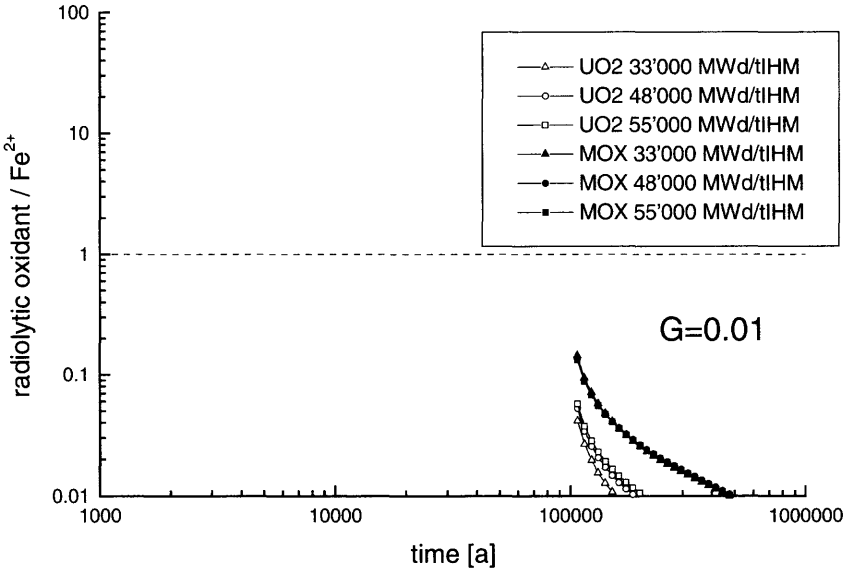

No redox front in the bentonite in this case.

(ii) Canister failure at a single point

1000 a canister lifetime, variations in bentonite minerals acting as reductants.

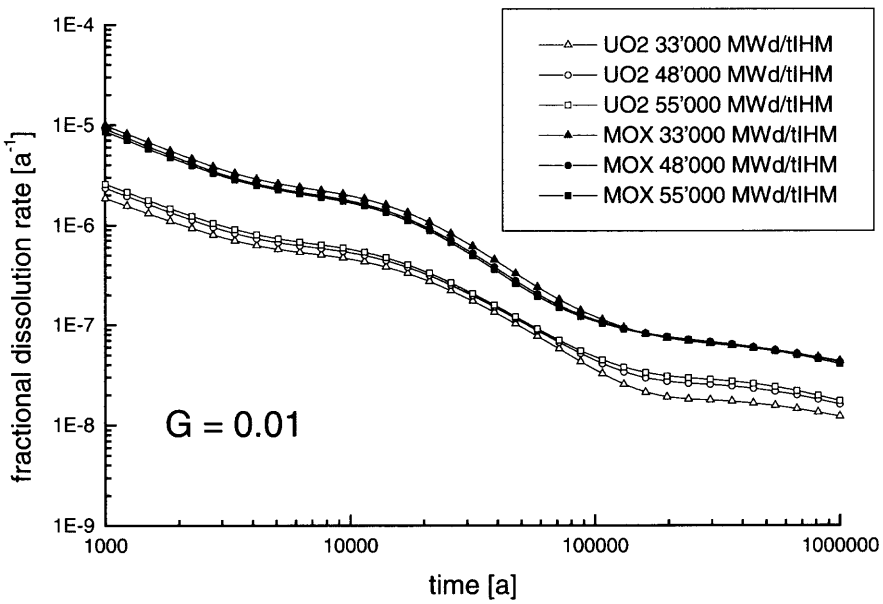

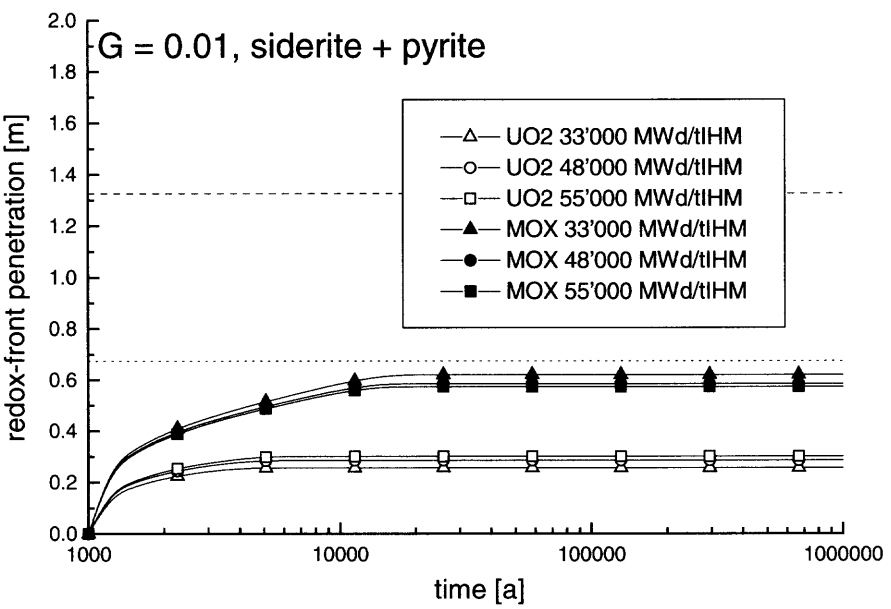

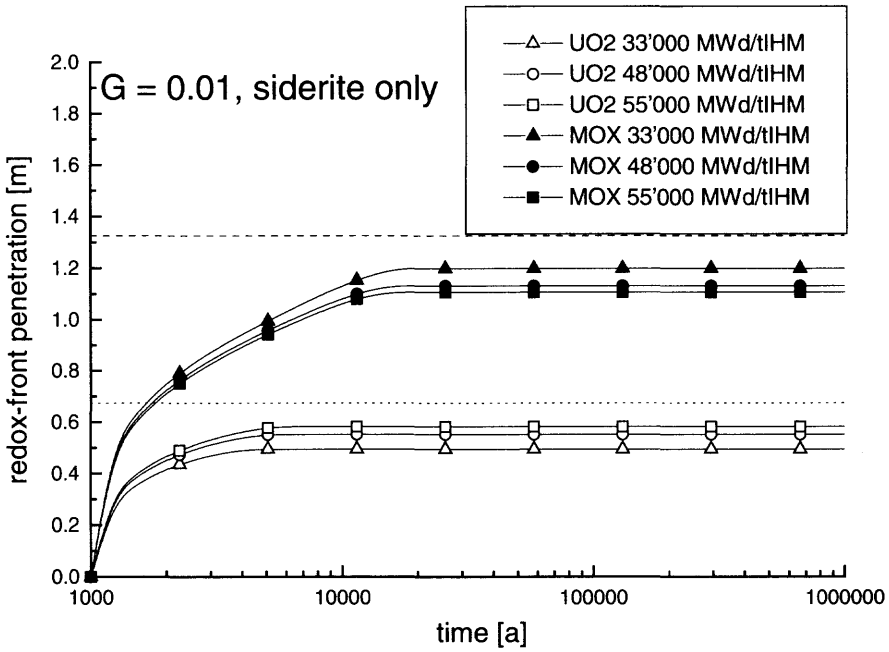
G = 0.01, siderite only
UO2 33'000 MWd/tIHM
UO2 48'000 MWd/tIHM
UO2 55'000 MWd/tIHM
MOX 33'000 MWd/tIHM
MOX 48'000 MWd/tIHM
MOX 55'000 MWd/tIHM
redox-front penetration [m]
time [a]
0.0
0.2
0.4
0.6
0.8
1.0
1.2
1.4
1.6
1.8
2.0
1000
10000
100000
1000000

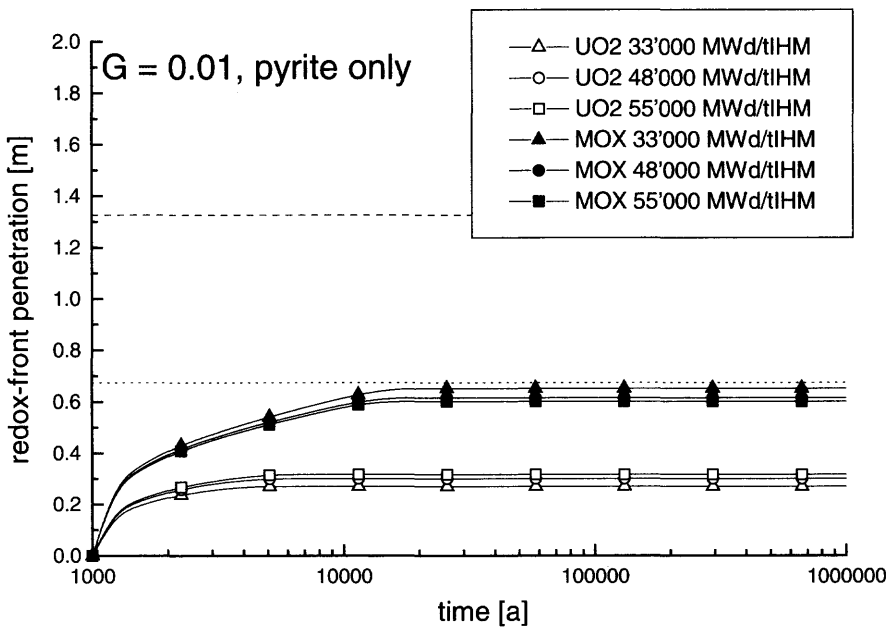
G = 0.01, pyrite only
UO2 33'000 MWd/tIHM
UO2 48'000 MWd/tIHM
UO2 55'000 MWd/tIHM
MOX 33'000 MWd/tIHM
MOX 48'000 MWd/tIHM
MOX 55'000 MWd/tIHM
redox-front penetration [m]
time [a]
0.0
0.2
0.4
0.6
0.8
1.0
1.2
1.4
1.6
1.8
2.0
1000
10000
100000
1000000

10000 a canister lifetime, variations in bentonite minerals acting as reductants.

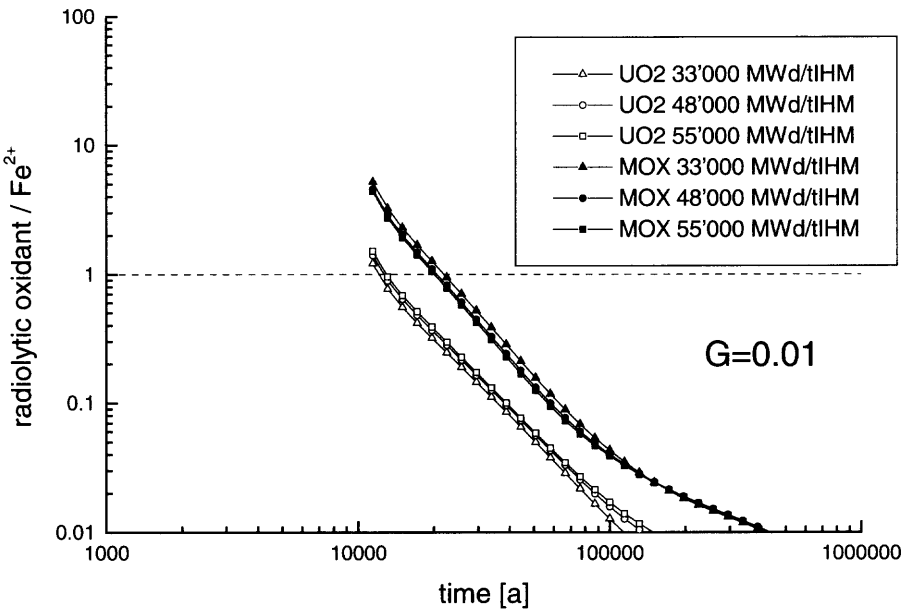

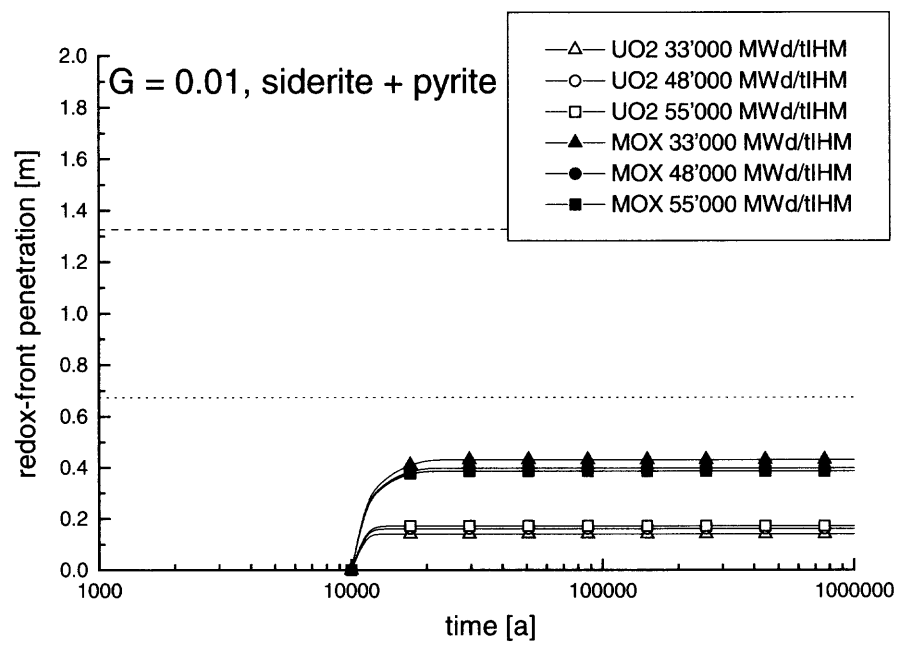

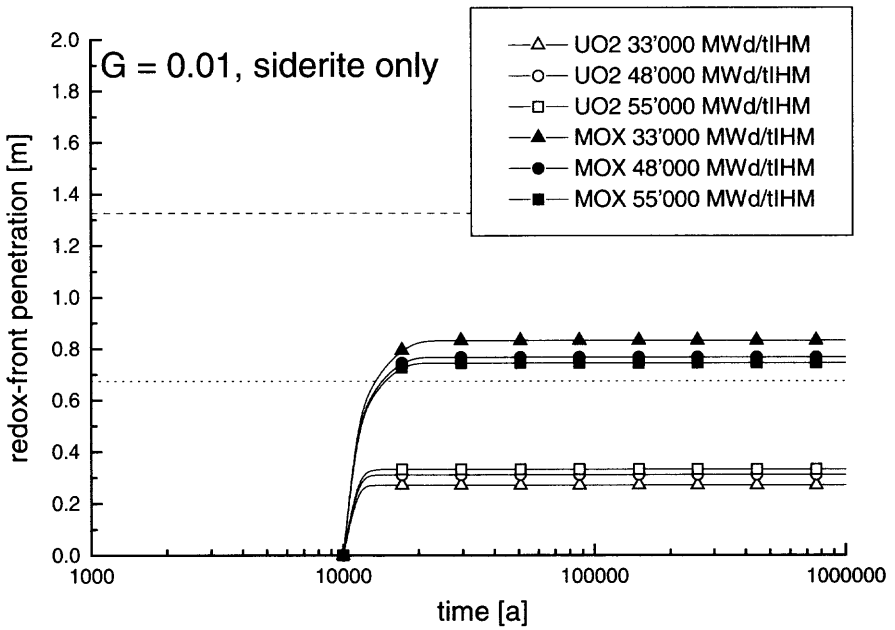
G = 0.01, siderite only
UO2 33'000 MWd/tIHM
UO2 48'000 MWd/tIHM
UO2 55'000 MWd/tIHM
MOX 33'000 MWd/tIHM
MOX 48'000 MWd/tIHM
MOX 55'000 MWd/tIHM
redox-front penetration [m]
time [a]
2.0
1.8
1.6
1.4
1.2
1.0
0.8
0.6
0.4
0.2
0.0
1000
10000
100000
1000000

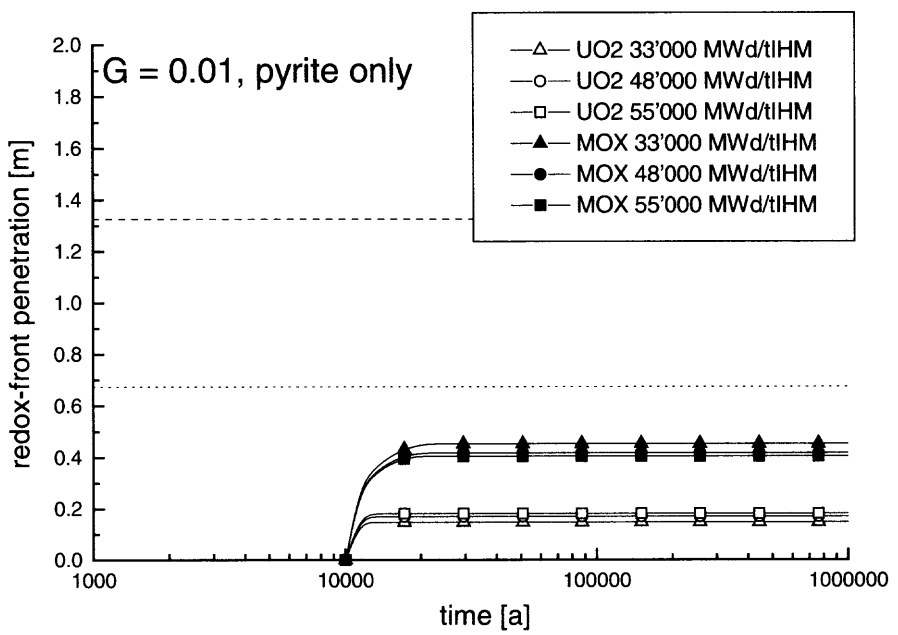
G = 0.01, pyrite only
UO2 33'000 MWd/tIHM
UO2 48'000 MWd/tIHM
UO2 55'000 MWd/tIHM
MOX 33'000 MWd/tIHM
MOX 48'000 MWd/tIHM
MOX 55'000 MWd/tIHM
redox-front penetration [m]
time [a]
2.0
1.8
1.6
1.4
1.2
1.0
0.8
0.6
0.4
0.2
0.0
1000
10000
100000
1000000

100000 a canister lifetime.

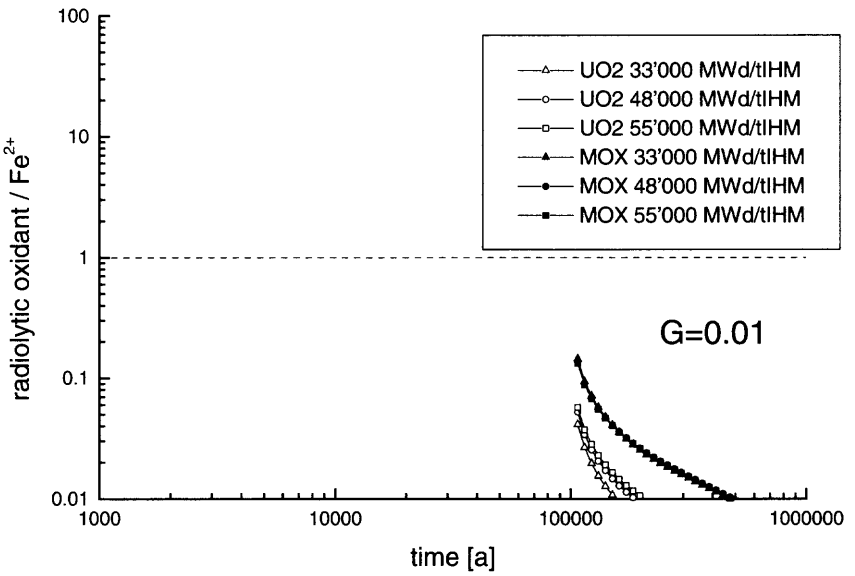

No redox front in the bentonite in this case.

APPENDIX F: EVALUATION OF THE CONCENTRATIONS OF NEAR-FIELD REDUCTANTS

From Table 3.4.1 of NAGRA (1994), in the case of a repository for reprocessed high-level waste in a crystalline host rock (tunnel diameter 3.7 m), the mass of bentonite per canister (excluding the water contained in bentonite pores) is 9.0×10^4 kg. This mass occupies a volume of 52.8 m^2, giving a density of 1704.5 kg m^{-3}. Assuming the same bentonite density applies, this value can be used to evaluate the concentrations of near-field reductants in a spent-fuel repository in either crystalline or Opalinus Clay host rocks, in spite of their different geometrical configurations.

From Table A3 of MÜLLER-VONMOOS & KAHR (1983), 1.4% of this mass is composed of carbonate minerals, of which one half is $FeCO_3$, giving a density of $FeCO_3$ of 11.9 kg m^{-3}. 0.3% of the mass is composed of FeS_2, giving a density of FeS_2 of 5.11 kg m^{-3}.

One mole of $FeCO_3$ weighs 0.116 kg and, if Fe(II) in $FeCO_3$ is oxidised to Fe(III), then 11.9/0.116 = 103 moles of reducing equivalents are available per cubic metre of bentonite. One mole of FeS_2 weighs 0.120 kg and, if Fe(II) and S(-1) in FeS_2 are oxidised to Fe(III) and S(VI), respectively, then $15 \times 5.11/0.120 = 639$ moles of reducing equivalents are available per cubic metre of bentonite. Considering both $FeCO_3$ and FeS_2 inventories, 103 + 639 = 742 mol m^{-3} of reducing equivalents are available.

References

MUELLER-VONMOOS, M & KAHR, G. (1983): Minerlogische Untersuchungen von Wyoming Bentonite MX-80 und Montigel, Nagra Technical Report NTB 83-12, Nagra, Wettingen, Switzerland.

NAGRA (1994): Kristallin-I Safety Assessment Report, Nagra Technical Report 93-22, Nagra, Wettingen, Switzerland.